New Routes to II-VI Materials

Saeed, Tahir

New Routes to II-VI Materials

by

Tahir Saeed, M. Sc.

A thesis submitted to the University of London

for the Degree of Doctor of Philosophy

Department of Chemistry

Queen Mary and Westfield College

Mile End Road

London E1 4NS

August 1995

Abstract

Zinc and cadmium dithiocarbamates were synthesized and used as single molecule precursors for the deposition of zinc or cadmium chalcogenides. The precursors were based on trimethylpropylenediamine including bis(trimethylpropylene-diaminedithiocarbamato)zinc(II)\cadmium(II) (**3**), (**4**) and methyl(trimethylpropylene-diaminedithiocarbamato)zinc(II)\cadmium(II) (**5**), (**6**). These compounds have been chracterized by I.R, NMR (^{1}H, ^{13}C and ^{113}Cd) and mass spectrometry. The single crystal x-ray structures of bis(trimethylpropylenediminedthiocarbamato)zinc(II) (**3**) and methyl-(trimethylpropylenediaminedithiocarbamato)cadmium(II) (**6**) have been determined, both compounds were polymeric. Thin films of zinc or cadmium sulfide by MOCVD method have been grown from (**3**), (**4**), (**5**) and (**6**). The cadmium compounds gave good films on both glass and GaAs substrates, but the films grown from corresponding zinc compounds were of poorer quality. Some t-butyl- and neopentyl(di-alkylamido)zinc compounds have been synthesized and characterized.

Thin films of CdS, ZnS, $Cd_xZn_{1-x}S$, and ZnO were grown by chemical bath deposition method. CdS films were deposited by using cadmium/ethylenediamine-/thiourea system whereas ZnS films were grown from zinc/ammonia/hydrazine/thiourea system. Films of ternary $Cd_xZn_{1-x}S$ have been obtained by the addition of cadmium to the ZnS system. Calculation were carried out for the speciation of the solution for which CdS was deposited. Films of ZnO were deposited from solution containing zinc/ethylenediamine in presence of NaOH. The various parameters controlling the film quality, growth rates, morphology and crystallinity were investigated. The films deposited were characterized by several methods including scanning electron microscopy, tramission electron microscopy, X-ray powder diffraction, reflection high energy electron diffraction and the electronic spectroscopy.

Dedicated To My Parents

Acknowledgements

I would like to thanks Prof. Paul O'Brien for his constant guidance, encouragement and unfailing support, which enabled me to finish this project. I am also very grateful to Dr. M. Azad Malik for his help throughout this work, from initial training to proof-reading. I would also like to acknowledge my indebtedness to Dr. Issac Abrahams for giving me a firm foundation of X-ray diffraction patterns. I would also like to thanks Dr. Angli Gayani for her useful suggestions regarding speciation and final proof-reading.

I would like to give enormous thanks to the people who have helped me with this great task over the years, including Liz, John, Lee, Izaque, Paola, Tito, Charlotte, Ian (H) and Ian (W). A special thanks must go to Steve, Liaquat (chacha) and Mo(tu) for making my life hell for the past four years.

I am grateful to the following people for their contribution: Mr. K. Pell for SEM; Mr. G. Coumbarides for ^{1}H, ^{13}C and ^{113}Cd nmr spectroscopy; Mr. M. Motevalli for X-ray crystal structures; Mr. P. Cook for mass spectra; Mr. J. Pratt and Mr. C. Whitehead for technical assistance; Mr. J. Cowley for glassblowing and Mr. A. Bradshaw in the stores for his help.

Finally I would like to thanks BP (solar) for financial assistance.

Contents **Page**

List of figures

List of tables

Chapter 1

Deposition methods for semiconducting materials

1.1 Introduction

Semiconducting II-VI materials have considerable potential in photoelectronic or optoelectronic applications, because of their wide range of direct band gaps. A number of growth methods for the deposition of semiconductor materials are described in this chapter. Solid-state materials used in electronics can be grouped into the following classes: insulators, semiconductors, conductors and superconductors.

Semiconductors may be single elements such as silicon or may consist of the combination of different elements (compound semiconductors) of various groups in the periodic table. Semiconductors have conductivities in the range of 10^{-8} S cm^{-1} and 10^{3} S cm^{-1}, a value which lies between that of insulators and conductors. Table 1.1 lists some of the binary semiconductors formed from group II-VI, III-V and IV-VI. In addition to binary compounds, semiconductors may be made from ternary or quaternary combinations such as: $Cd_xHg_{1-x}Te$ or $Ga_xAl_{1-x}As_yP_{1-y}$.

Table 1.1 Some important semiconductors

Elements	IV-VI compds.	III-V compds.	II-VI compds.
Si	PbS	AlAs	CdS
Ge	PbTe	AlSb	CdSe
		GaAs	CdTe
		GaP	ZnO
		InP	ZnS
		InAs	ZnSe
		InSb	ZnTe

The distinction between insulators, semiconductors and metals can also be made in terms of their band gap energies. If we consider the energy bands of insulators, semiconductors and conductors, in the case of a metal the conduction band is partially filled or overlaps the valance band as is illustrated in figure 1.1. Semiconductors and insulators have a forbidden energy gap between the valance band and the conduction band. The magnitude of this gap is small in the case of semiconductors and electrons that gain sufficient energy can move across the gap into the conduction band. Insulators have a large band gap and electrons in these materials cannot normally gain enough energy to move into the conduction band.

The present work is mainly concerned with compounds containing group II and group VI elements.

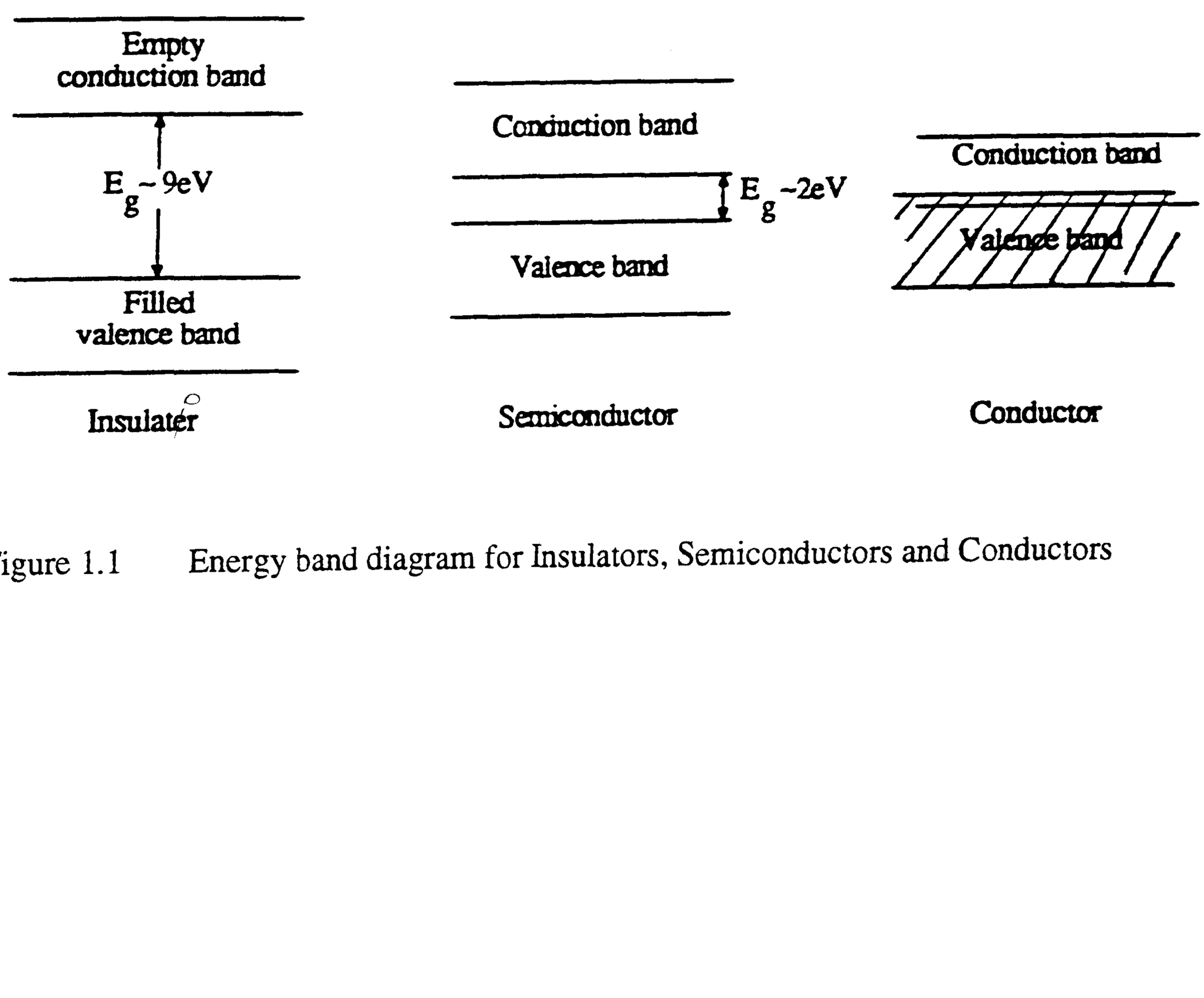

Figure 1.1 Energy band diagram for Insulators, Semiconductors and Conductors

1.2 Application of II-VI materials

The wide range of band gaps in II-VI compounds make them suitable for use in photoelectric devices [1] and optoelectronic devices [2].

1.2.1 Photoelectric devices

These devices convert optical signals into electrical signals and generate charge carriers, transport the carriers and finally interact the resultant current with an external circuit. Such devices function in the visible region and include infra red sensors and detectors. The electronic requirement for photodetection includes a high response to the incident radiation and a high signal noise-ratio, which varies with the wave length. An other requirement is the availability of high quality large single crystals (ideally about 10 cm^2 in area).

In order to obtain maximum efficiency in such detectors, it is necessary to use sensitising centres lying deep in the band gap. Cadmium sulfide (2.42 eV) is doped with halogen and becomes n-type (eg. CdS:Cl), then doped with sensitiser (usually copper) which has deep-lying energy level as low as 1.7 eV. These sites behave as hole traps (holes being more easily trapped than electrons due to their higher effective mass) and when a carrier pair is generated by an incident photon, the carriers travel towards the appropriate electrode. The hole which is trapped will remain so, causing another electron to be released from the cathode, resulting in recombination at the sensitising centre. Hence, the effect of incident radiation is to increase the conductivity of the semiconductor, enabling current to flow.

The same basic principals apply to photovoltaic detectors however their operation (unlike the standard photodetectors) is based on the movement of minority carriers, photogenerated species which are transferred to the opposite conductivity region in the material where they become majority carrier. As with the previous devices, a p-n heterojunction is involved, the two materials often resulting in lattice mismatching, creating point defects which in turn cause recombination by trapping carriers, reducing the electronic qualities of the device.

Another slightly different device involves photo-resistance in which the speed of response to radiation in the material is important. Compensated CdS provides the best example of such a material, operating in the 500-550 nm region (visible radiation) making the device suitable for example, as an exposure meter for cameras.

Solar cells

These devices are the basis of the conversion of solar energy to electrical energy; for economic viability and maximum efficiency the devices require a high surface area (due to the low density of the solar energy). Investigations have been made into many II-VI materials but a promising combination is the p-Cu_2S/n-CdS system which overcomes the lattice mismatch problem in the fabrication of the p-n heterojunction [3,4]. The material is produced by "topotaxy", whereby CdS is contacted with a solid source of copper or a copper containing solution. Diffusion causes exchange (2 copper atoms for 1 cadmium atom) within the lattice, the sulfur lattice arrangement remaining unchanged.

1.2.2 Optoelectronic devices

These devices show luminescence i.e. the efficient emission of electromagnetic radiation when placed in an electric field. They include light emitting diodes (LED's) [2,5] and lasers [6].

Light-emitting diodes

Because of their direct band gap and the possibility of alloy formation, II-VI compounds can have energy gaps encompassing the whole of the visible region of the electromagnetic spectrum. Red, green and yellow LED's can be fabricated, but problems in producing blue LED's based on ZnSe and $ZnS_{1-x}Se_x$ have plagued engineers for many years [7]. It is not yet practical to fabricate a blue LED which functions at room temperature since the shallow donor atoms required trigger self-activated luminescence in the yellow region. One option may be to utilise the alloy $ZnS_{1-x}Se_x$ which covers the whole spectral range including the blue region [8]. ZnS can emit in the visible region in crystalline or powder form [9,10]. However with certain dopants deep centres can lead to emission at visible wavelengths.

Lasers

In order for a semiconductor material to lase, the band gap must be direct and allow sufficient generation of charge carriers when under the influence of a forward biased external current. The behaviour of a laser device is based on the population inversion of the carriers, allowing incident radiation to force the relaxation of the carriers

resulting in the emission of highly concentrated monochromatic radiation. The advantage of the semiconductor laser include its efficiency and very small size.

The two main ways to obtain and maintain population inversion in II-VI semiconductors involve excitation of the material by either separate lasers (optical pumping) or the action of an electron beam. The former has been used to produce lasing action in CdSe (using a $GaAs_xP_{1-x}$ laser) and $CdS_{1-x}Se_x$ (using flash tubes). The latter involves an electron beam penetrating several microns into the materials and producing large number of carriers (ca 100 per incident electron) resulting in a laser action (operating 4K and 77K) at right angle to the incident beam. This method has been applied to materials such as ZnS, ZnO, CdS, CdSe and various alloys [11].

1.3 Deposition methods for II-VI materials

As specified earlier, the need for good quality and purity in the production of thin film and single crystal is of prime importance. To avoid the presence of point defects, dislocation and unwanted impurities, much care must be taken to ensure the purity of the constituent elements, the transport for the sources efficient, and the careful deposition of the material. Various methods are available for deposition of II-VI materials, and some of them are discussed in this chapter.

1.3.1 Electrodeposition

In electrodeposition an electric current is allowed to flow between two electrodes in an electrolytic cell. An electrolytic cell comprises a cathode, an anode, a cathodic reactant, an anodic reactant and an electrolyte. A typical electrolyte for the deposition of CdS may consist of an aqueous solution of cadmium hydroxide and thiourea.

Pawar [12] performed detailed studies on the electrodeposition method which included the speed of rotation of the substrate, the temperature of the bath, the concentration of electrolyte and the strength of the applied electric field. Ultrasonically cleaned chromium-plated stainless steel substrates rotated at 75 rpm were placed in a stirred solution of cadmium hydroxide and the temperature was maintained at 90 °C. After applying an electric current (0.15 mA, 900 mV dc.) between the substrate and the stainless steel electrode, a solution of thiourea was added to the reaction vessel (0.7 ml/min).Thin films of CdS were found to be deposited both at the anode and the cathode.

It was found that at low rotation speeds of the substrate (50-60 rpm), the films were thick, nonspecular and nonuniform, whereas at higher speeds (150 rpm), the films were thin, specular and adhesive. At intermediate speeds (70-80 rpm), the films were smooth, specularly reflecting, adhesive and uniform. The films formed on an equivalent stationary substrate were porous, powdery, thick, and non-uniform. Additionally, anodically grown films were more adherent, physically coherent and smoother than cathodic ones.

The rate of deposition of CdS onto the substrate surface has been shown to increase when the substrate was at positive bias and vice versa. Stirring of the solution also increased the rate of deposition of CdS.

Studies into the mechanism of the electrodeposition process shows that film formation proceeds via a thin layer of cadmium hydroxide on the substrate which acts as catalyst promoting the decomposition of thiourea, which supplies sulfide (S^{2-}) ions which then combine with cadmium hydroxide to form CdS.

Other studies on the mechanism of electrodeposition have been carried out in dimethyl sulfoxide [13], and diethyl glycol [14] solutions. Cyclic voltammetry at stationary electrodes and pulse polarography at dropping mercury electrodes in solution containing both Cd^{2+} ions and elemental sulfur provide evidence that sulfur is chemisorbed at these electrodes and that the formation of at least a monolayer of metal sulfide takes place. For this system it has also been shown that the potential at which CdS is formed is strongly dependent on the concentration of sulfur, whereas the opposite is true at an electrode covered with a CdS layer.

Electrodeposition of ZnS and CdZnS [15] has also been carried out from an alkaline aqueous bath using the corresponding metal salts and sodium thiosulfate (as a sulfur source) at pH 2 - 2.5. The films were reported to be polycrystalline containing free Zn and S in addition to ZnS. CdSe [16,17] thin films have been prepared by a repeated cathodic-deposition process and the films have been shown to give a better performance than the solar cell . Thin films of $CuInS_2$ [18,19], $CuInSe_2$ [20], CdSeTe [21], and CdTe [22-24] have also been successfully electrodeposited onto titanium, graphite and indium tin oxide substrates by electrodeposition method.

Most recently polycrystalline films of cubic ZnSe [25] and hexagonal CdS [26] have been deposited onto stainless steel plates, titanium and tin oxide coated glass. ZnSe films showed a sharp change in reflectance at 670 nm, indicating semiconductor nature.

1.3.2 Electroless Deposition or Chemical bath deposition

Deposition from solutions is a convenient and cheap method for depositing thin semiconducting films of CdS, CdSe, ZnS, ZnSe, CdZnS, CdHgS, PbSe, CoSe and Bi_2Se_3. This technique was first introduced by Bell, Hemmatt, and Wald [27], and since then has been used widely. It is a similar technique to electrodeposition but a chemical redox process, rather than an external potential source is responsible for the deposition process. The rate is controlled by altering the bath temperature, the pH of the solution, and the concentration of the reactants.

Electroless deposition has been carried out using the following exchange reaction.

$$M^{2+} + (NH_2)_2CS + 2OH^- \text{-----> } MS \text{ (film)} + 2NH_3 + CO_2 \quad \text{(Eq. 1)}$$

where M = Cd, Zn

$$[Zn(TEA)]^{2+} + (NH_2)_2CS + 2OH^- \text{------> } ZnS \text{ (film)} + TEA + 2NH_3 + CO_2$$

TEA = Triethanolamine

It has been suggested [28] that the hydroxyl ions act both as a complexing agent and base in the reaction. When the hydroxyl concentration is low, the Zn^{2+} concentration in the solution is high, due to the pH of the bath. The reverse situation applies if the hydroxyl ion concentration is high. In both instances the maximum thickness obtained is low, but at the higher pH values, the rate of deposition is enhanced.

The dependence of growth rate on various deposition parameters may be understood by considering the growth mechanism : ions from the solution reach the

surface and migrate onto it to react with each other to form stable nuclei which grow with further arrival of ions. The rate of growth is high during early stages (due to high concentration of reactants) but as the time passes it gradually falls to zero. The initial rate of growth has been found to depend on the concentration of ions in the solution i.e. bath concentration and on their mobility on the substrates, which is a function of the reaction bath temperature and the nature of the substrate surface. If a thicker film is required, the deposition process may be repeated.

Electroless deposition of thin films of CdS, ZnS, PbS, CdZnS, CdSe, and PbSe have been carried out by the decomposition of thiourea in an alkaline solution of salts of corresponding cations [29-32]. Triethanolamine (TEA) has been used as a complexing agent in the deposition of thin films of ZnS [28], CdZnS [33], ZnSe [34], CoSe [35], and MnS [36]. Multicomponent semiconductors such as $Cd_{1-x}Zn_x$ S, $Cd_{1-x}Hg_x$ S, $Cd_{1-x}Pb_x$S, and $Pb_{1-x}Hg_x$S have also been prepared [29,37] by electroless deposition process.

The composition of such multicomponent film may be varied by altering the concentration of one component e.g. $HgCl_2$ in the deposition solution. Bhattacharya [38] successfully deposited Bi_2S_3 from thiourea solution at pH 9.8. The overall reaction is

$$Bi(A)^{3+} + (NH_2)_2CS \text{ --------> } Bi_2S_3 + (NH_2)_2CO + nA \qquad \text{(Eq. 2)}$$

Where $A = N(CH_2CH_2OH)_3$

CdS [39,40] thin films of thickness 0.2 μm have been deposited onto glass, SnO_2, and $CuInSe_2$ substrates from thiourea and cadmium sulfate. The thin films were continuous, homogeneous and appear granular. A chemical method for the growth of ternary II-VI materials has been described [41], where GaAs wafers were successfully

used to grow thin films of ZnSSe. The films obtained were uniform and polycrystalline, with a cubic structure.

Recently the electroless deposition of CdS thin films have been carried out on a range of substrates such as glass, graphite, silicon and tin oxide coated glass, using various deposition baths. A bath containing cadmium salt, ammonium nitrate and thiourea was used by Rieke and Bentjen [42] and Sahu et al. [43] to deposit mixed phase CdS films, which were characterised by XRD and SEM. In other work a cadmium\triethanolamine\ammonia\thiourea system was employed to deposit CdS films. The best films were reported at bath containing Cd:TEA:NH_3:Th mole ratios of about 1:3.75:14.4:1 [44].

Crystalline ZnS thin films (cubic) have also been grown onto glass slides by Dono and Herrero [45]. Similar work was carried out using zinc sulfate, ammonia, hydrazine, and thiourea and is discussed in detail in chapter 3 of this thesis. CdS, $Cd_xZn_{1-x}S$ and ZnO thin films were deposited by using different deposition baths.

1.3.3 Spray Pyrolysis

The spray pyrolysis process was first introduced in the mid 1940's for the preparation of oxide films [46]. Since then it has become one of the most intensively studied low-cost techniques and has become a production method for applying transparent electrically conducting films of SnO_x onto glass [47]. The method was first applied to the preparation of CdS by Chamberlin and Skarman [48] in 1966. The technique was later adopted by Bube [49] who deposited a wide range of compound semiconductors.

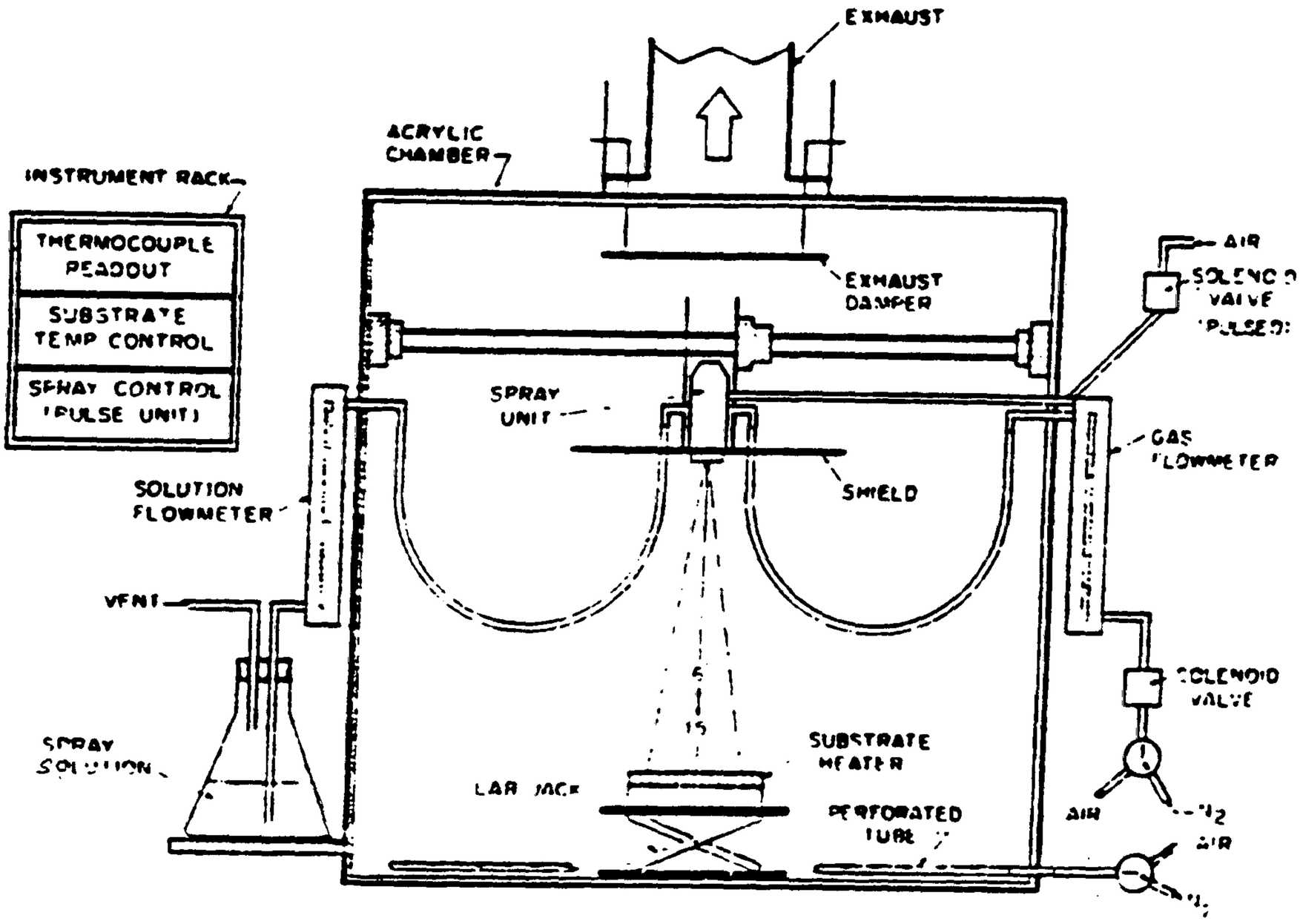

Figure 1.2 Spray pyrolysis apparatus

The spray pyrolysis technique consists of spraying a finally atomised solution of the precursor onto a heated substrate. A diagram of a spray pyrolysis apparatus is shown in figure 1.2. Deposition is normally carried out under a blanket of nitrogen. The substrate can be heated in two ways: by direct illumination by a tungsten filament lamp or a hot plate. It can be held at a constant temperature by a feedback arrangement. A reservoir of the spray solution is held under pressure and allowed to flow to the spray nozzle.

Atomisation of the solution at the spray nozzle can be achieved in many ways. At a conventional spray head, a free stream of spray solution is struck by a jet of carrier gas travelling at a high speed and atomisation takes place as the necessary condition are satisfied. Alternatively, atomisation may be achieved by forcing the liquid through a small orifice at high pressure.

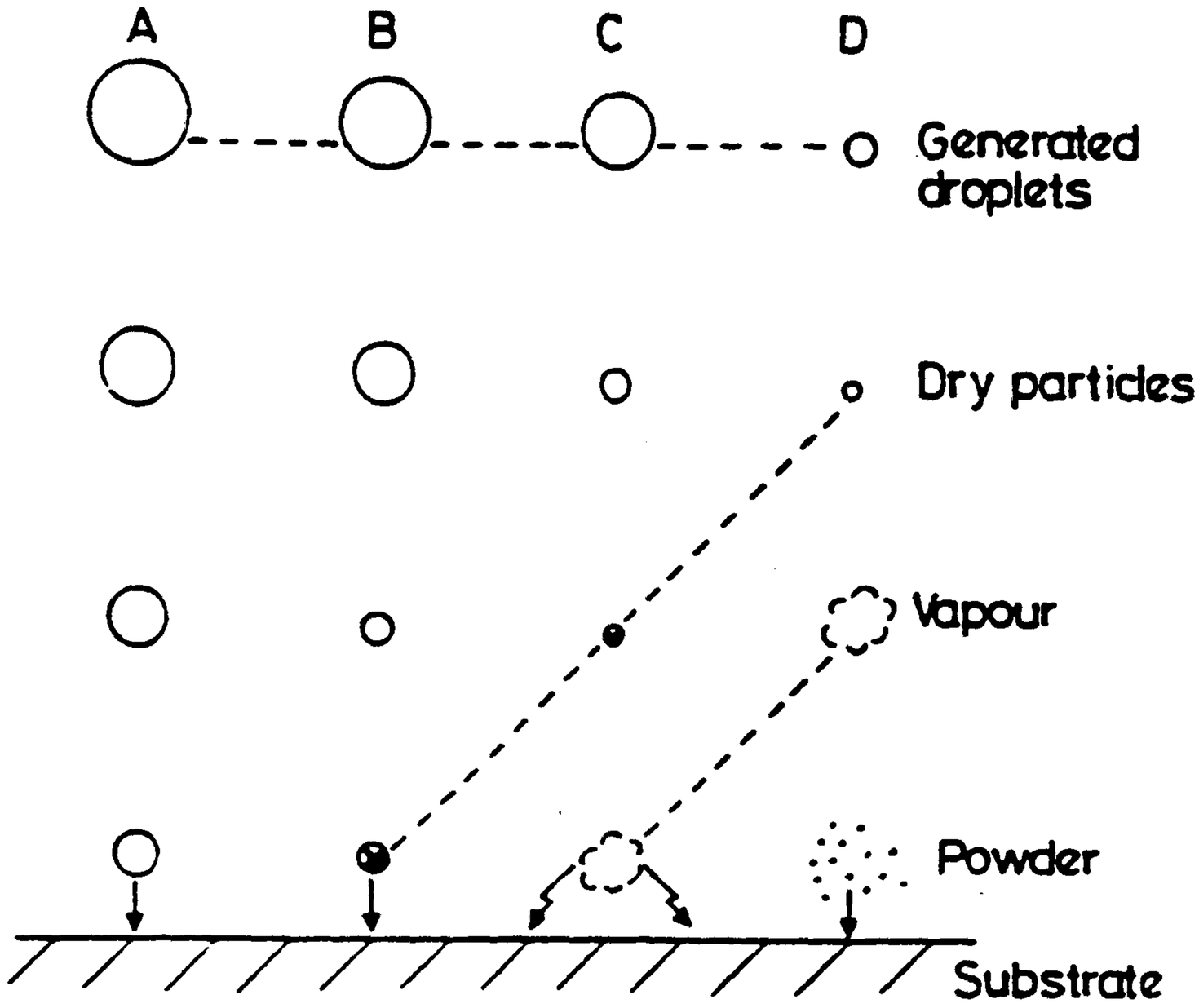

Figure 1.3 The relationship between deposition processes and droplet sizes

To ensure even heating and uniform coverage of the substrate surface by the spray solution, the substrate is usually mounted onto a platform which can be moved transversely and rotated. Movement in the spray head can also be used to promote uniform deposition. There are many factors that influence the quality of films obtained by spray pyrolysis; droplet size, solution spray rate, temperature of the substrate etc. Of these factors, one of the most important is droplet size.

If we consider droplets of four different sizes travelling from the nozzle to the substrate, there are different deposition processes that can occur. These are illustrated in figure 1.3.

A The droplet is so large that the heat absorbed during transport to the substrate surface is insufficient to evaporate all the solvent. The droplet reaches the substrate surface and the solvent subsequently evaporates leaving dry particles which melt and

then decompose to give the desired compound and gaseous products. Evaporation of the solvent on the substrate surface results in localised cooling and a correspondingly poor quality film

B The droplet size is such that all the solvent evaporates just before reaching the substrate, leaving behind precipitated particles of the precursor. These are deposited onto the substrate surface where they melt/sublime and then decompose to give the desired compound. Again cool spots result from the melting of the precursor which lead to inferior quality films.

C Here we have the ideal droplet size. The solvent evaporates completely before reaching the substrate surface. The precipitates then melt, vaporise, and diffuse to the substrate surface where they undergo adsorption, surface diffusion and reaction leading to nucleation and layer growth. The later part of the process can be described as chemical vapour deposition [47].

D In this case the droplet size is too small and the reaction is complete before the substrate is reached. This results in a powder of the desired compound adhering to the substrate and films of very poor quality.

ZnS [50] thin films have been deposited by spraying a toluene solution of bisdiethyldithiocarbamatozinc (II) onto silicon, sapphire and GaAs substrates at 460 - 520°C. The films grown on silicon or sapphire showed a highly oriented hexagonal structure, whereas those grown on GaAs showed a highly oriented cubic structure. The films grown on silicon displayed high transparency in the I. R. and the principal lattice absorption band occurred at 278 cm^{-1}, which is in good agreement with the literature value for ZnS [51].

1.3.4 Hot Wall Epitaxy (HWE)

The simplest vacuum process is evaporation. Thin films may be formed on a substrate by heating the source material to a sufficiently high temperature to give a high rate of sublimation. The vapours then condense onto the cooler substrate. A typical system [52] for film growth by thermal evaporation is shown in the figure 1.4.

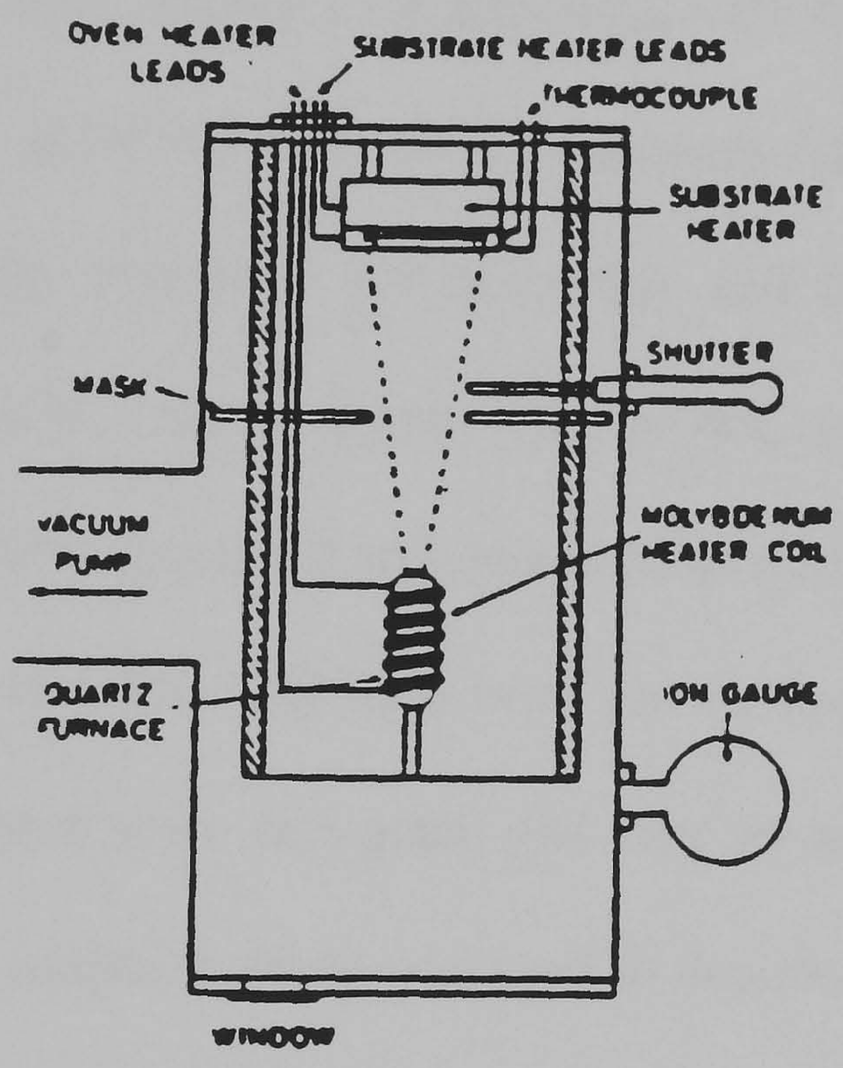

Figure 1.4 Diagram of an evaporating system

The source and substrate are usually placed at a distance of 5 - 15 cm apart. A shutter placed between the source and the substrate prevents deposition on the substrate before growth conditions have reached a steady state. The ideal condition for film growth is to have the substrate temperature high enough for the incident atoms or molecules to have sufficient surface mobility to form a well ordered structure. The substrate temperature for the condensation of most materials is limited to about 300 - 400 °C. This is because higher temperatures will cause re-evaporation of the incident

molecules from the heated substrate, leading to a lower growth rate and loss of material due to condensation in cooler parts of the system.

A number of studies on the growth of cadmium and zinc chalcogenides have been carried out by Hudoch [53], and Muravyeva and co-workers [54]. Depositions were performed in a small quartz sublimation shell using a sapphire substrate. Crystalline CdTe layers [55] and Mn doped ZnS and ZnS-CdS superlattices [56] have been grown on a misoriented sapphire (0001) substrate using hot wall epitaxy.

A modified hot wall epitaxy [57] apparatus with double source tubes has been developed and used to grow epitaxial heterostructures and multilayers. The reaction chamber and the vacuum chamber were combined, and the vacuum system was thus greatly simplified. ZnS_xSe_{1-x} single crystal films grown on GaAs substrates using this apparatus showed excellent crystalline and optical properties.

Epitaxial layers of CdSe [58] have been grown by HWE onto GaAs and BaF_2 substrates. These epilayers were hexagonal and very smooth. Recently a HWE [59] system with a gold tube radiation shield was used to deposit high quality CdTe layers on GaAs substrate. It was found that the gold tube radiation shield is more effective in heat confinement and allows better temperature stability than a stainless steel tube radiation shield.

1.3.5 Molecular Beam Epitaxy (MBE)

Molecular beam epitaxy is a high vacuum technique in which beams of atoms are generated by heating the corresponding elemental source at a high temperature under vacuum. The atoms are adsorbed onto the heated substrate surface where they move to

their appropriate lattice sites. The growth rate is determined by the arrival of group II atoms, since an excess of group VI atoms is required to prevent the deposition of the metal.

Two ovens are shown in figure 1.5 but more ovens can be used for the growth of ternary materials, or for doping. The cells are usually made of low vapour pressure materials such as graphite or boron nitride held at accurately controlled temperatures which govern the beam intensity.

In order to ensure uniform coverage of large substrates (5-8 cm), the substrate stage is rotated at a speed between 0.03 to 2 Hz [61]. In order to achieve the high crystallinity of the epitaxial layers, the substrate temperature must be sufficiently high so that the atoms desorbing on the substrate have high surface mobility and can migrate to an appropriate lattice sites.

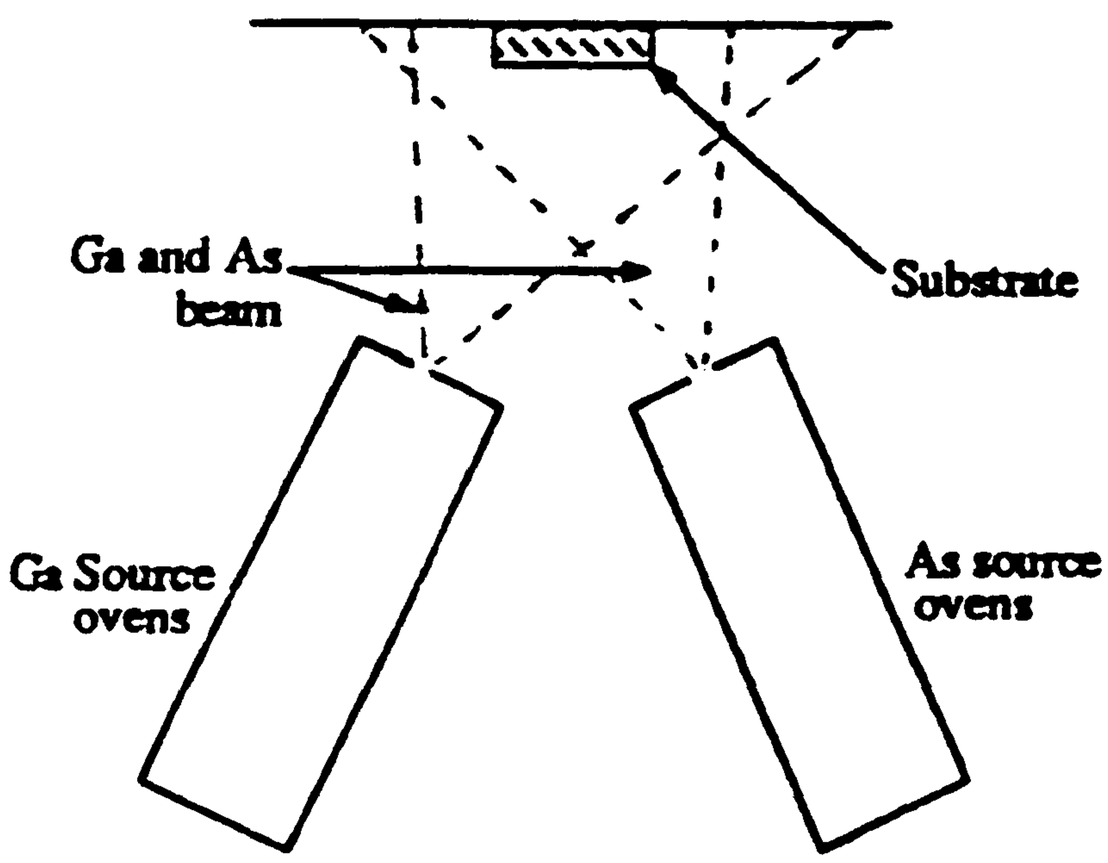

Figure 1.5 Schematic representation of MBE

This technique can be used for the growth of thin semiconductor films of very high quality. Heterostructures, multilayered structures having lattice-matched component layers which differ in composition, form the basis of optoelectronic devices such as lasers. The preparation of these materials by MBE [60] is particularly attractive because MBE allows very fine control for example, over the film thickness and doping although deposition rates are very slow.

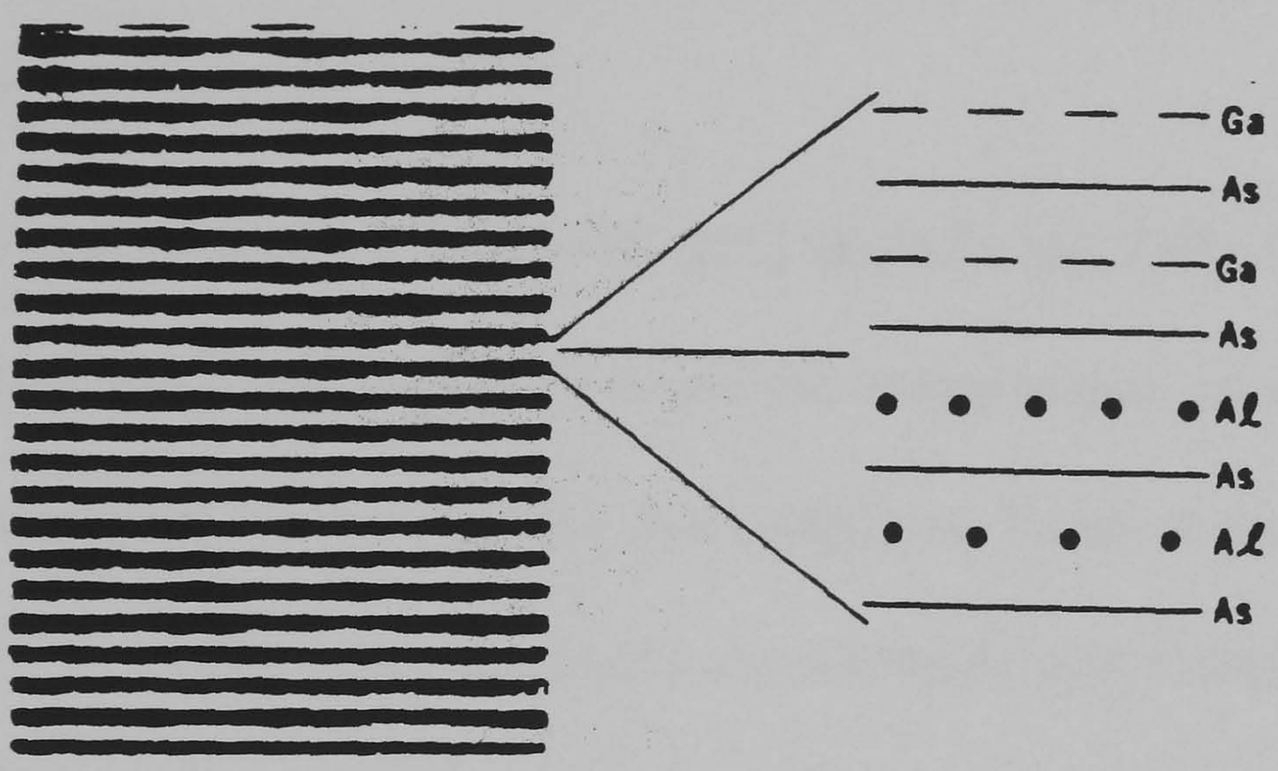

Figure 1.6 Cross-sectional Transmission Electron Micrograph of GaAs/AlAs

A system for the MBE growth of semiconductors consist of an ultra high vacuum chamber containing sources for the atomic or molecular beams, and a heated substrate. The molecular beams which emerge from the source ovens through small orifices are directed at the heated substrate. The ultrahigh vacuum employed (as low as 10^{-12} Torr) increases the mean free path of the constituents elements by removing most of the gas molecules from the path way. This results in the molecules travelling towards the substrate without collisions in the beam.

One of the greatest advantages of having ultrahigh vacuum is the possibility to study the film surface in situ with electron beam analysis technique. The major drawbacks of the method are its requirement for high vacuum and its slow growth rate. The majority of films which have been grown by MBE are III-V semiconductors. The first growth of CdS by the use of multiple beams was reported by Miller and Bachman [62], in which cadmium and sulfur were formed into beams which were directed to the heated substrate. During the last ten years much interest has been shown in the growth of selenides and tellurides of cadmium and zinc [63], the growth of CdS has also been reported [64].

Molecular beam epitaxial growth [65] of ZnTe and ZnTe-CdTe superlattices on GaAs substrate has been studied, and growth temperatures as low as 300 °C were reported. ZnSe [66] has been grown successfully on GaAs at growth temperatures as low as 100 °C using hot molecular beams generating by post heating at 600 °C both for Zn and Se. ZnSe epilayers showed good low temperature photoluminescence properties. Recent developments [67] in the MBE growth of II-VI materials for laser diodes and LED's have involved p-type doping of ZnSe, using active nitrogen. In another paper by Hommel et al. [68], it has been shown that MBE grown ZnSe epilayers deposited directly on a GaAs substrate were of better quality than to those grown on a GaAs buffer layer.

Indium [69] and antimony [70] have been used as dopants to deposit thin films of CdTe, ZnTe, and CdMnTe. This method has also been used to deposit thin films of the quaternary ZnMgSSe [71] onto GaAs in the fabrication of blue laser diodes.

The ternary alloy $Cd_{1-x}Mg_xTe$ and $Cd_{1-x}Mg_xTe/CdTe$ [72] quantum well structure have been deposited by MBE. The band gap in the ternary material was determined as a

function of Mg concentration. $Cd_{1-x}Mg_xTe$ thin films with x-values of up to 0.75 were fabricated, corresponding to a band gap of 2.8 eV at low temperature. Therefore the whole band gap range can be covered . In another paper [73] CdMgTe films were shown to have a band gap up to 2.2 eV at a different Mg concentration.

The epitaxial growth of HgSe [74] was studied for the first time by MBE growth on GaAs substrates. It was found that the growth rate was very low at substrate temperatures above 120°C. At 120°C and at lower temperatures the growth rate was appreciably high and electrical properties were improved compared with samples grown at higher temperatures.

1.3.6 Metalorganic Molecular Beam Epitaxy (MOMBE)

An ultrahigh vacuum technique similar to MBE. In MOMBE metalorganic group VI sources are used with an elemental group II source. This technique is a hybrid developed from MBE and MOCVD. The use of the gas source was first proposed by Cawala [75] who used arsine for the growth of GaAs. Afterwards metal alkyls were also used in this growth technique [76]. MOMBE is related to MBE, in that the beams of reactant sources travel toward the heated substrate and are adsorbed onto the surface at the appropriate sites. The choice of precursor is increased because volatility is no longer a problem. Similarities to MOCVD are that the sources are metal alkyls and group V hydrides.

The developments in MOMBE [77] for wide band gap II-VI compounds have been studied by considering both film properties and a novel growth technique. MOMBE using $(Me)_2Zn$ and H_2Se has enabled the growth of p-type ZnSe doped with nitrogen using ammonia as dopant source. More recently ZnSe [78] thin films were deposited by using thermally pre-craked $(Et)_2Zn$ and $(Et)_2Se$ on GaAs (001) substrates.

A schematic diagram of the processes involved (MBE, MOCVD and MOMBE) is shown in figure 1.7.

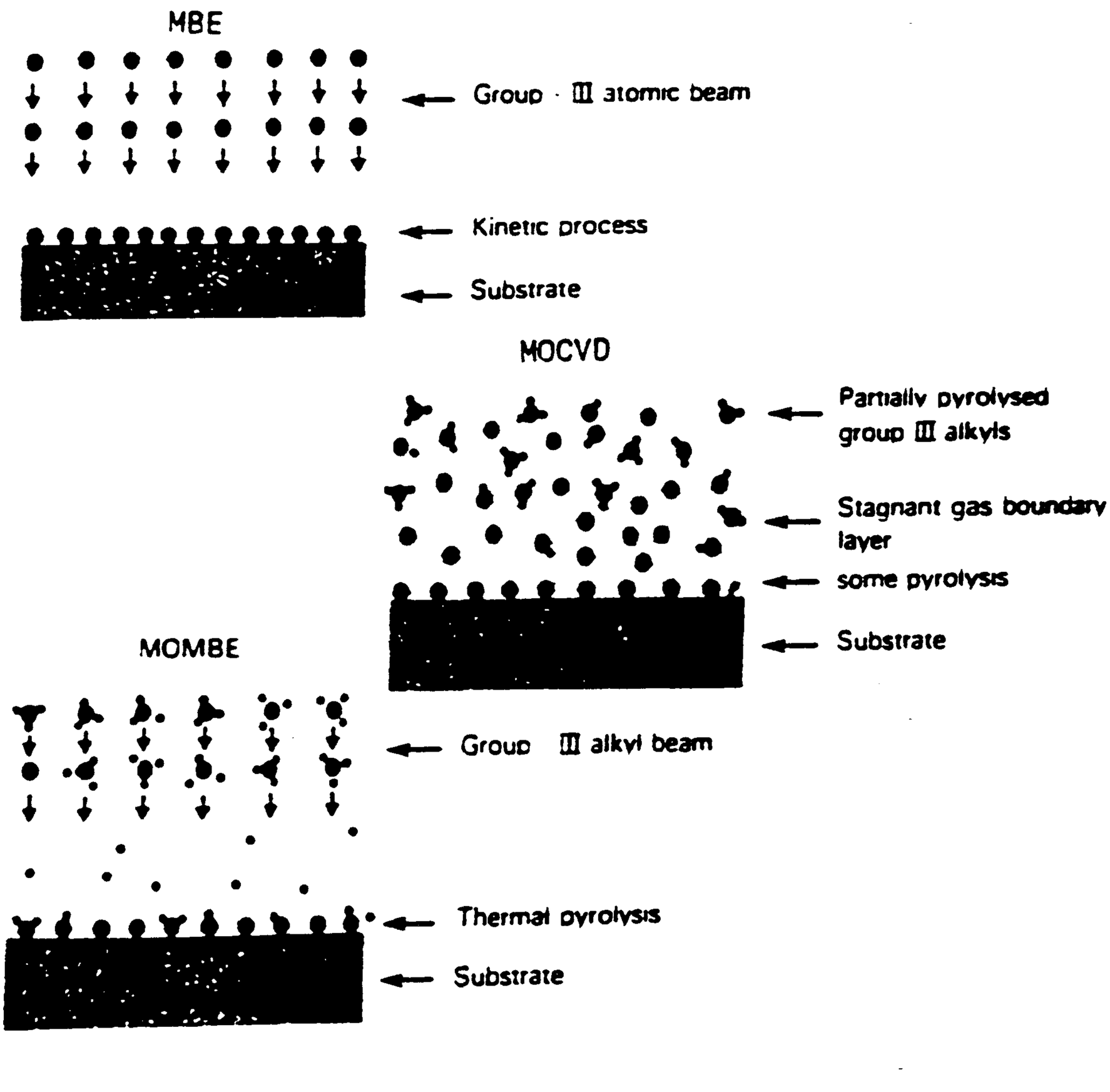

Figure 1.7 A schematic diagram of MBE, MOCVD and MOMBE

1.3.7 Atomic Layer Epitaxy (ALE)

Atomic layer epitaxy (ALE) was first introduced by Suntola and Anston who deposited thin films of ZnS, SnO_2, and GaP [79]. The technique is closely related to Molecular Beam Epitaxy (MBE) in which a beam of constituent molecules is targeted at a substrate surface under an ultra-high vacuum. Since the first experiment in 1974, this technique has been extended to the growth of III-V semiconductors such as GaAs and AlAs [80].

ALE involves the growth of thin films of one monolayer at a time. Since group II elements and group VI elements are much more volatile than their corresponding binary compounds, when a monolayer is adsorbed onto a surface, any excess atoms will immediately re-evaporate at the growth temperature. If we consider the evaporation of zinc onto a substrate, this is continued until the heated substrate is entirely covered, then all but a monolayer of chemisorbed zinc atoms re-evaporate into the vacuum system.

At the next stage, sulfur is evaporated onto the zinc layer. A monolayer of sulfur covers the zinc layer with the formation of Zn-S bonds. Excess sulfur is weakly held and consequently desorbs into the vacuum system. This process can then be repeated until the desired thickness of film is achieved. The film thickness can be monitored by counting the number of cycles (each cycle corresponds to one monolayer of the binary compound).

Precursors for ALE do not have to be constituent elements of the binary or ternary semiconductor, but can also be volatile compounds. For example the growth of ZnS can be achieved by chemisorption of zinc chloride onto a substrate, followed by

reaction with chemisorbed hydrogen sulfide. The unwanted volatile side-products (in this case HCl) are desorbed leaving behind the ZnS monolayer.

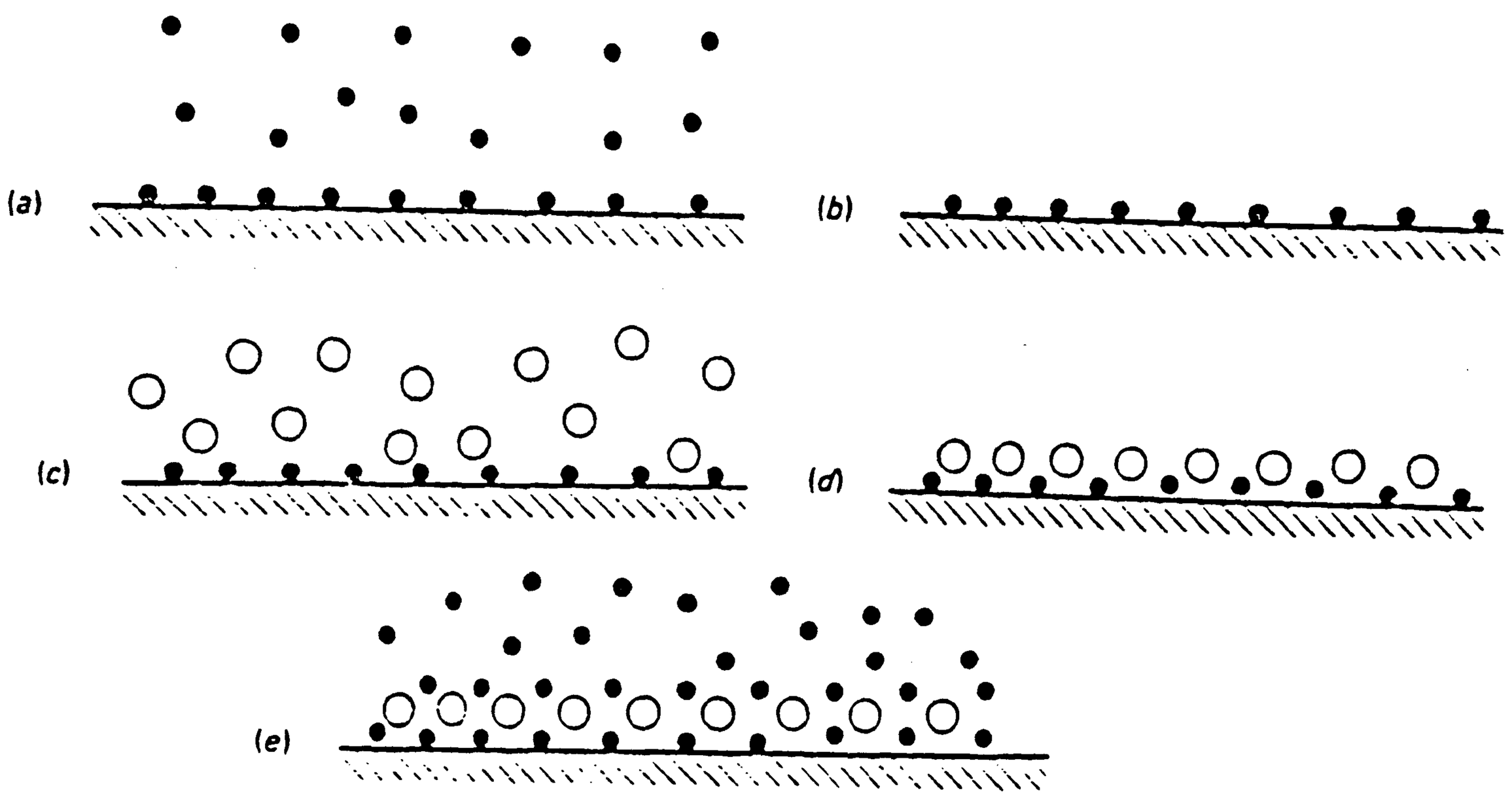

Figure 1.8 The Atomic Layer Epitaxy process

Zinc acetate and water were used as the source materials in the growth of ZnO [81]. However, it appears that ZnO is formed from the decomposition of zinc acetate and not from the reaction with water.

Superlattices of CdS/ZnS [82,83] and ZnTe [84] have been fabricated on GaAs at low temperatures of 185-190 °C by ALE using a MBE system. The film thickness of cubic CdS [84] was uniform in the whole area of the epilayer and the surface morphology was flat and smooth. Atomic layer epitaxy of ZnS [85] has been studied by

LP-MOVPE using dimethylzinc and hydrogen sulfide. In another paper [86] $ZnCl_2$ and H_2Se were used to deposit thin films of ZnSe. CdTe, HgTe and HgCdTe [87] have been deposited by ALE using dimethylcadmium and dimethylmercury along with methylallyltelluride. The films deposited at 250°C were of high quality with excellent surface morphology.

Short period superlattices of $[(CdSe)_n(ZnSe)_{10}]_m$ [88] and CdTe(ZnTe)/MnTe [89] have been deposited on GaAs (100) substrate using ALE in a MBE system. One monolayer per cycle growth of ZnSe was obtained over a range of substrate temperatures of 280 - 360°C.

A great disadvantage of the ALE growth technique is that it takes about 5 hours to grow a 1500 nm thick ZnTe film. There appears to be no way in which growth rates can be increased because ALE requires time for chemisorption and desorption of species at the substrate surface. This together with the vacuum system needed limits to the extent to which this technique can be used as a manufacturing technique.

1.3.8 Liquid Phase Epitaxy (LPE)

The growth of epitaxial layers on crystalline surfaces from solution is termed liquid phase epitaxy. This technique is particularly attractive for the growth of III-V compounds because the low melting points and the high boiling points of gallium and indium make them ideal solvents. This technique is used in the manufacture of numerous semiconductor devices, especially for opto-electronics applications.

The choice of solvents for the growth of II-VI semiconductors is less straight forward because group II metals have relatively high vapour pressures, and the group

elements are often used as the solvents [90]. A brief description of the technique is given below.

The configuration for the boat used for LPE is shown in figure 1.9. One or two wells in the graphite block serve to hold the reactant solutions. A graphite slider holding the substrate can be moved to locate them under the wells. The whole apparatus, under an inert atmosphere, is placed in a furnace.

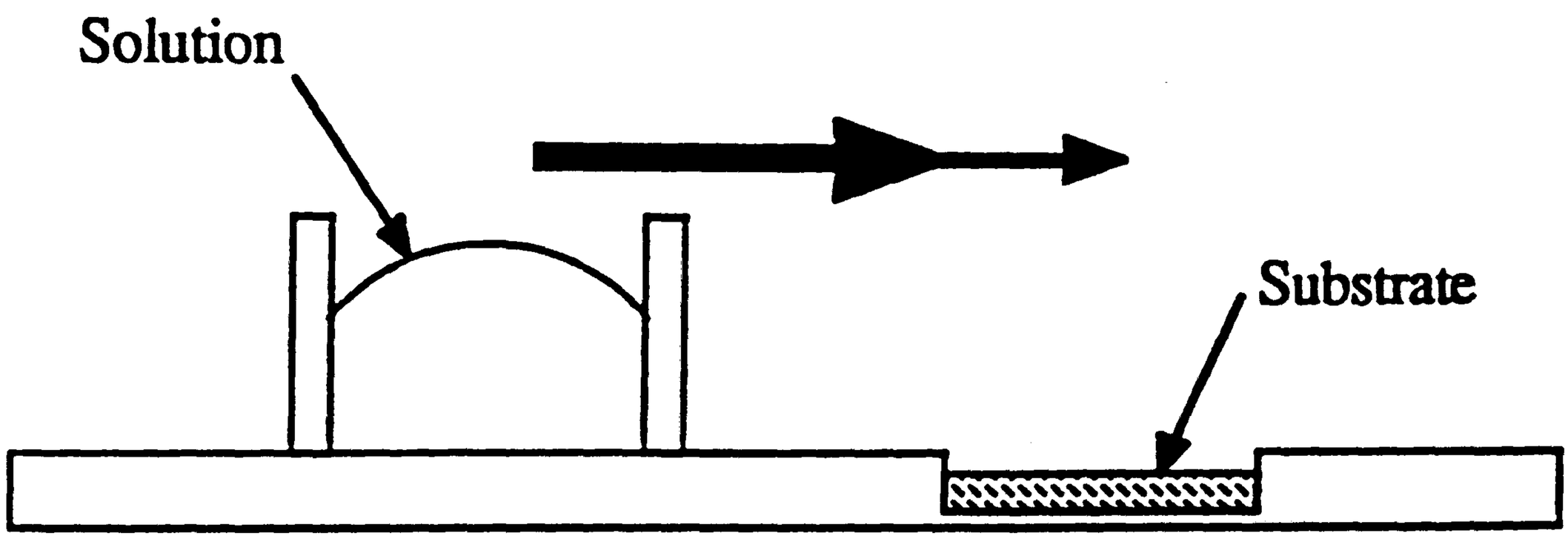

Figure 1.9 The LPE boat

During operation while the system is being heated to the required temperature, the substrate is covered by part of the graphite block. When the desired temperature is reached, the substrate is then moved under the well. To terminate the growth process, the substrate is moved out from the solution.

The growth of thin films can be controlled precisely, because the growth rate is slow. Additional layers of other semiconductors can also be grown by moving the substrate under other wells.

Various aspects of liquid phase epitaxy have been reviewed by Greene [91], and other workers [92,93]. Most recently, liquid phase epitaxial growth of CdHgTe [94,95] has been studied using powdered HgTe as a source of mercury in a graphite sliding boat from a tellurium rich solution at 460 °C.

1.3.9 Metalorganic Chemical Vapour Deposition (MOCVD)

Metalorganic chemical vapour deposition has been used to fabricate II-VI semiconductors. The low growth temperature (<500 °C) and improved control of gas phase ratios have resulted in materials with lower impurity incorporation as compared to other deposition techniques. In MOCVD metal-organic compounds are passed over a heated substrate where they pyrolyse. The pyrolysis products become adsorbed onto the heated substrate, migrate across to their appropriate lattice sites and after loss of their hydrocarbon fragments becomes part of the growing crystal. If the deposition is epitaxial then the technique can be called Metalorganic Vapour Phase Epitaxy (MOVPE).

In contrast to III-V materials MOCVD technology has some difficulities with II-VI materials. The main problem for II-VI materials is the difficulity to grow high quality single crystals to use as substrates. The majority of II-VI materials exist in both cubic and hexagonal phases, the facts derived polytypism can form during the growth of thin films [96]. A third problem concerns the reproduceable control of the conductivity type and conductivity. Other problems include the nature of the reactions in the MOCVD reactor which usually occur when using conventional precursors such as metal alkyls and chalcogen hydrides.

The basic MOCVD process is often modified to facilitate the deposition of II-VI materials. LP-MOCVD [97,98] and photoassisted MOCVD [99] processes are simple

examples which may lead to the growth of II-VI superlattice for the preparation of blue/blue-green emitting laser diodes.

The mechanism involved in the growth of films by MOCVD has been described by Faktor [100] and involves the interaction of a stagnant gas boundary layer with the hot substrate surface such that the alkyl molecules undergo dissociation. The substrate temperature may impart sufficient mobility at the growth interface such that the crystal to grow epitaxially, i.e. MOVPE.

Thin films of ZnS on GaAs have been grown from dimethylzinc or diethylzinc in the presence of hydrogen sulfide [101]. The gaseous reaction in the vapour phase between the precursor materials can seriously limit film uniformity. The reaction arises from the co-ordination of the electron donating Lewis base H_2S with the electron accepting Lewis acid dimethylzinc or diethylzinc, elimination of an alkyl group from group VI precursors which do not contain active hydrogen atoms, such as Me_2S and Et_2S, has been used to grow thin films of ZnS.

The use of such precursors promote the uniformity but invoke the use of the higher temperatures due to the higher thermal stability of these alkyls and heterocyclic group VI derivatives. Hence alternative group II precursors such as adducts of dimethyl-zinc with 1,4-thioxan have enabled the reduction of the temperature necessary for growth [101]. There are two basic types of reaction chambers used in MOCVD, the original vertical design as used by Manasevit [102], and a horizontal version originally developed by Bass and Oliver [103].

Iodine-doped ZnS films have been grown [104] using ethyliodide as a source. It has also been shown that the electron density of the film can be controlled from 5×10^6

to 2 x 10^{19} cm^{-3} by changing the doping conditions. Thus ethyliodide can be used as a useful donor dopant source for the growth of ZnS films.

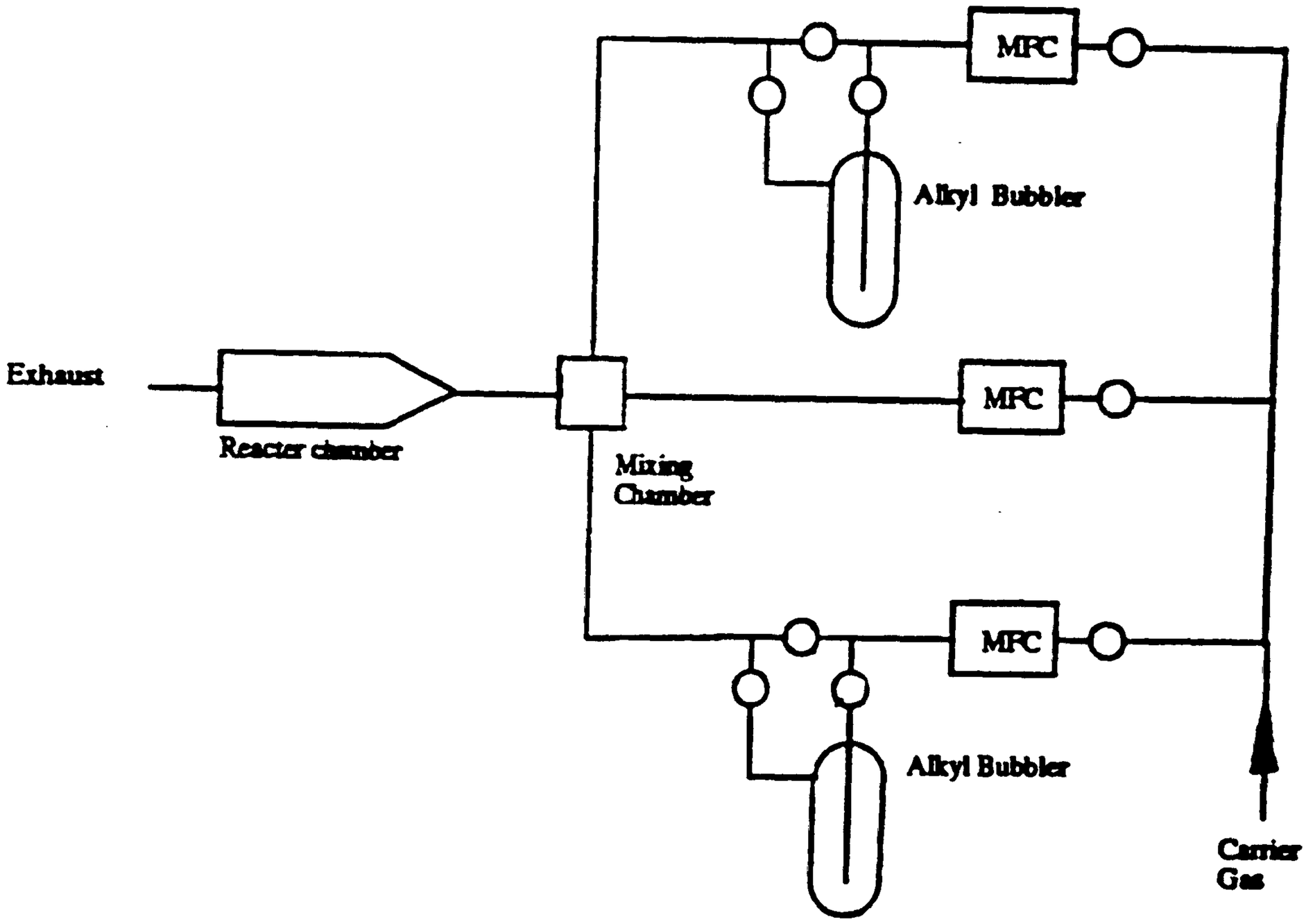

MFC = Mass Flow Controller

Figure 1.10 Schematic diagram of MOCVD apparatus

ZnSe epilayers have been grown on GaAs using laser enhanced MOCVD [105] and the growth rate and the crystallinity of the films were shown to be improved. The growth of the superlattice systems ZnSe-CdSe and ZnS-CdS has been reported [106]. These superlattices have good structural and optical properties at lower temperature (300 °C), but at higher temperature (500 °C) these properties deteriorate due to diffusion between adjacent layers.

MOCVD has been employed to deposit ZnO [107] using dimethylzinc, tetrahydrofurane and water. It was found that water acts as an oxygen source in the

formation of ZnO. A film of stoichiometric CdS [108] on quartz substrates has been deposited from single molecular precursor (bis-morpholinodithioato-S,S)cadmium) by MOCVD. The band gap of 2.4 eV of the deposited CdS was confirmed by optical absorption measurements. ZnS has been grown using dimethylzinc and hydrogen sulfide on to indium tin oxide substrates and the crystalline quality of ZnS has been studied [109]. High quality ZnS film, with strongly preferred orientation was grown under optimised conditions of substrate temperature. In another related work [110] Al-doped n-type ZnSe thin films were prepared under Zn-rich growth conditions by LP-MOCVD. High conductivity of n-type ZnSe with $\rho = 0.01$ cm and $n = 2.4 \times 10^{18}$ was reported on GaAs (100) substrates.

Nomura et al [111] have prepared low conductive ZnS epitaxial layers on Si(111) by low-pressure MOCVD using N_2 carrier gas system, $Zn(S_2CNEt_2)_2$ was employed as a source and the net carrier concentration of the ZnS (1 micron thick deposited at 400 °C) was as low as 10^{15} cm^{-3}. Zinc sulfide has been deposited by a dip-dry method [112] from a solution, in chloroform, containing an equimolar mixture of $EtZnPr^i$ and $Zn(S_2CNBu_2)_2$, pyrolysis was carried out at 300 °C under N_2, and the resultant films were free from oxide contamination, polycrystalline and cubic. Recently mixed alkyl zinc or cadmium complexes [113] of dialkyl thio- or selenocarbamates $(RME_2CNR'_2)_2$ have been successfully used to deposit thin films of zinc and cadmium chalcogenides. Good quality thin films of CdS and ZnS have been deposited by MOCVD using single molecule precursors and discussed in chapter 2 of this thesis.

References

1. J. B. Dance, "Photoelectronic Devices", Iliffe Books Ltd., 1969.

2. S. M. Sze, "Semiconducting Devices-Physics and Technology", John Wiley and Sons, 1985.

3. J. Kimmerle, R. Menner, F. Pfisterer and H. W. Schock, J. Cryst. Growth, 1985, 72, 525.

4. R. Menner, B. Dimmler, R. H. Mauch and H. W. Schock, J. Cryst.Growth, 1988, 86, 906.

5. H. Hartmann, R. Mach and B. Selle, in "Current Topics in Material Science", [Ed. E. Kaldis], North Holland, Amsterdam,1982, 1.

6. B. Ray, "II-VI Compounds", Pergamon Press, 1969.

7. H. Kukimoto, Semicond. Sci. Technol., 1991, 6, A14.

8. W. Stutius, J. Cryst. Growth, 1982, 59, 1.

9. H. Katayama, S. Oda and H. Kukimoto, Appl. Phys. Lett., 1975, 27, 697.

10. S. Iida, T. Sugimoto, S. Suzuki, S. Kishimoto and Y. Yagi, J. Cryst. Growth, 1985, 72, 51.

11. S. Colak, B. J. Fitzpatrick and R. N. Bargava, J. Cryst. Growth, 1985, 72, 504.

12. S. H. Pawar, C. H. Bhosale, and P. Deshmukh, Bull. Material Sci., 1986, 8, 419.

13. A. S. Baranski, and W. R. Fawcett, J. Electroanal. Chem., Interfacial Electrochem., 1984, 160, 271.

14. A. S. Baranski, and W. R. Fawcett, J. Electrochem. Soc., 1984, 131, 2509.

15. C. D. Lokhande, M. S. Jadhav, and S. H. Pawar, J. Electrochem. Soc., 1989, 136, 2756.

16. P. K. Pandey, S. R. Kumar, A. J. N. Rooz, and S. Chandra, Thin Solid Films, 1991, 200, 1.

17. S. Licht, and J. Manassen, J. Electrochem. Soc., 1987, 134, 1064.

18. S. Moorthy Babu, R. Dhanasekaran, and P. Ramasamy, Thin Solid Films, 1991, 198, 269.

19. C. Guillen, E. Galiano, and J. Herrero, Thin Solid Films, 1991, 195, 137.

20. A. N. Molin, A. I. Dikusar, G. A. Kiosse, P. A. Petrenko, A. I. Sokolovsky and Yu. G. Saltanovsky, Thin Solid Films, 1994, 237, 66.

21. S. Moorthy Babu, T. Rajalakshmi, R. Dhanasekaran, and P. Ramasamy, J. Cryst. Growth, 1991, 110, 423.

22. S. Moorthy Babu, R. Dhanasekaran, and P. Ramasamy, Thin Solid Films, 1991, 202, 67.

23. S. Bonilla, and E. A. Dalchiele, Thin Solid Films, 1991, 204, 397.

24. L. Gheorghita, M. Cocivera, Art J. Nelson and A. B. Swatrzlander, J. Electro. Chem. Soc., 1994, 141, 529.

25. C. Natarajan, M. Sharon, C. Levy-Clement and M. Neumann-Spallart, Thin Solid Films, 1994, 237, 118.

26. T. Edamura and Jun'ichiro Muto, Thin Solid Films, 1993, 235, 198.

27. R. O. Bells, M. Hammatt, and F. Wald, Phys. Stat. Sol., 1970, 1, 375.

28. S. Biswas, P. Pramanik, and P. K. Basu, Mat. Lett. 1986, 4, 81.

29. N. C. Sharma, R. C. Kainthla, D. K. Pandya, and K. L. Chopra, Thin Solid Films, 1979, 60, 55.

30. I. Kaur, D. K. Pandya, and K. L. Chopra, J. Electrochem. Soc., 1980, 127, 943.

31. G. A. Kitaev, A. A. Uritskaya, and S. G. Mokrushin, Russian J. Physical Chem., 1965, 39, 1101.

32. R. C. Kainthla, D. K. Pandya, and K. L. Chopra, J. Electrochem. Soc., 1980, 127, 277.

33. G. K. Padam, G. L. Malhotra, and S. U. M. Rao, J. Appl. Phys., 1988, 63, 770.

34. P. Pramanik, and S. Biswas, J. Electrochem. Soc., 1986, 133 ,350.

35. P. Pramanik, S. Bhattacharya, and P. K. Basu, Thin Solid Films, 1987, 149, L81.

36. P. Pramanik, M. A. Akhter, and P. K. Basu, Thin Solid Films, 1988, 158, 271.

37. M. Skyllas-Kazacos, J. F. McCann, and R. Arruzza, Appl. Sur. Sci. 1985, 22, 1091.

38. R. N. Bhattacharya, and P. Pramanik, J. Electrochem. Soc., 1982, 129, 332.

39. D. Lincot, and J. Vedel, 10th European Photovoltaic Conference Lisbon, 8-12 April 1991.

40. T. L. Chu, S. S. Chu, and C. Wang, J. Appl. Phys, 1991, 70, 7608.

41. G. N. Chaudhari, S. Manorama, and V. J. Rao, Thin Solid Films, 1992, 208, 243.

42. P. C. Rieke and S. B. Bentjen, Chem, Mater., 1993,5, 43.

43. S. C. Sahu and S. N. Sahu, Thin Solid Films, 1993, 235, 17.

44. P. J. Sebastian, J. Campos and P. K. Nair, Thin Solid Films, 1993, 227,190.

45. J. M. Dono and J. Herrero, J. Electrochem. Soc. 1994, 141, 205.

46. M. Foex, Bull. Soc. Chim. France, 1944, 11, 6.

47. J. B. Mooney, and J. S. Skarman, Ann. Rev. Mater. Sci., 1982, 12, 81 and references therin.

48. R. R. Chamberlin, and J. S. Skarman, J. Electrochem. Soc., 1966, 113, 86.

49. C. Wu, R. S. Feigelson, and R. H. Bube, J. Appl. Phys., 1972, 43, 156.

50. D. Pike, H. Cui, R. Kershaw, K. Dwight, A. Wold, N. Blanton, A. Wernberg and H. J. Gysling, Thin Solid Films, 1993, 224, 221.

51. Y. M. Gao, P. Wu, J. Baglio, K. Dwight and A. Wold, Matr. Res. Bull.,1989, 24, 1215.

52. R. B. Schoolbar, and J. N. Zemel, J. Appl. Phys., 1964, 35, 1848.

53. P. Hudock, Trans. Metall. Soc. AIME, 1967, 239, 338.

54. K. K. Muravyeva, I. P. Kalinkin, L. A. Sergeeva, V. B. Aleskovsky, and N. B. Bagomlov, Inorg. Mater., 1970, 6, 330.

55. H. Tatsuoka, H. Kuwabara, Y. Nakanishi, and H. Fujiyasu, Thin Solid Films, 1992, 213, 1.

56. H. Fujiyasu, Y. Takeuchi, K. Hikida, K. Ishino, and A. Ishida, J. Cryst. Growth, 1992, 117, 1026.

57. Q. Meng, B. Chen, G. Hou, L. Wu, and G. Dong, J. Cryst. Growth, 1992,121, 191.

58. M. Grun, U. Becker, M. Scheib, H. Giessen and G. Klingshirn, J. Cryst. Growth, 1993, 126, 505.

59. J. S. Hwang, B. J. Koo, I. H. Chung, H. L. Park and C. H. Chung, J. Cryst. Growth, 1993, 130, 617.

60. K. Ploog, Ann. Rev. Mater. Sci., 1982, 12, 123.

61. A. Y. Cho, and K. Y. Cheng, Appl. Phys. Lett., 1981, 38, 360.

62. R. J. Miller, and C. H. Backman, J. Appl. Phys., 1958, 29, 1277.

63. D. L. Smith, and V. Y. Pickhardt, J. Appl. Phys., 1975, 46, 2366.

64. D. C. Cameron, W. Duncan, and W. M. Stung, Thin Solid Films, 1979, 58, 61.

65. J. Li, L. He, N. Zhu, P. Lao, and S. Yuan, J. Cryst. Growth, 1992, 119, 322.

66. M. Ohishi, H. Satio, M. Yoneta, and Y. Fujisaki, J. Cryst. Growth, 1992,117, 125.

67. J. Qiu, H. Cheng, J. M. DePuydt and M. A. Haase, J. Cryst. Growth, 1993, 127,279.

68. P. Ruppert, D. Hommel, T. Behr, H. Heinke, A. Waag and G. Landwehr, J. Cryst. Growth, 1994, 138,48.

69. A. Waag, T. A. Kuhn, S. Schmeusser, B. Schmied, M. M. Kraus, N. Kallis, W. Ossau, R. N. Bicknell-Tassius, and G. Candwehr, J. Cryst. Growth, 1992, 117, 820.

70. R. D. Feldman, R. F. Austin, and A. Sher, J. Cryst. Growth, 1992, 118, 295.

71. H. Okuyama, K. Nakano, T, Miyajima, and K. Akimoto, J. Cryst. Growth, 1992, 117, 139.

72. A. Waag, F. Fischer, Th. Litz, B. Kuhn-Heinrich, U. Zehnder, W. Ossau, W. Spahn, H Heinke and G. Landwehr, J. Cryst. Growth, 1994, 138, 155.

73. F. Fischer, A. Wagg, G. Bilger, Th. Litz, S. Scholl, M. Schmitt and G. Landwehr, J. Cryst. Growth, 1994, 141, 93.

74. C. R. Becker, L. He, S. Einfeldt, Y. S. Wu, G. Lerondel, H. Heinke, S. Oehling, R. N. Bicknell-Tassius and G. Landwehr, J. Cryst. Growth, 1993, 127, 331.

75. A. R. Cawala, Appl. Phys. Lett., 1981, 38, 701.

76. E. Veuhoff, W. Pletschen, P. Balk, and H. Luth, J. Cryst. Growth, 1981, 55, 30.

77. M. Konagai, J. Cryst. Growth, 1992, 120, 261.

78. D. Rajavel, J. J. Zinch and J. E. Jensen, J. Cryst. Growth, 1994, 138, 19.

79. T. Suntola, and J. Anston, US Patent, 4058430, 1970.

80. S. M. Bedair, M. A. Tischler, T. Katsuyarna, and N. A. El-Masry, Appl. Phys. Lett., 1985, 47, 51.

81. M. Tammenmaa, T. Koskinen, and M. Leskela, Thin Solid Films, 1985, 124, 125.

82. S. Ohta, S. Kobayashi, and F. Kaneko, J. Cryst. Growth, 1990, 106, 166.

83. T. Tadokoro, S. Ohta, T. Ishiguro, Y. Ichinose, S. Kobayashi and N. Yamamoto, J. Cryst. Growth, 1993, 130, 29.

84. Y. Takemura, M. Konagai, H. Nakanishi, and K. Takahashi, J. Cryst. Growth, 1992, 117, 144.

85. S. Yamaga, and A. Yoshikawa, J. Cryst. Growth, 1992, 117, 152.

86. C. D. Lee, B. H. Lim, C. Lim, H. L. Park, C. H. Chung and S. K. Chang, J. Cryst. Growth, 1992, 117, 148.

87. N. H. Karam, R. G. Wolfson, I. B .Bhat, H. Ehsani and S. K. Ghandhi, Thin Solid Films, 1993, 225, 261.

88. T. Matsumoto, T. Iwashita, K. Sasamoto and T. Kato, J. Cryst. Growth, 1994, 138,63.

89. E. Abramof, W. Faschinger, H. Sitter and A. Pesek, J. Cryst. Growth, 1994, 135, 447.

90. M. G. Astles, G. Blackmore, N. Gordon, and D. R. White, J. Cryst. Growth, 1985, 72, 61.

91. P. D. Greene, Chemistry of Semiconductor Industry, Ed. Ledwith, and S. J. Moss, Blackie, 1987.

92. M. H. Kelisher, J. Cryst. Growth, 1984, 70, 365.

93. L. R. Dawson, Prog. in Solid State Chem., 1972, 7, 117.

94. M. G. Astles, N. Shaw, G. Blackmore, and R. S. Hall, J. Cryst. Growth, 1992, 117, 213.

95. A. Takami, Z. Kawazu, T. Takiguchi, K. Mitsui, K. Mizuguchi, and T. Murotani, J. Cryst. Growth, 1992, 117, 16.

96. R. Dahmani, L. Salamanca-Riba, N. Y. Ngugen, D. Chandler-Horowitz and B. T. Jonker, J. Appl. Phys., 1989, 76, 514.

97. S. Fujita, T. Yodo and A. Sasaki, J. Cryst. Growth, 1985, 72, 27.

98. A. Yosikawa, S. Yamaga, K. Tanaka and H. Kasai, J. Cryst. Growth, 1985, 72, 13.

99. Sg. Fujita, A. Tanabe, T. Sakamoto, M. Isemura and Sz. Fujita, Jpn. J. Appl. Phys., 1987, 26, L2000.

100. M. Faktor, Chemtronics, 1988, 3, 3.

101. A. C. Jones, P. J. Wrigth, and B. Cockayne, Chemtronics, 1988, 3, 35.

102. H. M. Manasevit, and W. I. Simpson, J. Electrochem. Soc., 1971, 118, 644.

103. S. J. Bass, and P. E. Oliver, Inst. Phys. Conf. Ser., 1977, 33b, 1.

104. S. Yamaga, A. Yoshikawa, and H. Kasai, J. Cryst. Growth, 1990, 106, 683.

105. M. Y. Yeh, C. C. Hu, G. L. Lin, and M. K. Lee, Thin Solid Films, 1992, 215, 142.

106. P. J. Parbrook, P. J. Wright, B. Cockayne, A. G. Cullis, Henderson, and K. P. O'Donnell, J. Cryst. Growth, 1990, 106, 503.

107. W. Wieldraaijer, J. Van Balen Blanken and E. W. Kuipers, J. Cryst. Growth, 1993, 126,305.

108. O. B. Ajayi, O. K. Osuntola, I. A. Ojo and C. Jeynes, Thin Solid Films, 1994, 248, 57.

109. J. W. Li, J. D. Chiang, Y. K. Su and M. Yokoyama, J. Cryst. Growth, 1994, 137, 421.

110. M. Y. Yeh, S. J. Guo, H. D. Huang and M. K. Lee, Thin Solid Films, 1994, 240, 116.

111. R. Nomura, T. Murai, T. Toyosaki, H. Matsuda, A. Baba, to be published elsewhere.

112. R. Nomura, K. Konishi, S. Futenma and H. Matsuda, Appl. Organomet. Chem., 1990, 4, 607.

113. M. A. Malik and P. O'Brien, Adv. Mater. Optics and Electronics, 1994, 3, 171.

Chapter 2

Novel precursors for the deposition of zinc or cadmium chalcogenides by MOCVD

2.1 Introduction

Zinc and cadmium have the electronic configurations [K] $3d^{10}4s^2$ and [K] $4d^{10}5s^2$ and lie at the end of the first or second row of transition elements respectively. The oxidation state of these elements is almost invariably two. In all of their compounds zinc and cadmium have a complete 3d and 4d shell respectively and consequently no crystal field stabilization effects present. The stereochemistry of zinc and cadmium is determined by considering the size, covalent bonding and the ligand geometry.

The coordination numbers for both zinc and cadmium range from low values such as 2 in Me_2Zn and Me_2Cd to higher coordination numbers such as 6 in $(N_2H_5)_2Zn(SO_4)_2$ [1] and 8 in cadmium $CaCd(OAc)_4.6H_2O$ [2]. However, for both zinc and cadmium tetrahedral coordination is common and such complexes are formed with a variety of ligands such as ammonia and amines. The coordination chemistry of cadmium has been reviewed by Constable [3], Aylett [4,5] and Prince [6].

The problems associated with the use of the group II metal alkyls as precursors for MOCVD were discussed in chapter 1. Complexes containing a chelate ring show an enhanced stability, and use of such compounds as precursors for MOCVD appears to be attractive because the precursors are likely to be non-pyrophoric and their use may inhibit homogenous reaction. If the ligand chelates through an atom such as sulfur or selenium, then a separate group VI source may no longer be necessary because both group II and group VI can be transported in the same molecule.

A number of research workers have reported the deposition of II-VI semiconductors from single source precursors by MOCVD. Chalcogenides have been deposited using: thiophosphinates [7,8], thiocarbamates [9,10], selenocarbamates [11], thiolates [12-15] and alkylmetaldithio- or diselenocarbamates [16-19]. ZnS, ZnSe, CdS, CdSe and related ternary materials have been grown from such precursors [20,21].

In present work dithiocarbamates of zinc or cadmium were prepared by the reaction of trimethylethylenediamine (TMEDA) or trimethylpropylenediamine (TMPDA) with CS_2. The resulting thiocarbamic acids gave the corresponding complex on reaction with Zn or Cd salt. The bisdithiocarbamato derivatives of TMEDA with Zn and Cd are intractable white solids, insoluble in common organic solvents and presumably polymeric materials, whereas bisdithiocarbamato derivatives of TMPDA with Zn and Cd are microcrystalline solids. The bis(trimethylpropylenediaminedithiocarbamato)zinc complex was characterized by X-ray crystallography. Both zinc and cadmium compounds were used to deposit good quality thin films of the chalcogenide.

In order to increase the volatility and reactivity of these complexes, mixed alkyl-Zn/Cd dithiocarbamates were prepared and characterized. Preliminary growth results showed that these complexes are better precursors than the parent bis compounds.

2.2 Results and Discussion

2.2.1 Bis(trimethylethylenediaminedithiocarbamato) zinc\cadmium

The zinc and cadmium carbamato complexes were prepared with N,N,N-trimethylethylenediamine. Bis(trimethylethylenediaminedithiocarbamato)zinc(II) **(1)** and bis(trimethylethylenediaminedithiocarbamato)cadmium(II) **(2)** compounds are intractable white solids, stable at room temperature for unlimited period and insoluble in organic solvents and hence are presumably polymeric materials. These compounds have been characterized by element analysis, infra red, solid state ^{13}C nmr, and solid state ^{113}Cd nmr spectroscopies. The solution state nmr studies could not be carried out because of the insolubility of these complexes.

Spectroscopic studies

IR spectra of both **(1)** and **(2)** show typical thiocarbamate stretching bands at 993 and 1008 cm^{-1} respectively.

Both the zinc and cadmium compounds are insoluble in common organic solvent, and ^{13}C nmr (solid state) spectroscopy was used to study these compounds. ^{13}C nmr (solid state) give clear six line spectra for both **(1)** and **(2)** which were very similar to ^{13}C nmr (solution state) spectra of **(3)** and **(4)** discussed later. For **(1)** and **(2)** the carbon associated with thiocarbamate sulfurs (CS_2) appear at 205.97 and 205.82 ppm respectively. The $N(CH_3)_2$ group gave two signals showing that the methyls are not equivalent. The signal for M-$N(CH_3)_2$ appeared at 49.19 and 49.35 ppm for **(1)** and **(2)** respectively. Methylene carbon signals were observed at lower field. The ^{13}C nmr (solid state) spectrum of compound **(2)** is shown in figure 2.1.

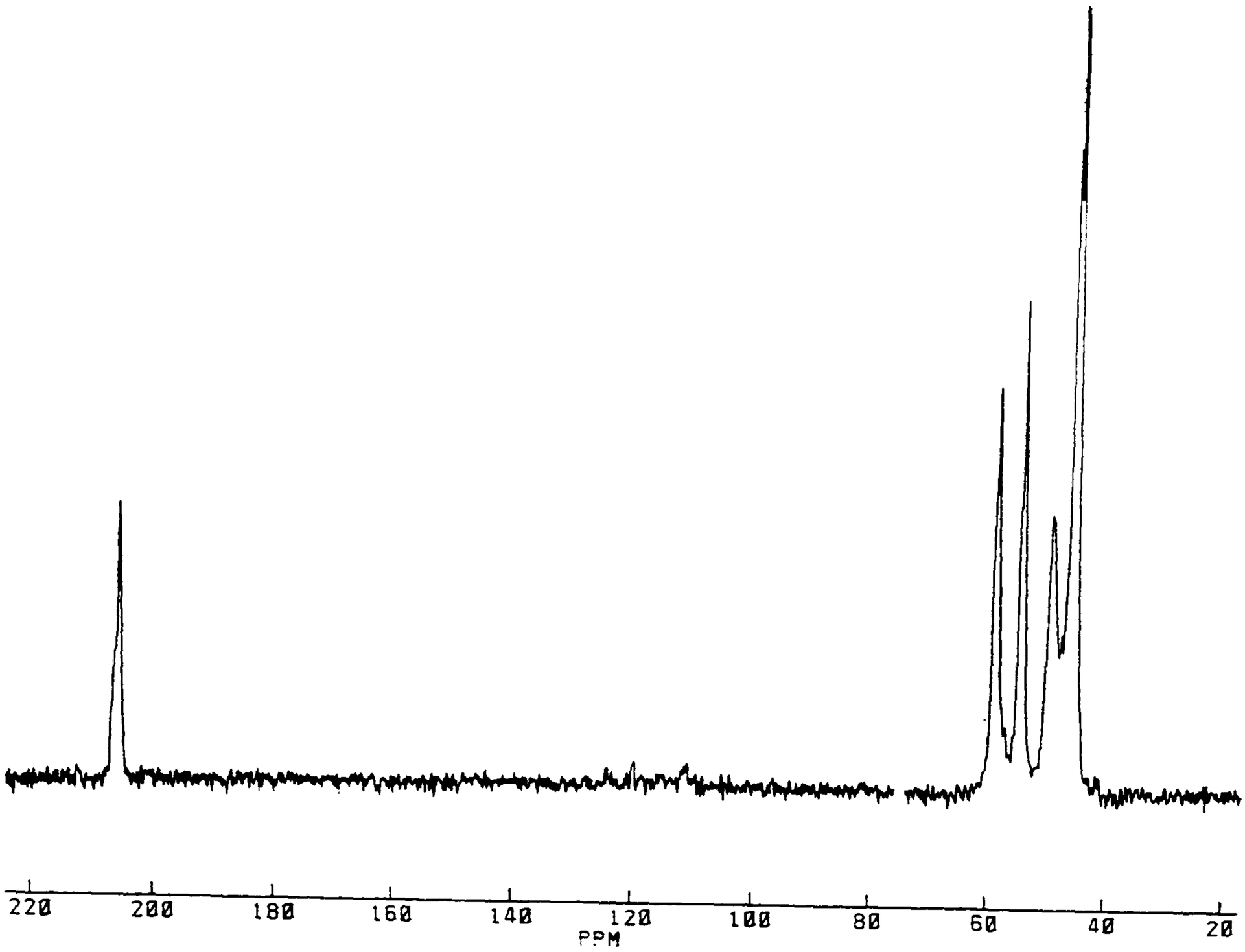

Figure 2.1 ^{13}C nmr (solid state) spectrum for bis(trimethylethylenediaminedithio-carbamato)cadmium

The ^{113}Cd (solid state) nmr spectra of (**2**) and bistrimethylpropylenediaminedithiocarbamatocadmium (**4**) were recorded. The spectrum of (**2**) shows a single line at δ 289 ppm with no evidence for quadrupolar coupling to nitrogen. The chemical shift of (**4**) δ 291 ppm is similar to that for (**2**) and indicates a similar environment. An analysis of the spinning side bands leads to anisotropy parameters similar to (**2**) suggesting similar coordination. The ^{113}Cd solution state nmr spectrum of (**4**) gives a singlet at δ 298 ppm which shows that Cd has similar coordination environment both in solution and solid state. The greater purity of (**4**) is not surprising as it was relatively easy to recrystallize the compound and has been studied in detail in this laboratory.

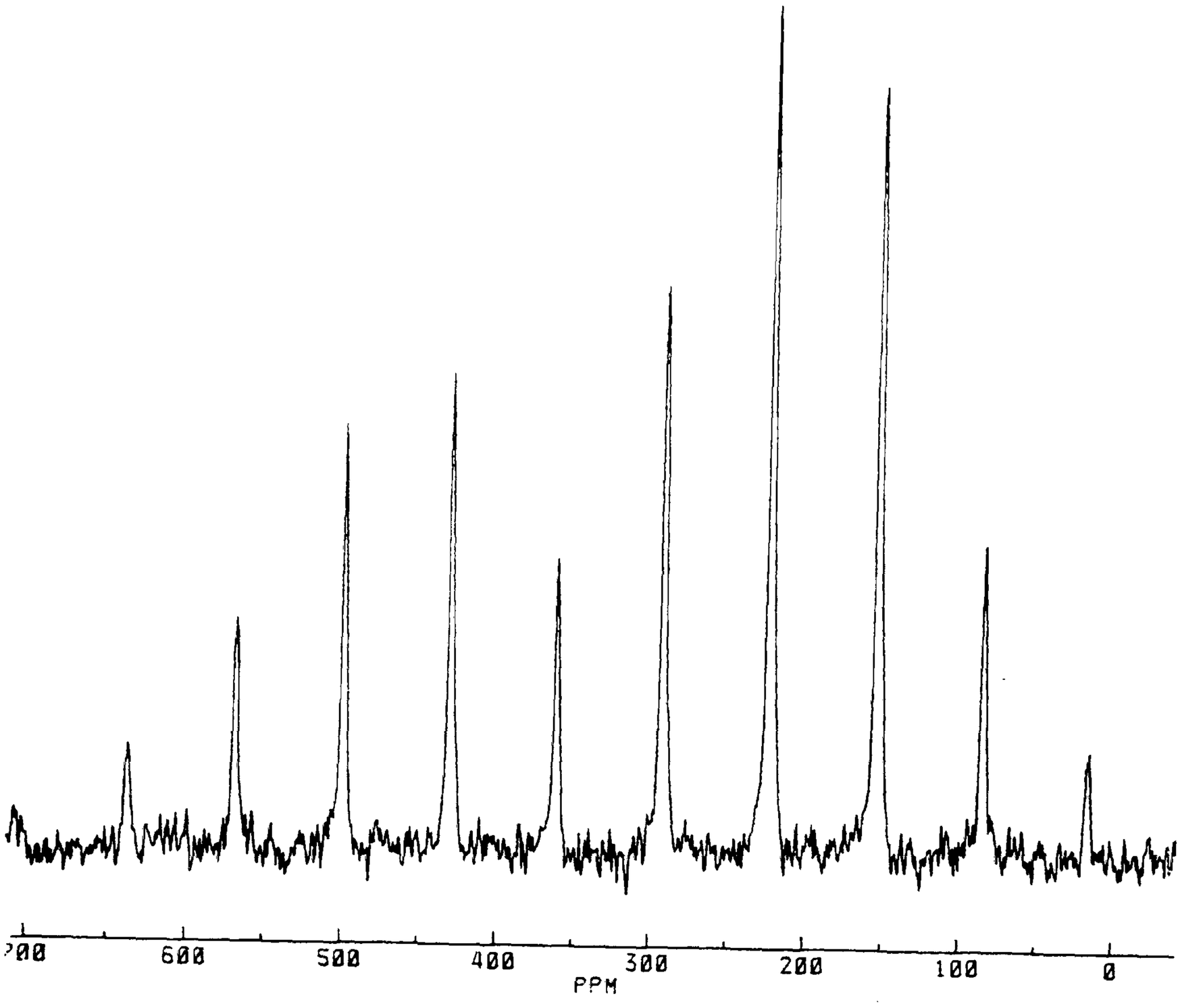

Figure 2.2 ^{113}Cd nmr (solid state) for bis(trimethylethylenediaminedithiocarbamato)-cadmium

2.2.2 Bis(trimethylpropylenediaminedithiocarbamato)zinc\cadmium

Bis(trimethylpropylenediaminedithiocarbamato)zinc(II) **(3)** and bis(trimethyl-propylenediaminedithiocarbamato)cadmium(II) **(4)** are microcrystalline solids, soluble in common organic solvents. These compounds may be useful precursors for deposition of II-VI materials. Both compounds have been characterized by element analysis, infra-red, ^{1}H nmr, ^{13}C nmr and mass spectroscopy and by an X-ray single crystal structure determination.

Spectroscopic studies

The infra-red spectra of compounds (**3**) and (**4**) contain bands at 424, 989, 1461 cm^{-1} typical of coordinated thiocarbamate functions [23].

Both compounds (**3**) and (**4**) gave similar ^{1}H nmr spectra. The α and γ-methylene protons give triplets due to coupling with ß-methylene protons with similar coupling constants. The ß-methylene protons appear as a quintet at higher field through coupling with four equivalent neighboring methylene protons. The $N(CH_3)_2$ and $N(CH_3)$ protons give singlets for both (**3**) and (**4**) with the expected 2:1 intensity ratio. The chemical shifts for the cadmium compound are at lower field for all protons compared to the corresponding zinc compound. ^{1}H nmr spectrum for (**4**) is shown in figure 2.3.

The ^{13}C nmr of both compounds (**3**) and (**4**) show the expected six line spectra. The ß-methylene carbon gives a signal at relatively higher field than those observed for α- and γ-methylene carbons. CS_2 carbons for (**3**) and (**4**) give clear signals at 204.3 and 205.71 ppm respectively. The $N(CH_3)_2$ carbons give one signal only in contrast to compounds (**1**) and (**2**) where two overlapping signals were observed which shows that these carbons are equivalent in solution. ^{13}C nmr spectrum of compound (**4**) is shown in figure 2.4.

Mass spectra of both compounds (**3**) and (**4**) showed similar major fragments. In both compounds the base peak was observed at m/e 58 which corresponds to $CH_2N(CH_3)_2$. Other fragments are listed in experimental section.

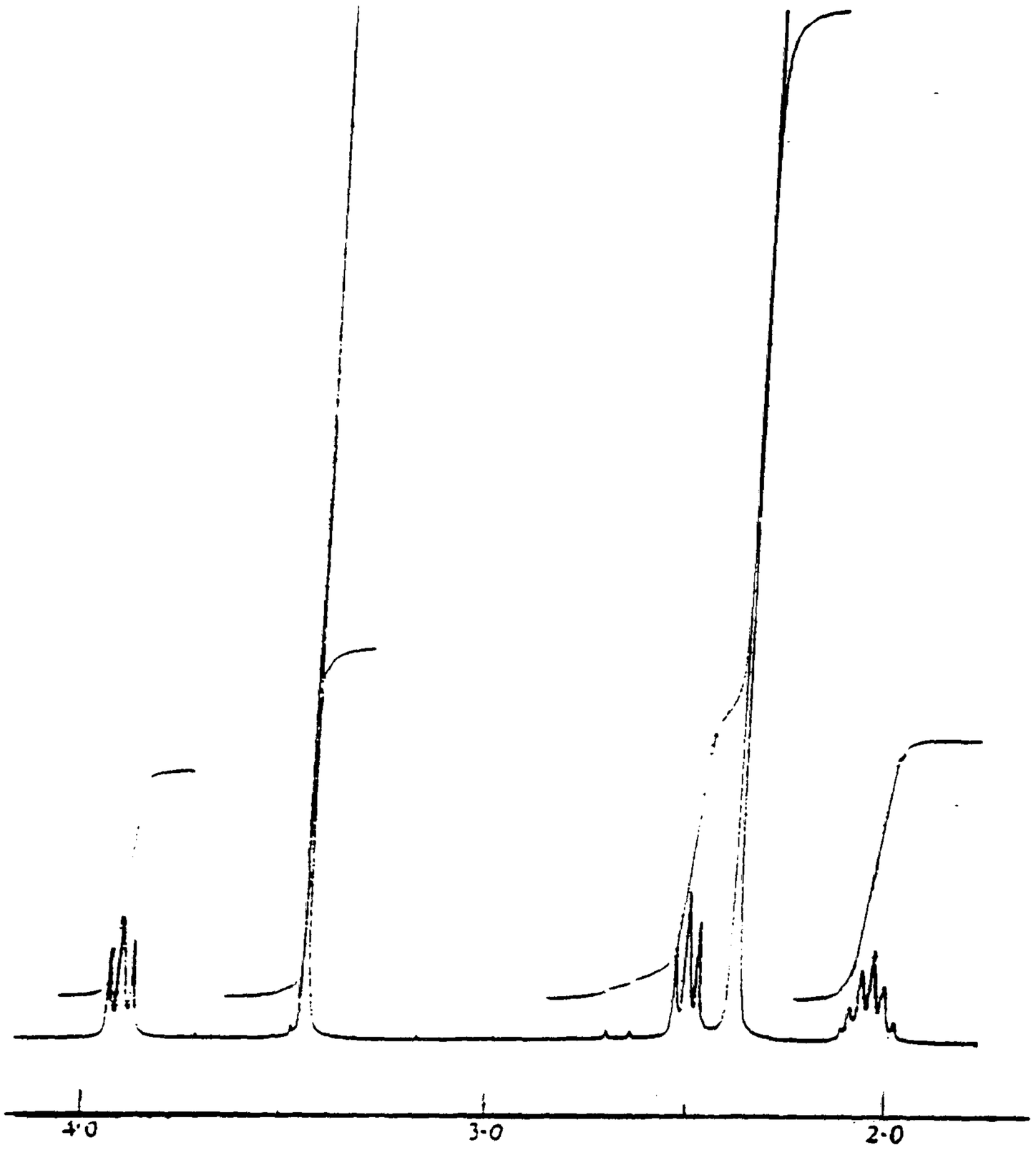

Figure 2.3 ^{1}H nmr spectrum for bis(trimethylpropylenediaminedithiocarbamato)-cadmium

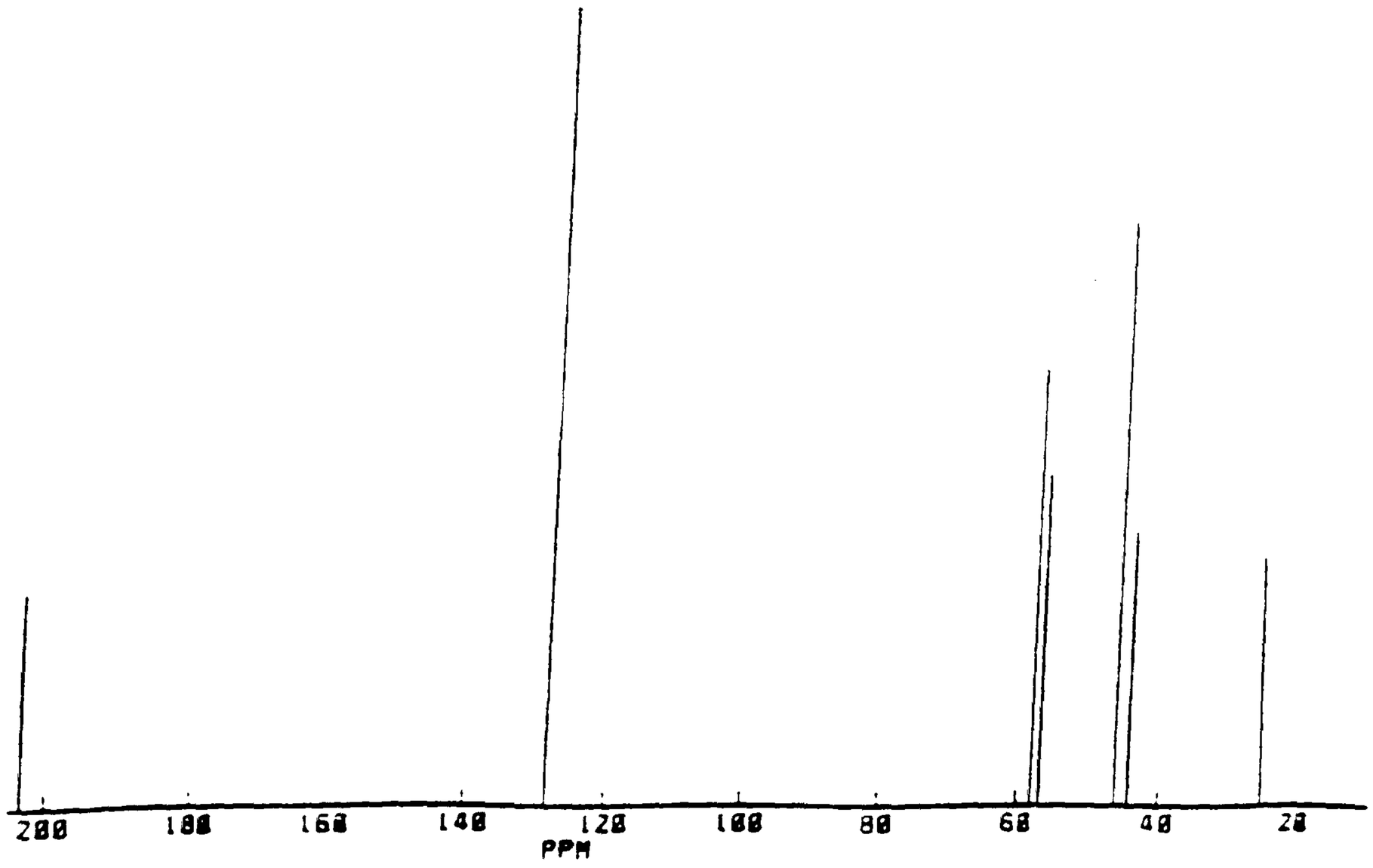

Figure 2.4 ^{13}C nmr spectrum for bis(trimethylpropylenediaminedithiocarbamato)-cadmium

Crystal structure of bis(trimethylpropylenediaminedithiocarbamato)zinc(II) (3)

Crystals of bis(trimethylpropylenediaminedithiocarbamato)zinc(II) were obtained by recrystallizing the product from benzene. Single crystal was mounted at the end of a glass capillary and the data was collected by a CAD4 diffractrometer. Crystal data and structure refinement is given in table 2.1.

The structure of (**3**) is a polymer. The monomeric $Zn(S_2CNMe(CH_2)_3NMe_2)$ units are linked through nitrogen atoms of the ligand. Each zinc is attached to four sulfur atoms and one nitrogen atom making it 5 coordinate. Thiocarbamate group chelates and the trimethylpropylenediamine bridges between the monomeric units through nitrogen to zinc centers. The coordination is intermediate between trigonal bipyramidal and square pyramidal as observed in the related N,N-diethyldithiocarbamatozinc [24], N,N-diethyldithiocarbamatocadmium [25], N,N-diethyldiselenocarbamatozinc [26], and N,N-diethyldiselenocarbamatocadmium [11].

The structure gives rise to two three-membered heterocyclic rings with a comparatively broader bite angle (71°) of chelating ligand as compared to those observed previously [11,24,26]. Zn-S bond distances (2.30 - 2.61) are shorter than those observed previously in dithiocarbamates (2.33 - 2.82) [11,24,27]. Zn-N bond length (2.15) is considerably shorter than those in $Me_2Zn[(CH_2NMe)_3]_2$ [28,29] (2.41), $Me_2N(CH_2)_2NMe_2]_2$ [30] (2.27), $[Me_2N(CH_2)_3]Zn$ [31] (2.31), but longer than $[(CNS)ZnS_2CNMe_2]_2$ [32] (1.95) and $C_5H_5NZn[S_2CNMe_2]_2$ [33] (2.08).

Table 2.1 Crystal data and structure refinement for (**3**)

Identification note	T56
Empirical formula	$C_{14} H_{30} N_4 S_4 Zn$
Formula weight	448.03
Temperature	293(2) K
Wavelength	0.71069 Å
Crystal system	Monoclinic
Space group	P21
Unit cell dimensions	a = 7.54(2) Å α = 90 ° b = 12.66(2) Å β= 108.80(14) ° c = 11.69(2) Å γ= 90 °
Volume	1056(3) $Å^3$
Z	2
Density (calculated)	1.409 g/cm^3
Absorption coefficient	1.561 mm^{-1}
F(000)	472
Theta range for data collection	1.84 to 22.99 deg.
Index ranges	-1<=h<=8, 0<=k<=13, -12<=l<=12
Reflections collected	1727
Independent reflections	1543 [R(int) = 0.0346]
Refinement method	Full-matrix least-squares on F^2
Data / restraints / parameters	1543 / 1 / 115
Goodness-of-fit on F^2	1.183
Final R indices [I>2σ(I)]	R1 = 0.1080, wR2 = 0.2287
R indices (all data)	R1 = 0.2555, wR2 = 0.5535
Absolute structure parameter	0.1(2)
Largest diff. peak and hole	2.176 and -1.692 $e.Å^{-3}$

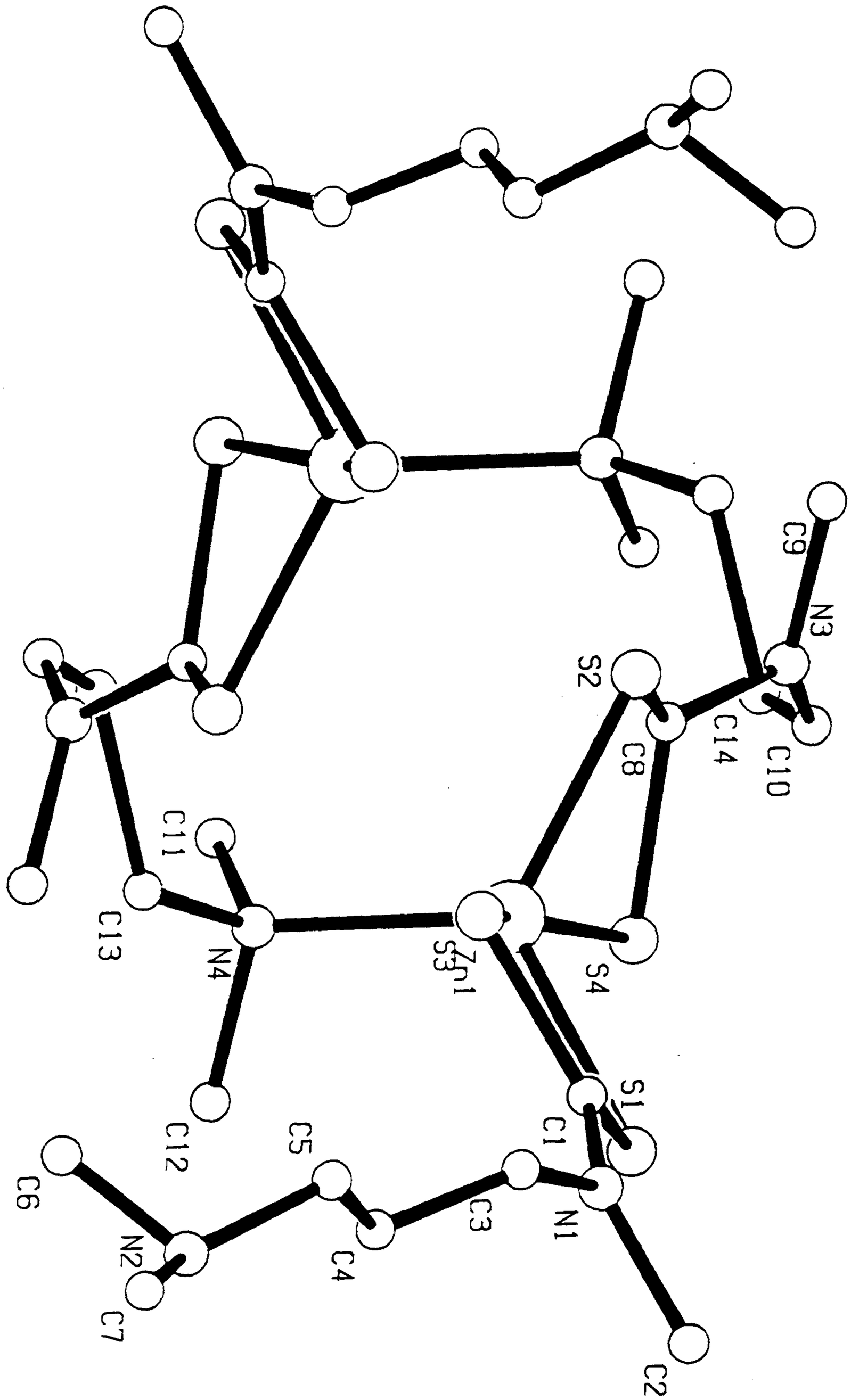

Figure 2.5 Crystal structure of bis(trimethylpropylenediaminedithiocarbamato)zinc

Table 2.2 Selected bond length (Å) and bond angles (°) for bis(trimethyl-propylenediaminedithiocarbamato)zinc

Zn(1)-N(4)	2.56(6)	Zn(1)-S(2)	2.30(2)
Zn(1)-S(1)	2.36(2)	Zn(1)-S(3)	2.58(2)
Zn(1)-S(4)	2.61(2)	S(1)-C(1)	1.68(10)
S(2)-C(8)	1.60(7)	S(3)-C(1)	1.75(10)
S(4)-C(8)	1.83(7)	N(1)-C(1)	1.21(11)
N(1)-C(2)	1.48(9)	N(1)-C(3)	1.71(12)
N(2)-C(6)	1.30(9)	N(2)-C(5)	1.41(8)
N(3)-C(10)	1.44(9)	N(3)-C(8)	1.42(9)
N(3)-C(9)	1.46(7)	N(4)-C(13)	1.32(8)
N(4)-C(12)	1.53(9)	N(4)-C(11)	1.70(7)
C(10)-C(14)	1.20(11)	C(13)-C(14)	1.74(10)
N(4)-Zn(1)-S(2)	114(2)	N(4)-Zn(1)-S(1)	119(2)
S(2)-Zn(1)-S(1)	127.4(6)	N(4)-Zn(1)-S(3)	97(2)
S(2)-Zn(1)-S(3)	106.1(6)	S(1)-Zn(1)-S(3)	71.3(5)
N(4)-Zn(1)-S(4)	101(2)	S(2)-Zn(1)-S(4)	70.7(6)
S(1)-Zn(1)-S(4)	96.1(6)	S(3)-Zn(1)-S(4)	161.8(6)
C(1)-S(1)-Zn(1)	91(3)	C(8)-S(2)-Zn(1)	95(2)
C(1)-S(3)-Zn(1)	83(3)	C(8)-S(4)-Zn(1)	80(2)
C(1)-N(1)-C(2)	129(8)	C(1)-N(1)-C(3)	129(7)
C(2)-N(1)-C(3)	103(6)	C(6)-N(2)-C(5)	113(6)
C(10)-N(3)-C(8)	126(5)	C(10)-N(3)-C(9)	127(5)
C(8)-N(3)-C(9)	103(5)	C(13)-N(4)-C(12)	104(5)
C(13)-N(4)-C(11)	112(4)	C(12)-N(4)-C(11)	97(4)
N(1)-C(1)-S(1)	123(8)	S(1)-C(1)-S(3)	115(6)

2.2.3 Methyl(trimethylpropylenediaminedithiocarbamato) zinc or cadmium

Methyl(trimethylpropylenediaminedithiocarbamato)zinc (**5**) and methyl(trimethyl-propylenediaminedithiocarbamato)cadmium (**6**) derivatives of compounds (**3**) and (**4**) were prepared in order to improve the volatility of the thiocarbamates for the deposition of thin films of ZnS and CdS at relatively lower temperatures.

Spectroscopic studies

Infra red spectra of both (**5**) and (**6**) show the typical thiocarbamate stretching bands at 997 and 1002 cm^{-1} respectively.

^{1}H nmr spectra of (**5**) and (**6**) show six multiplets with $N(CH_3)_2$ equivalent methyl protons. Chemical shifts and the mutiplicity of the signals is listed in experimental section. In general the cadmium complex gives lower field signals especially for $-NCH_3$ (δ 3.24) protons as compared to the corresponding zinc (δ 2.33) complex. CH_3-M protons in both complexes appear at higher field values than those of methylcadmium/zincdiethyldithiocarbamates values [16].

^{13}C nmr shows the same general trends in the chemical shifts as observed in ^{1}H nmr for (**5**) and (**6**) but in contrast to the large difference for $-NCH_3$ protons only a small change is noted for carbon. Chemical shift of -CS carbons of (**5**) and (**6**) is rather close whereas this difference is considerable in other related compounds [16]. ^{13}C nmr spectrum for (**5**) is shown in figure 2.6.

The mass spectra of compounds (**5**) and (**6**) showed similar trends in their patterns of fragmentation. Molecular ion peaks correspond to the molecular mass of corresponding dimers and the base peaks at m/e 58 corresponds to $CH_2N(CH_3)_2$ fragment. Although the X-ray crystal investigation showed the structure to be polymeric

but it appears that the nitrogen to cadmium bond is not strong enough to keep up the polymer but gives a relatively stable dimeric fragment which on further fragmentation gives monomer.

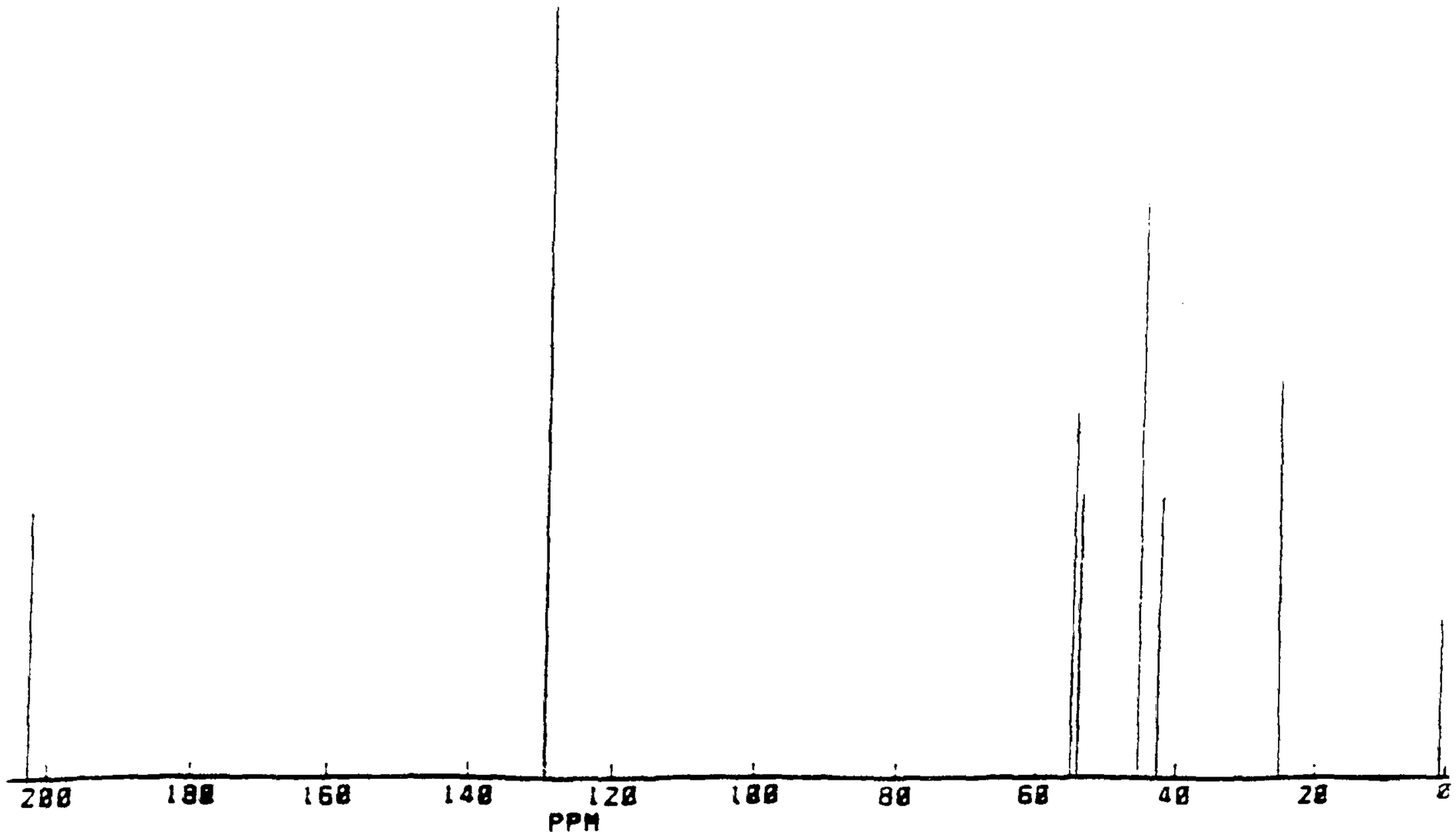

Figure 2.6 ^{13}C nmr spectrum for methyl(trimethylpropylenediaminedithiocarbamato)-zinc

Crystal Structure of Methyl(trimethylpropylenediaminedithiocarbamato)cadmium

The compound was recrystallized from benzene to obtain X-ray quality crystals. A good quality single crystal was mounted at the end of a glass capillary under nitrogen and the data was collected on CAD4 diffractrometer. Crystal data and structure refinement is given in table 2.3. The structure of methyl(trimethylpropylenediaminedithiocarbamato)cadmium is shown in figure 2.7. Selected bond lengths and angles are summarized in table 2.4.

The structure consists of a polymer in which the monomers are connected through terminal nitrogen to cadmium. Each cadmium is four coordinate through bonding to two sulfurs, one carbon, and one nitrogen. S1, S2, and C1 are in the same plane with Cd slightly out of plane (0 Å) and N2 clearly (2.63 Å) occupying an axial position in a distorted tripodal pyramid. The structure has no unusual bond lengths or angles. Cd-S (2.58 Å) and Cd-N (2.44 Å) bond lengths are slightly shorter than the Cd-S (2.62 Å) bond lengths in bisdiethyldithiocarbamatocadmium(II) [10], and Cd-N (2.49 - 2.57 Å) in $Me_2Cd[Me_2N(CH_2)_2NMe_2]$ and $(Me_3CCH_2)_2Cd[Me_2N(CH_2)_2NMe_2]$ [22] and those previously observed [34-37] in ordinary coordination compounds but is longer than that of the proper Cd-N (2.33 Å) bond. Cd-C (2.15 Å) bond lengths are close to those observed previously [34-37].

Table 2.3 Crystal data and structure refinement for (**6**)

Formula	$C_{11}H_{18}N_2S_2Cd$
M	354.820
Crystal system	Monoclinic
Space group	$P_{21/n}$
a (Å)	9.307(1)
b (Å)	8.097(1)
c (Å)	21.535(2)
a (°)	90
b (°)	102.43(1)
g (°)	90
U (Å^3)	1584.81(0.30)
Z	4
D_C (g cm^{-1})	1.487
F(000)	712
radiation	Mo Ka
l/(Å)	0.71069
m (cm^{-1})	16.066
qmin/max	1.5,25°
Total no. of reflections.	3598
No. of unique reflections.	2781
No. of observed reflections. (F_O>3s(F_O))	1008
No. of refined parameters.	194
Weighting scheme parameter g in w=1/[s^2(F)+gF^2]	0.000463
Final *R*	0.0778
Final R_G	0.0637

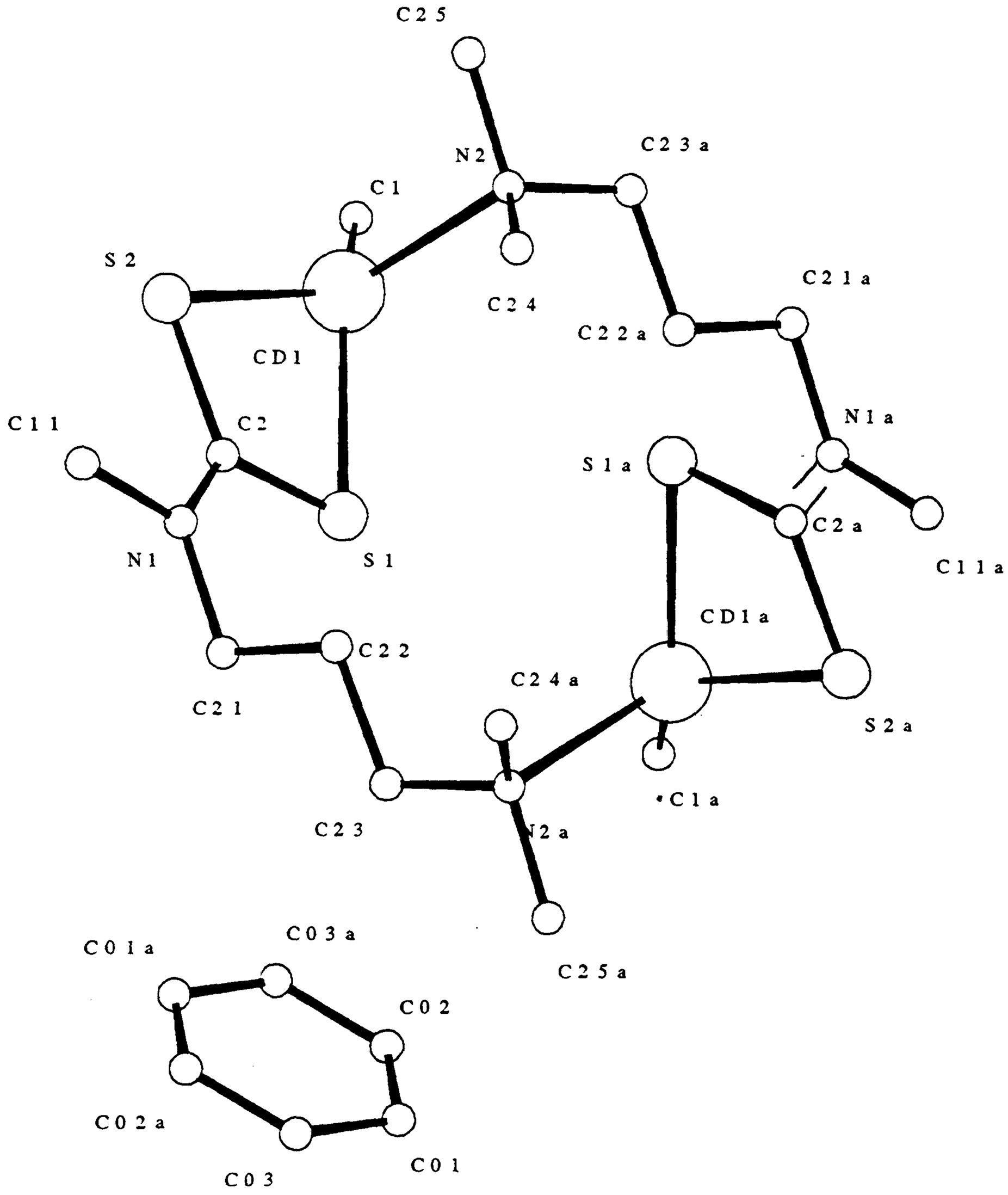

Figure 2.7 Crystal structure of methyl(N,N,N-trimethylpropylenediaminedithio-carbamato)cadmium

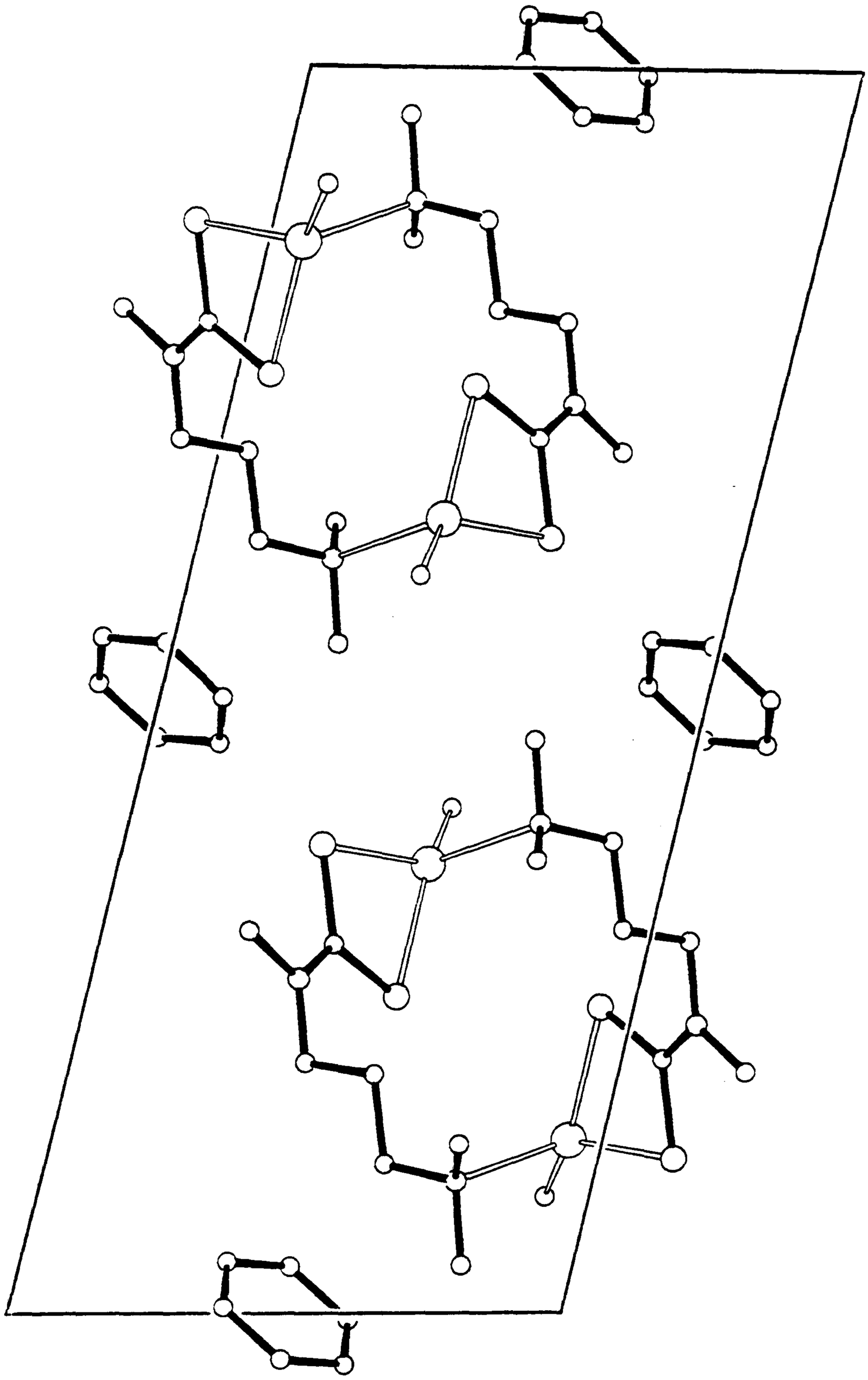

Figure 2.8 Packing diagram for methyl(N,N,N-trimethylpropylenediaminedithio-carbamato)cadmium

Table 2.4 Selected bond lengths (Å) and bond angles (°) for methylcadmium-trimethylpropylenediaminedithiocarbamate

S(1)-Cd(1)	2.577(8)	S(2)-Cd(1)	2.583(8)
C(1)-Cd(1)	2.149(18)	N(2)-Cd(1)	2.436(15)
C(2)-S(1)	1.718(19)	C(2)-S(2)	1.740(19)
C(2)-N(1)	1.307(20)	C(11)-N(1)	1.450(19)
C(21)-N(1)	1.451(20)	C(22)-C(21)	1.517(23)
C(21)-C(22)	1.535(23)	C(24)-N(2)	1.478(18)
C(25)-N(2)	1.437(20)	C(03)-C(01)	1.389(26)
C(03)-C(02)	1.349(26)		
S(2)-Cd(1)-S(1)	69.8(3)	C(1)-Cd(1)-S(1)	137.2(6)
C(1)-Cd(1)-S(2)	135.2(5)	N(2)-Cd(1)-S(1)	98.2(4)
N(2)-Cd(1)-S(2)	96.3(4)	N(2)-Cd(1)-C(1)	109.4(7)
C(2)-S(1)-Cd(1)	86.6(7)	C(2)-S(2)-Cd(1)	86.0(7)
C(11)-N(1)-C(2)	118.7(16)	C(21)-N(1)-C(2)	123.7(16)
C(21)-N(1)-C(11)	117.7(15)	S(2)-C(2)-S(1)	117.3(12)
N(1)-C(2)-S(1)	120.5(15)	N(1)-C(2)-S(2)	122.1(15)
C(22)-C(21)-N(1)	109.4(16)	C(23)-C(22)-C(21)	108.8(15)
C(24)-N(2)-Cd(1)	111.5(11)	C(25)-N(2)-Cd(1)	105.3(12)
C(25)-N(2)-C(24)	110.1(15)	C(02)-C(03)-C(01)	120.3(20)

2.2.4 t-Butyl or neopentyl(dialkylamido)zinc

A series of alkyl(alkylamido)zinc(II) compounds with the general formula of RZnNR'(R = ^{i}Pr, ^{t}Bu; R' = Me, Et, ^{i}Pr, ^{i}Bu) have been synthesized and characterized by ^{1}H and ^{13}C nmr. The t-Butyl derivatives are unstable and decompose at room temperature, whereas the neopentyl compounds are low boiling volatile liquids with the vapour pressure of ca 4 Torr at 0 °C. The purity, stability, and vapour pressure of neopentyl compounds make them potentially useful zinc precursors for the p-doping of ZnSe.

In present work t-butyl(dimethylamido)zinc (**7**), t-butyl(diethylamido)zinc (**8**), t-butyl(di-iso-propylamido)zinc (**9**), t-butyl(di-iso-butylamido)zinc (**10**), neopentyl-(dimethylamido)zinc (**11**), neopentyl(diethylamido)zinc (**12**), neopentyl(di-iso-propylamido)zinc (**13**) and neopentyl(di-iso-butylamido)zinc (**14**) have been prepared and characterized by ^{1}H and ^{13}C nmr spectroscopy. (**11**) and (**13**) were white intractable solids, insoluble in organic solvents presumably polymeric materials. All other compounds are liquid and characterized by ^{1}H and ^{13}C nmr spectroscopy. t-Butyl derivatives were unstable and decomposed at room temperature, whereas neopentyl derivatives were quite stable.

^{1}H nmr data for the t-butyl derivatives are summarized in experimental section and the spectrum for t-butyl(diethylamido)zinc is shown in figure 2.9. The t-butyl group showed a singlet for methyl protons at 1.15 to 1.35 ppm. The largest change in the chemical shift of these protons was observed for iso-propylamido compound which appeared at the highest field (1.15 ppm). In others the chemical shift was close. t-Butyl(diethylamido)zinc (**8**) showed a triplet and quartet for N-ethyl protons and iso-propyl derivative (**9**) gave a doublet and septet as expected. The methylamido

compound (**7**) gave a doublet instead of a singlet for N-methyl protons which may be due to the mixture of monomer and dimer in solution. Similarly a triplet for N-methylene protons in iso-butyl derivative (**10**) is actually a overlapping doublet which again shows that the compound may be a mixture of a monomer and dimer. All other signals are clear and show no sign of a mixture.

^{13}C nmr of t-butyl derivatives gave a higher field signal for quartenary carbon (Zn-C) as expected and at mid-field for methyl carbons. Again the iso-propylamido compound (**8**) showed a large shift for Zn-C whereas the others gave similar chemical shift. All other signals appeared as expected. ^{13}C nmr spectrum of t-butyl(diethylamido)zinc is shown in figure 2.10.

The ^{1}H nmr spectrum of neopentyl(di-iso-butylamido)zinc is shown in figure 2.11. Neopentyl group gave a singlet for Zn-methylene protons at high field and a singlet for methyl protons at mid-field. N-ethyl protons as usual gave triplet and quartet. iso-Butyl group gave a multiplet for CH proton, a doublet for CH_3 protons, and a overlapping doublet for CH_2 protons which indicates the presence of more than one form of this compound in solution.

^{13}C nmr data are listed in experimental section and the spectrum of neopentyl(di-iso-butylamido)zinc is shown in figure 2.12. Neopentyl group gave three signals, one for methylene carbon, one for quartenary carbon and one for equivalent methyl groups. The iso-butyl group showed three signals, one for equivalent methyl carbons, and one for each of methyne and methylene carbon. All chemical shifts shown are as expected.

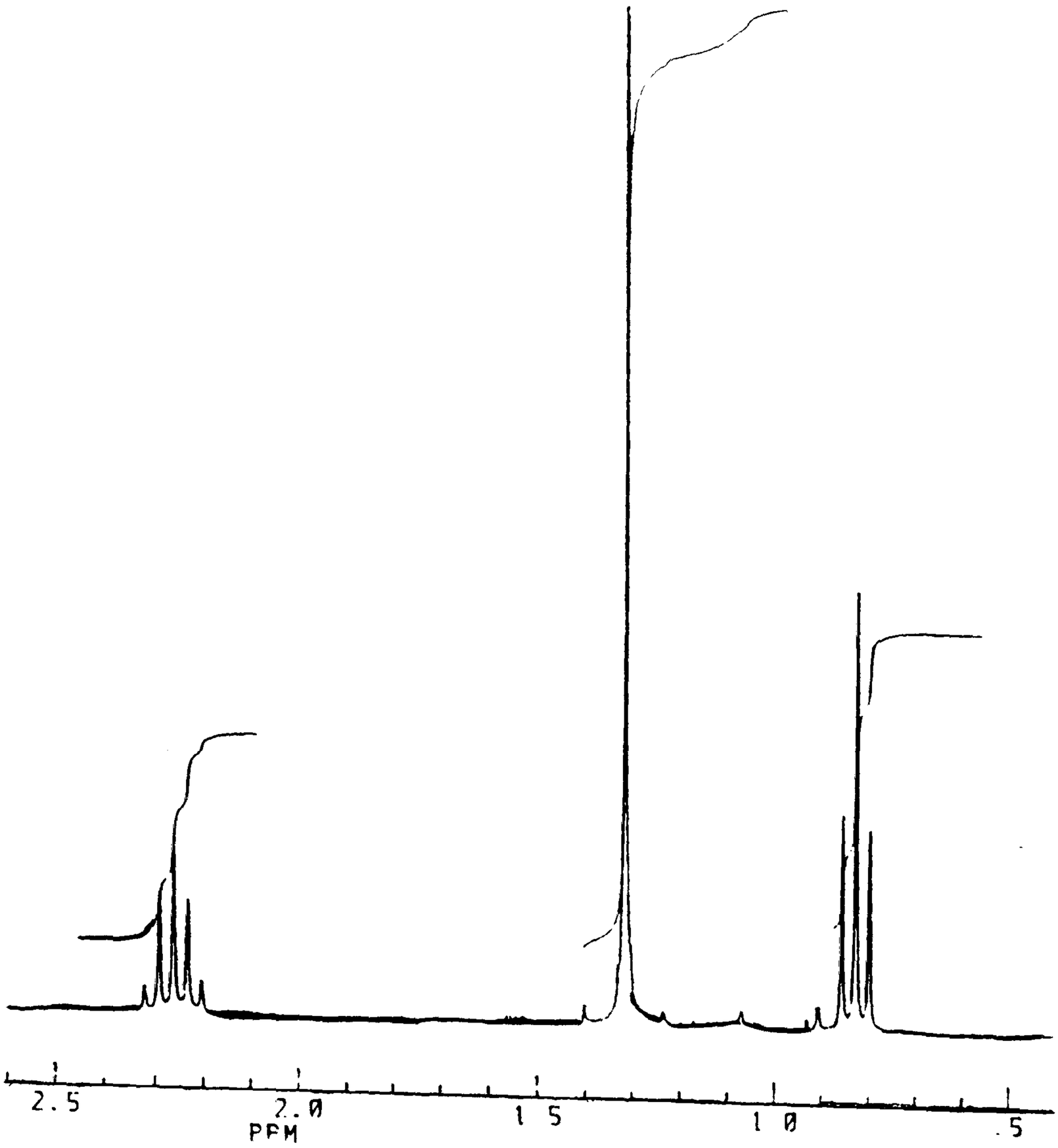

Figure 2.9 ^{1}H nmr spectrum for t-butyl(diethylamido)zinc

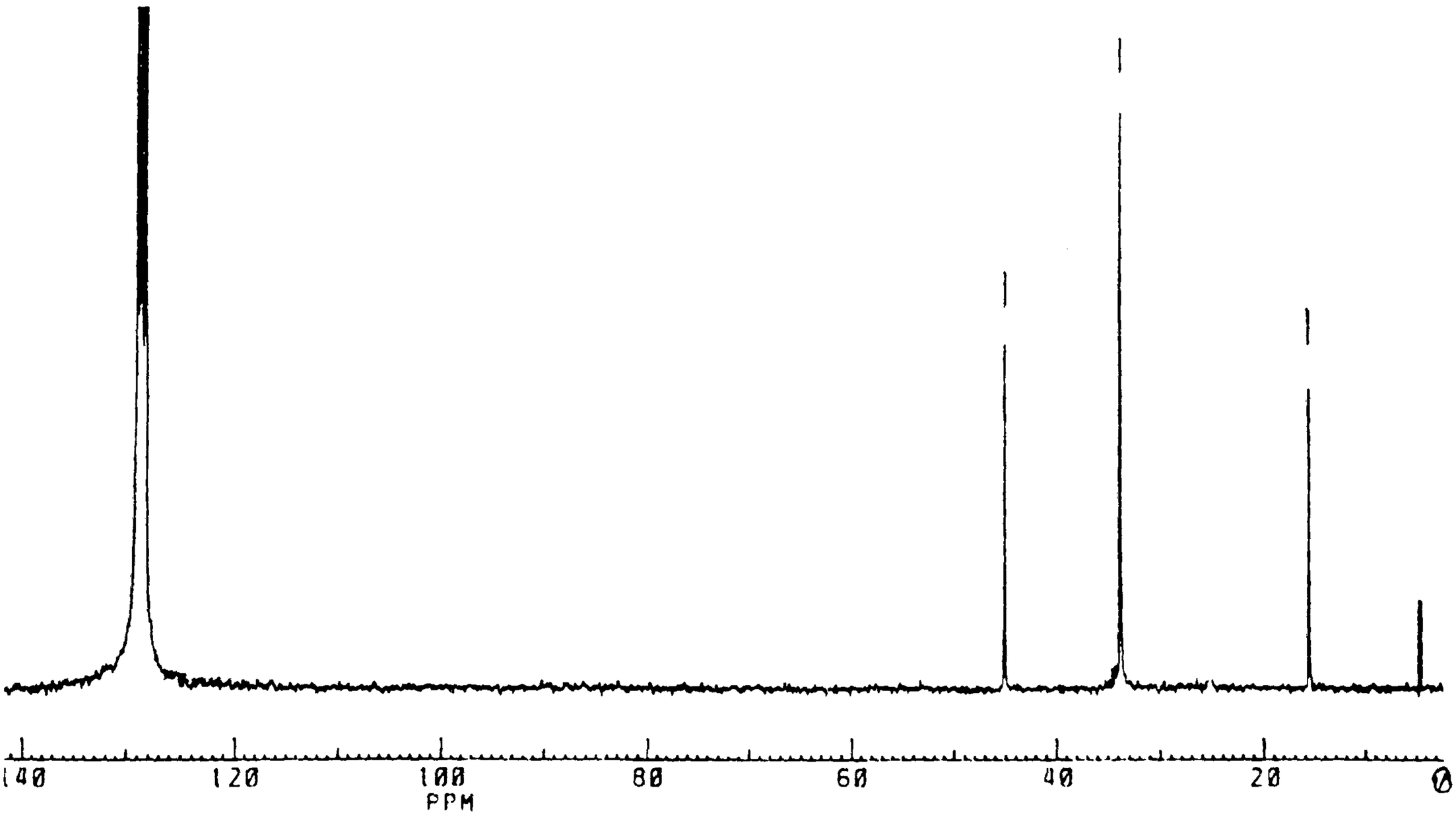

Figure 2.10 ^{13}C nmr spectrum for t-butyl(diethylamido)zinc

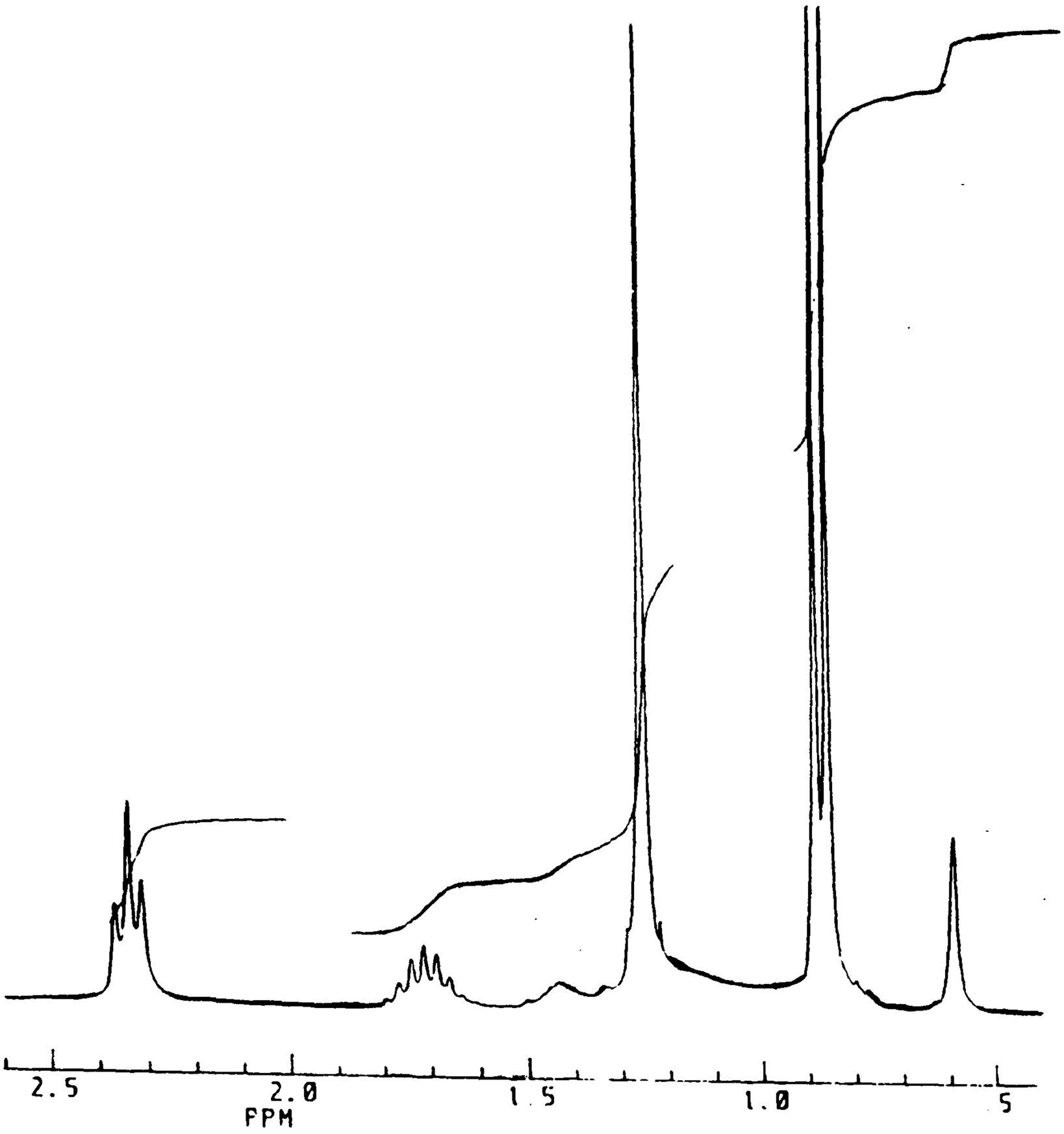

Figure 2.11 ^{1}H nmr spectrum for neopentyl(di-iso-butylamido)zinc

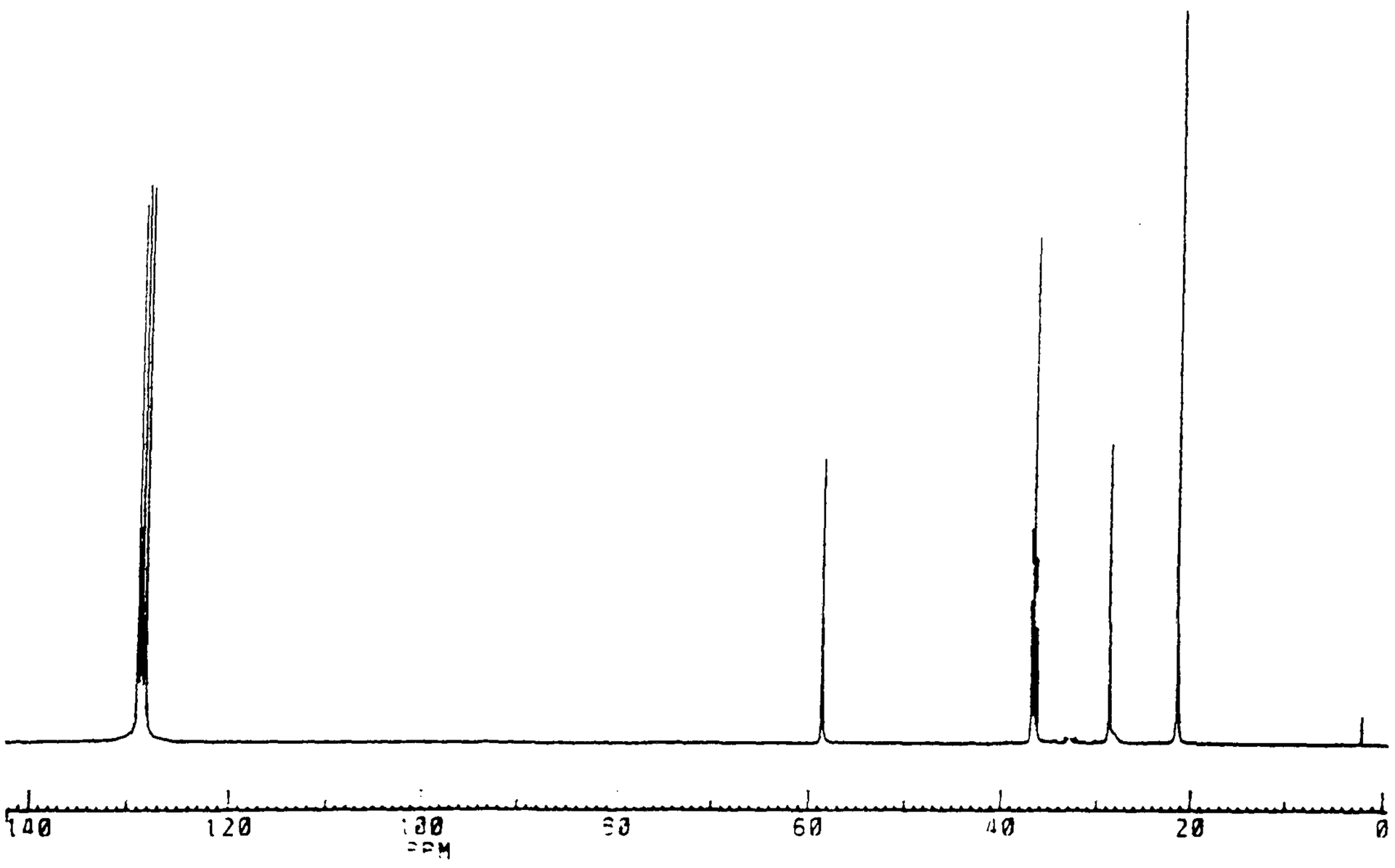

Figure 2.12 ^{13}C nmr spectrum for neopentyl(di-iso-butylamido)zinc

2.3 Growth work

Bis(trimethylpropylenediaminedithiocarbamato)zinc or cadmium (**3**), (**4**) and bis(trimethylethylenediaminedithiocarbamato)zinc or cadmium (**1**), (**2**) were used in attempts to deposit thin films. Good quality thin films were deposited by using (**3**) and (**4**) whereas, no films were deposited with (**1**) and (**2**). The films grown by using methyl(trimethylpropylenediaminedithiocarbamato)zinc or cadmium (**5**) and (**6**) were qualitatively of better quality films than parents bis dithiocarbamates (**3**) and (**4**).

The films grown were characterized by electron diffraction analytical X-ray (EDAX) by using electron microscopy, reflection high energy electron diffraction (RHEED), UV visible and in some cases by X-ray powder diffraction measurements.

2.3.1 Growth apparatus

All LP-MOCVD experiments were carried out in a simple hot-walled growth apparatus as shown in figure 2.13. This consisted of a continuously evacuated Pyrex tube which passed through a tube furnace. The source was placed towards the end of the tube which protruded about 4 cm from the furnace and was brought to the temperature required for sublimation by insulating the end of the tube with glass wool. The whole apparatus was evacuated (ca 10^{-2} Torr) using an oil diffusion pump and the system heated to the temperature required for sublimation and growth.

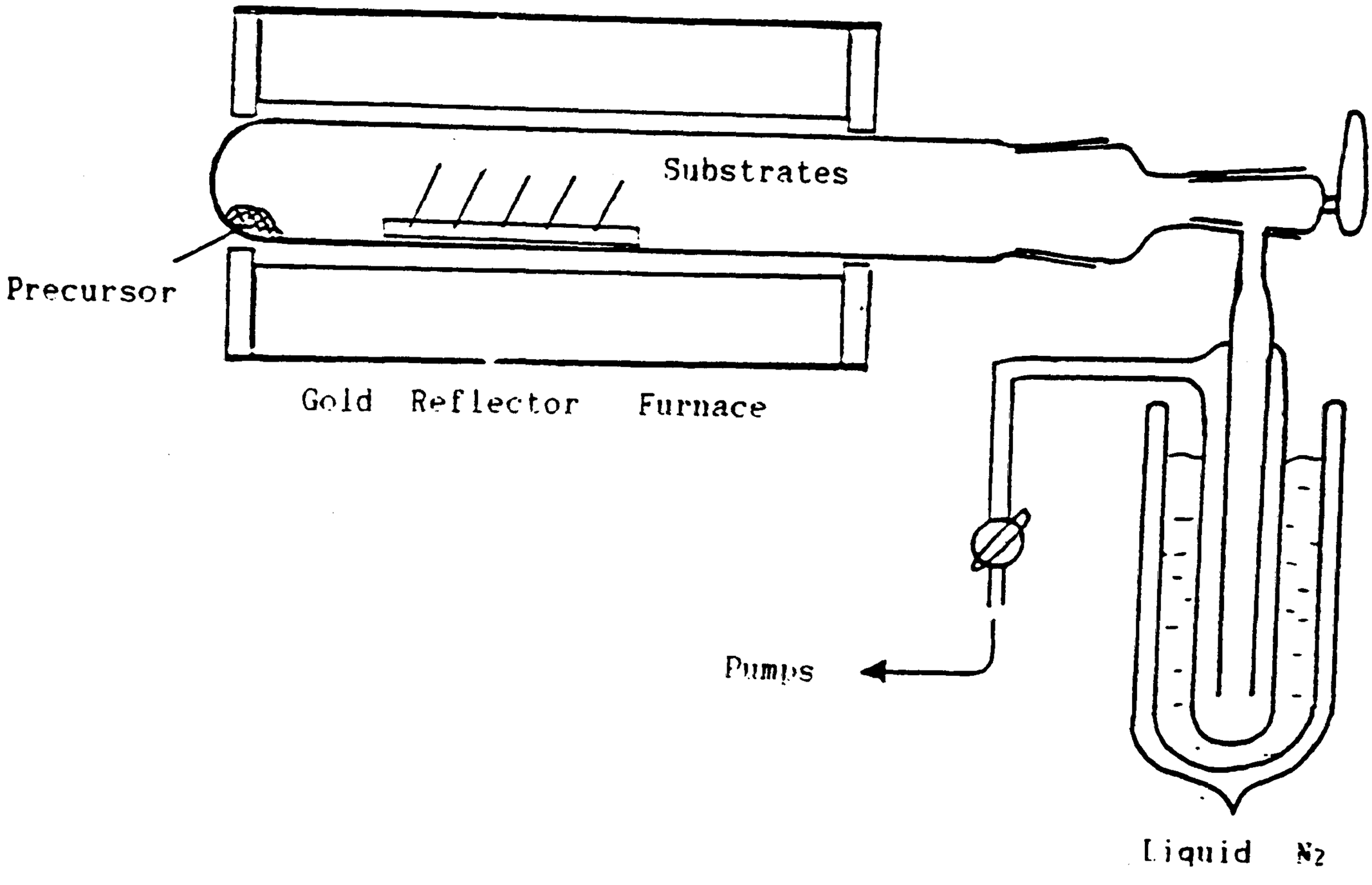

Figure 2.13 Schematic diagram of the LP-MOCVD growth apparatus

2.3.2 Growth of ZnS and CdS thin films using (3) and (4) as precursors

The precursors used in this work were bis(trimethylpropylenediamine-dithiocarbamato)zinc or cadmium (**3**) and (**4**). Thin specular films of CdS have been deposited onto glass and GaAs substrates at temperature range 325 to 375 °C. The 1:1 composition of Cd and S in the films have been confirmed by electron diffraction analytical X-ray (EDAX) using electron microscope (figure 2.14).

RHEED pattern of CdS films grown on GaAs at a growth temperature of 350 °C showed these films to be random, hexagonal, polycrystalline with no evidence for preferred orientation. The quality as judged by reflectivity of films grown from **(4)**

(>400 °C) was better than that of equivalent films grown from parent diethyldithiocarbamatocadmium (II) [10].

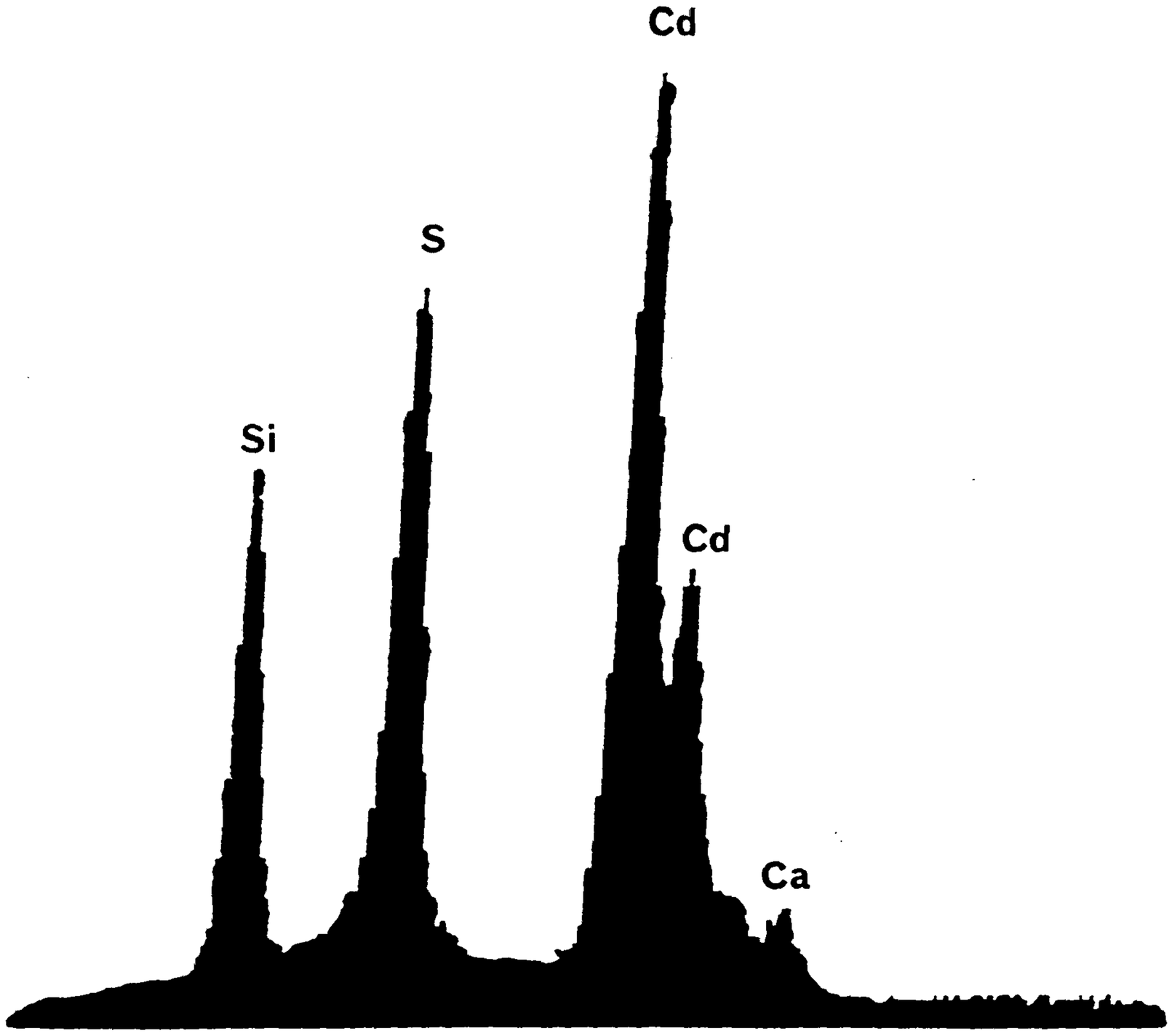

Figure 2.14 EDAX of CdS thin film as grown on glass at 350 °C using (4) as precursor

Scanning electron microscopy showed that CdS films grown on both glass and GaAs substrates at 350 °C were specular. adherent and uniform with crystallites of ca 0.25 μ micron as shown in figure 2.15. The films grown at 400 °C or higher temperatures were powdery, spotted and non-uniform. The morphology of such film is shown in figure 2.16. The band gap was found to be 2.43 eV (lit. 2.425 eV) [38] and was measured by using UV visible.

Figure 2.15 Scanning electron micrograph of CdS grown on glass for 20 minutes at 350 °C from (**4**) as precursor, ---------- = 1 μ

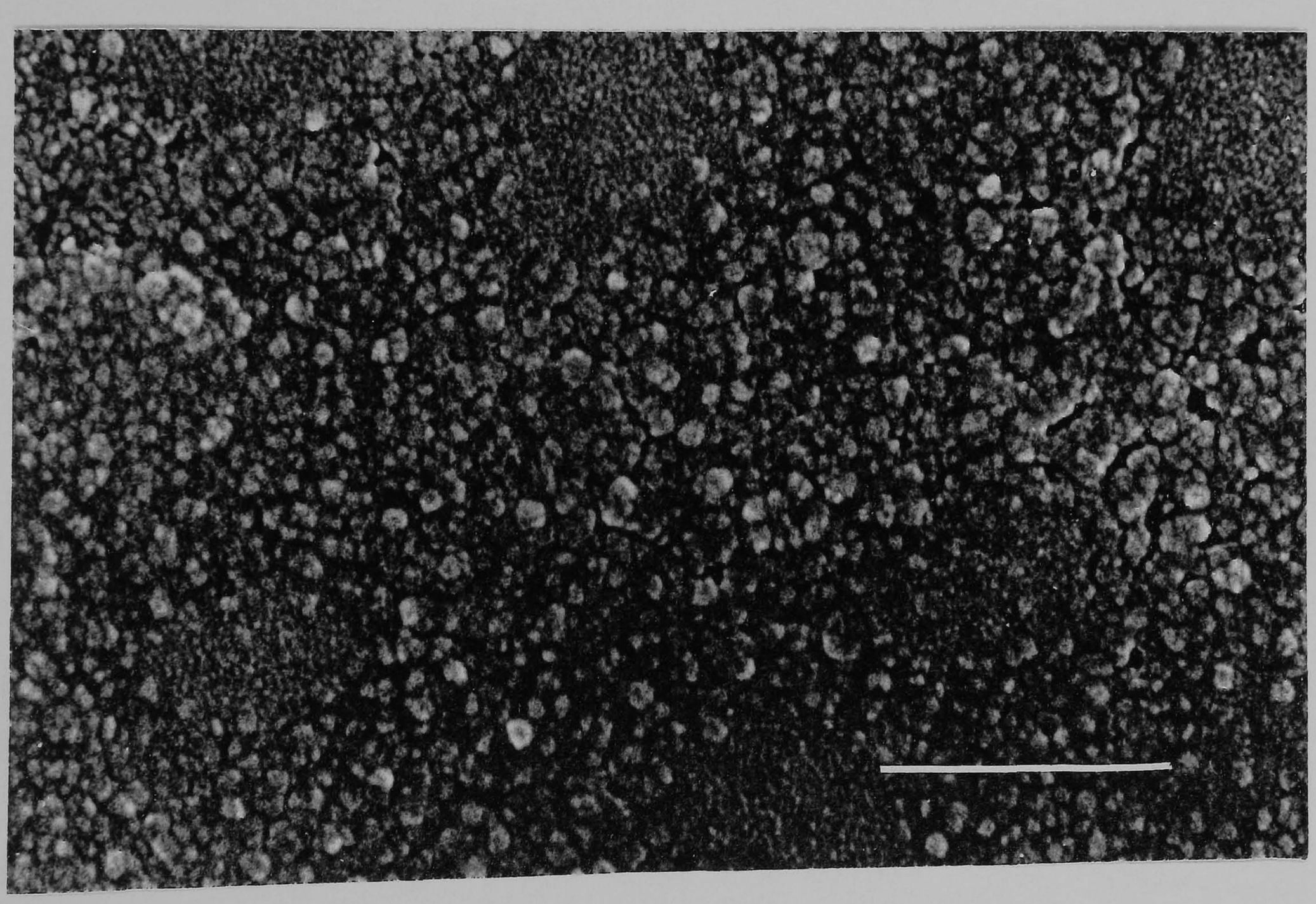

Figure 2.16 Scanning electron micrograph of CdS grown on glass for 20 minutes at 400 °C from (**4**) as precursor, ---------- = 1 μ

ZnS films grown on glass substrate in the temperature range 400 to 450 °C had a poor morphology and only very thin layers were deposited as compared to the parent diethyldithiocarbamatozinc (II). EDAX confirmed the 1:1 composition of Zn and S in ZnS films (figure 2.17). The band gap was found to be 3.57 eV which is in good agreement with the literature value 3.65 eV [38].

A summary of the deposition results onto both glass and GaAs substrates using bis(trimethylpropylenediaminedithiocarbamato)zinc or cadmium is given in table 2.5.

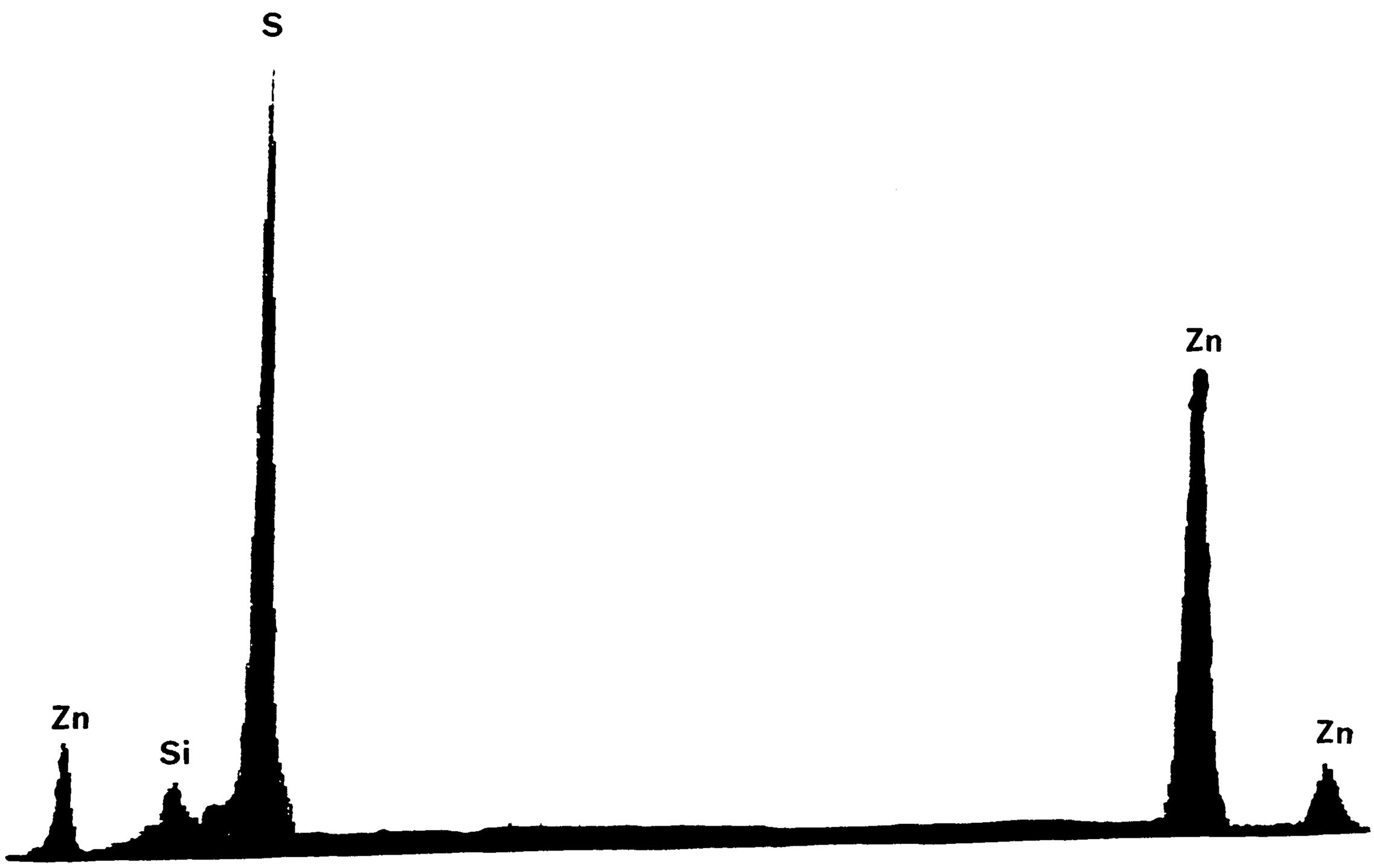

Figure 2.17 EDAX of ZnS thin film as grown on glass at 450 °C from (3)

Table 2.5 Summary of growth results using (**3**) and (**4**).

Compd.	Film	Time min.	Temp. °C	Substrate	Comments
(**3**)	ZnS	20	450	Glass	poor morphology and uneven film thickness
	ZnS	20	425	Glass	cloudy films appear
	ZnS	20	400	Glass GaAs	very thin layers on GaAs substrate
(**4**)	CdS	20	400	Glass GaAs	thick and even growth on both substrates
	CdS	20	375	Glass GaAs	good even growth on glass and GaAs
	CdS	20	350	Glass GaAs	thin even layers on both substrates
	CdS	20	325	Glass GaAs	good specular layer on GaAs substrate

In the apparatus used in the present study deposition from the parent diethyldithiocarbamates was not observed at temperatures <400 °C (20 minutes).

2.3.3 Growth of ZnS and CdS using (5) and (6) as precursors

CdS and ZnS films have been grown on glass and GaAs substrates using methyl(trimethylpropylenediaminedithiocarbamato)zinc (**5**) and methyl(trimethylpropylenediaminedithiocarbamato)cadmium (**6**) as precursors at temperature in the range 350 - 450 °C. Preliminary growth results showed that better quality films of CdS and ZnS have been obtained with higher growth rate as compared to the parent bistrimethylpropylenediaminedithiocarbamates (**3**) and (**4**). The EDAX profile confirmed the 1:1 composition of Cd and S in CdS and Zn and S in ZnS films. The film thickness was decreased at the lower temperature. CdS and ZnS gave crystallites of ca 1 μ micron and 0.5 μ micron respectively. The CdS films were specular and adherent as shown in figure 2.18, the band gaps were measured as 2.43 eV (literature 2.425 eV) [38]. Rapid deposition occurred and at a much lower temperature than for bisdiethyldithiocarbamatocadmium [10]. Powder diffraction of CdS revealed the film to be hexagonal. Powder diffraction results are given in table 2.7. The films grown from the zinc derivative (**5**) were usually powdery (figure 2.19), but the quality of films were better than those grown from zincdiethyldithiocarbamate [10]. The band gap measured (3.62 eV) was in good agreement to the literature value (3.65) [38]. A summary of the growth results using (**5**) and (**6**) as precursors is given in table 2.6.

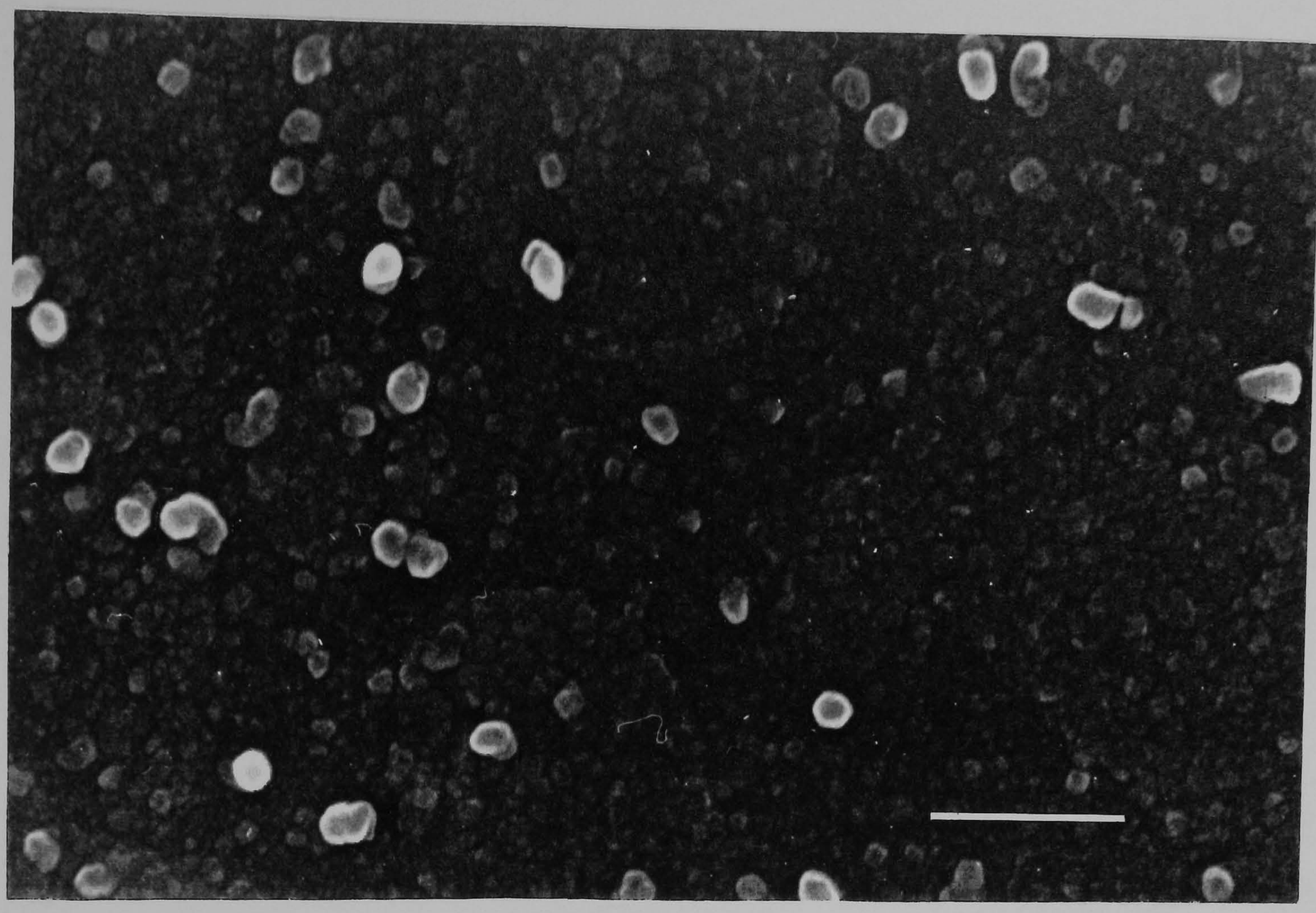

Figure 2.18 Scanning electron micrograph of CdS grown on Glass for 20 minutes at 350 °C from (**6**) as precursor, ---------- = 1 μ

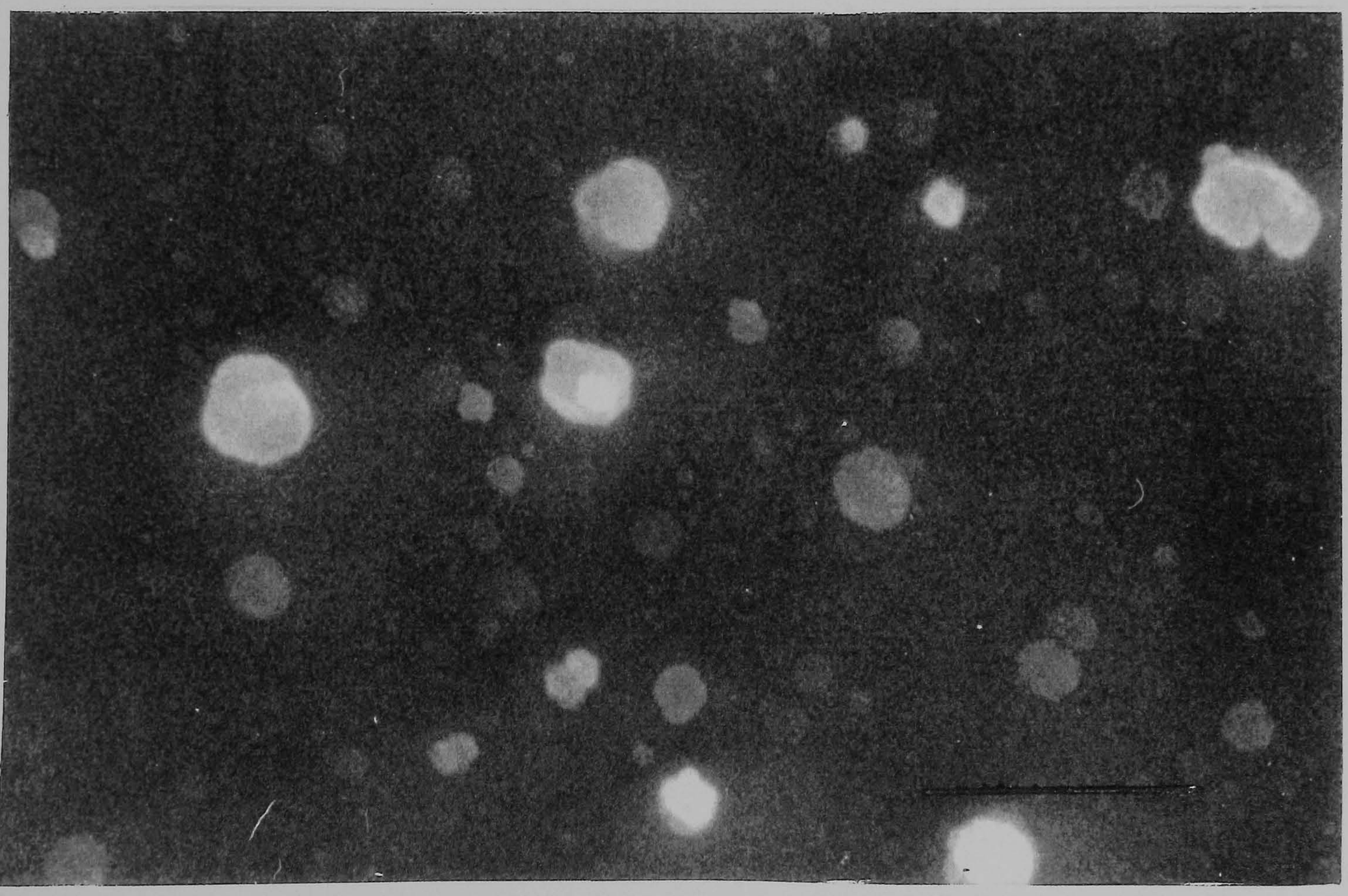

Figure 2.19 Scanning electron micrograph of ZnS grown on glass for 20 minutes at 350 °C from (**5**) as precursor, ---------- = 1 μ

Table 2.6 Summary of growth results using (**5**) and (**6**) as precursors

Compd.	Film	Time min.	Temp. °C	Substrate	Comments
(**5**)	ZnS	20	450	Glass	poor morphology and uneven film thickness
	ZnS	20	425	Glass	cloudy films with uneven growth.
	ZnS	20	400	Glass	very thin layer having poor morphology
(**6**)	CdS	20	400	Glass	Thick, spotted and nonuniform films
	CdS	20	375	Glass	specular films with even growth
	CdS	20	350	Glass	good even layers.
	CdS	20	325	Glass GaAs	thin, uniform film on both substrates

X-ray powder diffraction pattern of deposited CdS was carried out and the d-spacing were calculated and compared to the standard values as given in table 2.7. These values closely corresponds to the hexagonal phase of CdS with no sign of preferred orientation. Sealed tube pyrolysis at 350 °C for 20 minutes also gave micro-crystalline, hexagonal CdS.

Table 2.7 X-ray powder diffraction results [d(Å, % intensity) of CdS deposited at 350 °C on glass for 20 mins using (**6**)

CdS	ASTMS CdS (Hexagonal)	h	k	l
3.58(76)	3.58(75)	1	0	0
3.34(91)	3.36(59)	0	0	2
3.19(100)	3.16(100)	1	0	1
2.44(25)	2.45(25)	1	0	2
2.06(46)	2.06(57)	1	1	0
1.89(43)	1.89(42)	1	0	3
1.76(43)	1.76(45)	1	1	2
1.74(48)	1.73(18)	2	0	1
1.59(16)	1.58(7)	2	0	2
1.47(16)	1.52(2)	1	0	4
1.40(22)	1.40(15)	2	0	3

2.4 Experimental

The synthesis and manipulation of air sensitive compounds as carried out under an inert gas (nitrogen) or vacuum using standard Schlenk techniques which are briefly outlined below.

2.4.1 Vacuum line techniques

- Manipulations were normally carried out in an all glass Schlenk apparatus, connected by reinforced polythene and rubber vacuum tubing to an all-glass, double manifold system consisting of the following elements;
- A vacuum arm (10^{-2}-10^{-3} Torr) connected to a rotary oil pump via a liquid nitrogen cold trap.
- An inert gas line connected to the vacuum arm by two way taps.
- The inert gas (white spot nitrogen (BOC)) was delivered to the apparatus via purification columns to remove traces of oxygen and water. These columns contained:
- Manganese dioxide, reduced in a stream of hydrogen\nitrogen at 200 °C
- Grade "A" molecular sieves periodically regenerated by heating to 200 °C in a stream of nitrogen.
- Chromium trioxide doped of Kieselgel 60, heated to 300 °C in a stream of carbon monoxide.
- Reagents were introduced to the apparatus using Schlenk tubes for solids, and syringes and stainless steel tubing in conjunction with rubber septa for liquids and solutions. Metal alkyls were transferred by distillation in the case of dimethylzinc and by syringe in the case of dimethylcadmium.

2.4.2 Dry-Box techniques

A nitrogen-atmosphere dry-box (Barrett's Model 1089) fitted with a recirculating system to remove oxygen and water from the internal atmosphere further facilitated the handling of the air sensitive compounds.

2.4.3 Glassware and other apparatus

Pyrex glassware fitted with standard quickfit "B" joints were cleaned, using concentrated sulfuric acid, potassium dichromate or ethanolic potassium hydroxide baths, thoroughly rinsed with distilled water and finally with methylated spirits. Glassware was dried in an oven at 180 °C for at least 30 minutes before use. Glassware was assembled whilst hot and evacuated and flushed with inert gas (nitrogen) three times whilst cooling to room temperature. Dow corning grease was used to seal ground glass joints in all cases.

All melting points were measured on a Gallenkamp (MFB-595-010M) melting point apparatus.

2.4.4 Structural investigation

The following techniques were used to characterized thiocarbamates and related compounds.

Infra-red spectra (IR)

Infra-red spectroscopy in the region of 4000 to 400 cm^{-1} was carried out on a Mattson Fourier Transform infra-red spectrometer and calculations were carried out using Mattson's Icon software. Samples were prepared as mulls in nujol, and KBr disks were used to run the spectra.

Nuclear magnetic resonance spectra (nmr)

^{1}H and ^{13}C nmr spectra were recorded on a Bruker AM 250 pulsed Fourier Transform NMR Instrument. Samples were dissolved in deutrated chloroform, toluene or benzene.

Solid state ^{13}C and ^{113}Cd NMR were recorded on a Bruker MSL-300 nmr spectrometer. Magic angle spinning (MAS), cross polarization (CP) and proton decoupling were used for signal enhancement and to obtain high resolution spectra.

Mass spectra

Mass spectra were recorded on an AE1 MS902 mass spectrometer equipped with a MSS data system, and operating with an accelerating voltage of 70 eV.

X-ray crystallography

Single crystals for X-ray were mounted in 0.77 mm glass capillaries and sealed under nitrogen. Data were recorded using an Enraf-Nonius CAD4 diffractrometer operating in the w/2θ scan mode with graphite-monochromated Mo K_α radiation as described previously [39]. The structures were solved via standard heavy-atom procedures and refined by using full-matrix least-squares methods [40] with scattering factors calculated by using the reference data [41]. All non-hydrogen atoms were refined with anisotropic displacement factors; hydrogen atoms were fixed.

Electronic spectra

The absorbance of films were recorded with a Philips PU 8710 Spectrophotometer.

Scanning electron microscopy

Electron microscopy , including EDAX, was recorded with a JEOL 1200 EX II TEMSCAN microscope.

Transmission electron microscopy

Transmission electron microscopy with EDS was carried out on JEOL JEM 2010-200 KV. A solution of CdS was made in acetone and dispersed onto the carbon grid which were lowered into the microscope.

X-ray diffraction

X-ray diffraction pattern was recorded using a Siemens D5000 diffractrometer using CuK_α radiation and a LiF monochromator. The sample was mounted at 1° and scanned from 10-90° in steps of 0.02 with a count time of 2 seconds.

2.5 Synthesis

2.5.1 Preparation of bis(N,N,N-trimethyethylenediaminedithiocarbamato) zinc(II) or cadmium(II) (1) (2)

A mixture of carbon disulfide (10 mmol) and N,N,N-trimethylethylenediamine (TMEDA) (10 mmol) in water (20 cm^3) was stirred for 0.5 hour at 5 °C and then allowed to warm to room temperature. On addition of zinc nitrate (2.5 mmol) in water (10 ml) a white solid product was obtained. The product analysed as bistrimethylethylenediaminedithiocarbamatozinc(II), yield 41% , mp 140 °C.

The cadmium complex was prepared by same method using cadmium nitrate, yield 46%, mp 143 °C.

$Zn[S_2CNCH_3(CH_2)_2N(CH_3)_2]_2$ **(1).** ^{13}C NMR (solid state) δ (ppm) 205.97 (CS_2), 44.42 (NCH_3), 45.11 (NCH_3), 49.19 (NCH_3), 55.26 (CH_2N), 58.41 (NCH_2). IR ν (cm^{-1}) major bands and assignments are: 455 (M-S), 993 (C-S), 1462 (C=N). (Found: C, 33.9; H, 6.1; N, 12.9; S, 30.0, Calc. for $C_{12}H_{26}N_4S_4Zn$: C, 34.4; H, 6.2; N, 13.4; S, 30.5%).

$Cd[S_2CNCH_3(CH_2)_2N(CH_3)_2]_2$ **(2).** ^{13}C NMR (solid state) δ (ppm) 205.82 (CS_2), 45.21 (NCH_3), 45.82 (NCH_3), 49.35 (NCH_3), 54.15 (CH_2N), 58.53 (NCH_2). ^{113}Cd NMR (solid state) singlet at δ 289 ppm. IR ν (cm^{-1}) major bands and assignments are: 433 (M-S), 1008 (C-S), 1465 (C=N). (Found: C, 29.6; H, 5.7; N, 11.2; S, 26.2, Calc. for: $C_{12}H_{26}N_4S_4Cd$: C, 30.9; H, 5.6; N, 12.0; S, 27.5%).

2.5.2 Preparation of bis(N,N,N-trimethypropylenediaminedithiocarbamato) zinc(II) or cadmium(II) (3) (4)

Carbon disulfide (10mmol) was added to a stirred solution of N,N,N-trimethylpropylenediamine (TMPDA) (10 mmol) in water (20 cm^3) at 5 °C for 30 minutes. The mixture was warmed to room temperature and a solution of zinc nitrate (2.5 mmol) in water (10 ml) was added. A white solid product analysed as bis(trimethylpropylenediaminedithiocarbamato)zinc(II), yield 60%, mp 102 °C.

The cadmium complex was prepared by same method using cadmium nitrate. yield 60%, mp 131 °C.

$Zn[S_2CNCH_3(CH_2)_3N(CH_3)_2]_2$ **(3).** ^1H NMR solution ($[^2H_6]$ $CDCl_3$, 250 MHz) δ (ppm) 1.97 [(4H, t, $^3J_{(H-H)} = 7.5$ Hz), (CH_2-*CH_2*-CH_2)], 2.35 [12H, s, N(*CH_3*)$_2$], 2.41 [(4H, t, $^3J_{H-H} = 7.5$ Hz), (CH_2-*CH_2*N)], 3.44 (6H, s, NCH_3), 3.91 [(4H, t, $^3J_{H-H} = 7.5$ Hz), (NCH_2-CH_2)]. ^{13}C NMR ($[^2H_6]C_6H_6$, 250 MHz) δ (ppm) 204.38 (CS_2), 24.98 (-NCH_3), 42.83 (CH_2-*CH_2*-CH_2), 45.94 $N(CH_3)_2$, 55.50 (CH_2-CH_2N), 57.09 (NCH_2-CH_2). IR ν (cm^{-1}) major bands and assignments are 424 (M-S), 989 (C-S), 1461 (C=N). Mass spectrum (m/e): base peak 58.1 (100%) ($CH_2N(CH_3)_2$), other peaks at 44.1 (20.7%) [$N(CH_3)_2$], 88 (28.8%) [$CH_2N(CH_3)_2$], 111.1 (10.8%) [$CH_3(CH_2)_3N(CH_3)_2$], 159.1 (30.1%) [CH_3ZnCS_2], 255 [$ZnS_2CNCH_3(CH_2)_3N(CH_3)_2$] (7.9 %), 417 $Zn[S_2CNCH_3(CH_2)_3N(CH_3)]_2$ (12.7 %), 446 $Zn[S_2CNCH_3(CH_2)_3N(CH_3)_2]_2$ (16.8 %).

(Found: C, 36.4; H, 6.9; N, 11.8; S, 27.3, Calc. for $C_{14}H_{30}N_4S_4Zn$: C,37.6; H, 6.7; N, 12.6; S, 28.2%).

$Cd[S_2CNCH_3(CH_2)_3N(CH_3)_2]_2$ (**4**). ^1H NMR solution ($[^2H_6]$ $CDCl_3$, 250 MHz) δ (ppm) 2.10 [(4H, t, $^3J_{(H-H)}$ = 7.3 Hz), (CH_2-CH_2-CH_2)], 2.41 [12H, s, N(CH_3)$_2$], 2.52 [(4H, t, $^3J_{(H-H)}$ = 7.4 Hz), (CH_2-CH_2N)], 3.46 (6H, s, NCH_3), 3.95 [(4H, t, $^3J_{(H-H)}$ = 7.5 Hz), (NCH_2-CH_2)]. ^{13}C NMR ($[^2H_6]C_6H_6$, 250 MHz) δ (ppm) is 205.71 (CS_2), 25.22 (-NCH_3), 44.29 (CH_2-CH_2-CH_2), 46.24 N(CH_3)$_2$, 56.96 (CH_2-CH_2N), 57.47 (NCH_2-CH_2). ^{113}Cd NMR (solution state) singlet at δ 298 ppm. IR ν (cm^{-1}) major bands and assignments are 420 (M-S), 917 (C-S), 1461 (C=N). Mass spectrum (m/e): base peak 58.1 (100%) ($CH_2N(CH_3)_2$), other peaks at 44.1 (45.4%) [$N(CH_3)_2$], 88 (45.1%) [$CH_2N(CH_3)_2$], 111.1 (7.9%) [$CH_3(CH_2)_3N(CH_3)_2$], 159 (54.8%) [$CS_2CH_3N(CH_2)_3N$], 303 [$CdS_2CNCH_3(CH_2)_3N(CH_3)_2$] (1.4 %), 463 $Cd[S_2CNCH_3(CH_2)_3N(CH_3)]_2$ (4.5 %), 496 $Cd[S_2CNCH_3(CH_2)_3N(CH_3)_2]_2$(1.7 %). (Found: C, 33.7; H, 5.9; N, 10.9; S, 25.7, Calc. for $C_{14}H_{30}N_4S_4Cd$: C, 34.0; H, 6.1; N, 11.3; S, 25.2%).

2.5.3 Preparation of methyl(N,N,Ntrimethylpropylenediaminedithiocarbamato) zinc (II) or cadmium(II) (5) (6)

Both reactions were carried out, using standard Schlenck techniques. In a typical preparation, a solution of bis(N,N,N-trimethylpropylenediaminedithiocarbamato)zinc(II) (5 mmol) in 20 ml toluene was stirred with dimethylzinc (5 mmol) at room temperature for 0.5 hour. On concentration the solution under vacuum, a white solid product was identified as $CH_3ZnS_2CNCH_3(CH_2)_3N(CH_3)_2$, yield 59%, mp 177-180 °C.

The cadmium compound was prepared by same method using bis(N,N,N-trimethylpropylenediaminedithiocarbamato)cadmium. yield 54%, mp 122-124°C.

$CH_3ZnS_2CNCH_3(CH_2)_3N(CH_3)_2$ **(5).** ^1H NMR ($[^2H_6]C_6H_6$), 250 MHz) δ (ppm) 0.33 (3H, s, Zn*CH*$_3$), 1.71 [(2H, t, $^3JCH_2$-CH_2 =7.2 Hz), (CH_2-*CH*$_2$-CH_2)], 2.08 [6H, s, $N(CH_3)_2$], 2.18 [(2H, t, $^3JCH_2$-CH_2 =7.2 Hz, (CH_2N)], 2.33 (3H, s, NCH_3), 3.60 [(2H, t, $^3JCH_2$-CH_2 =7.1 Hz, NCH_2]. ^{13}C NMR ($[^2H_6]C_6H_6$ MHz) δ (ppm) 205.67 (CS_2), 2.03 (Zn*CH*$_3$), 25.83 (N*CH*$_3$), 43.09 (CH_2-*CH*$_2$-CH_2), 46.04 ($N(CH_3)_2$), 56.09 (*CH*$_2$N), 57.04 (N*CH*$_2$). IR ν (cm^{-1}) (major bands andassignments) 430 [(M-S)], 521 [(M-C)], 997 [(C-S)], 1469 [(C=N)]. Mass spectrum: m/e base peak 58 [$CH_2N(CH_3)_2$] (100 %), other peaks 42 [$N(CH_3)_2$] (40.7 %), 70 [$CH_2CH_2N(CH_3)_2$] (11.6 %), 84 [$(CH_2)_3N(CH_3)_2$] (41.6 %), 115 [$CH_3N(CH_2)_3N(CH_3)_2$] (27 %), 143 [CH_3ZnS_2] (23.8 %), 159 [CH_3ZnS_2C] (15.7 %), 255 [$ZnS_2CNCH_3(CH_2)_3N(CH_3)_2$] (7.6 %), 417 $Zn[S_2CNCH_3(CH_2)_3N(CH_3)]_2$ (9.7 %), 446 $Zn[S_2CNCH_3(CH_2)_3N(CH_3)_2]_2$ (8.8 %). (Found: C, 36.1; H, 6.3; N, 9.8. Calc. for $C_8H_{18}N_2S_2Zn$ C, 35.42; H, 6.6; N, 10.3%).

$CH_3CdS_2CNCH_3(CH_2)_3N(CH_3)_2$ **(6).** ^1H NMR ($[^2H_6]C_6H_6$), 250 MHz) δ (ppm) 0.32 (3H, s, Cd*CH*$_3$), 1.89 [(2H, t, $^3JCH_2$-CH_2 = 7.2 Hz)], (CH_2-*CH*$_2$-CH_2)], 2.18 [6H, s, $N(CH_3)_2$], 2.28 [(2H, t, $^3JCH_2$-CH_2 = 7.2 Hz, (*CH*$_2$N)], 3.24 (3H, s, N*CH*$_3$), 3.81 [(2H, t, $^3JCH_2$-CH_2 = 7.25 Hz, N*CH*$_2$]. ^{13}C NMR ($[^2H_6]C_6H_6$), 250 MHz) δ (ppm) 207.61 (CS_2), 2.03 ($CdCH_3$), 26.15 (NCH_3), 44.83 (CH_2-*CH*$_2$-CH_2), 46.56 ($N(CH_3)_2$), 57.67 (CH_2N), 58.20 (NCH_2). IR ν (cm^{-1}) (major bands and assignments) 427 [(M-S)], 514 [(M-C)], 1002 [(C-S)], 1468 [(C=N)]. Mass spectrum: m/e base peak 58.1 [$CH_2N(CH_3)_2$] (100 %), other peaks 44 [$N(CH_3)_2$] (38.7 %), 73 [$CH_2CH_2N(CH_3)_2$] (20 %), 84.1 [$(CH_2)_3N(CH_3)_2$] (39.9 %), 115 [$CH_3N(CH_2)_3N(CH_3)_2$] (9.7 %), 159.1 [$S_2CNCH_3(CH_2)_3N$] (24.6 %), 303 [$CdS_2CNCH_3(CH_2)_3N(CH_3)_2$] (1.1 %), 463 $Cd[S_2CNCH_3(CH_2)_3N(CH_3)]_2$ (4.5 %), 496 $Cd[S_2CNCH_3(CH_2)_3N(CH_3)_2]_2$(1.2 %).

(Found: C, 31.0; H, 5.9; N, 9.2; S, 19.9. Calc. for $C_8H_{18}N_2S_2Cd$ C, 30.2; H, 5.7; N, 8.8; S, 20.1%).

2.5.4 Preparation of t-butylmagnesiumchloride

Tert-butylmagnesiumchloride (429 mmol) was added dropwise to magnesium turnings (208 mmol), previously baked out with a crystal of iodene, stirring in (200 ml) of diethylether. After initation, the halide is added as to maintain a steady reflux. on complete addition, the reaction mixture was stirred until room temperature was reached then left to settle. After filteration the Grignard solution was standarised by titration of hydrolysed Grignard against dilute hydrochloric acid (0.92 M).

2.5.5 Preparation of bis-t-butylzinc

Tert-butylmagnesiumchloride (40 ml of 0.90 M solution) was added dropwise to zinc chloride (15 mmol) in diethylether (50 ml) at 0 °C, giving an immediate white precipitates. On complete addition, the mixture was stirred for 2 hours and left to settle. The solvent was then removed in *vacuo* leaving a white residue from which bistert-butylzinc distills (10^{-2} Torr, 125 °C), is collected at -196 °C and is left to warm up revealing a colourless liquid. Yield 2.14 g.

2.5.6 Preparation of t-butyl(dimethylamido)zinc (7)

Bistert-butylzinc (11.2 mmol) and dimethylamine (11.2 mmol) were reacted in toluene (30 ml) at 70-80 °C for 15 hours to prepare tert-butyl(dimethylamido)zinc. The mixture was allowed to cool and the solvent evaporated to dryness to give a colourless liquid which was identified as tert-butyl(dimethylamido)zinc, yield 2.56 g.

$(CH_3)_3CZnN(CH_3)_2$ (**7**). ^1H NMR ($[^2H_6]C_6H_6$), 250 MHz) δ (ppm) 1.28 [9H, s, $C(CH_3)_3$], 1.88 [6H, s, $(CH_3)_2$]. ^{13}C NMR ($[^2H_6]C_6H_6$), 250 MHz) δ (ppm) 1.16 $(CH_3)_3C$, 25.08 $N(CH_3)_2$, 32.54 $C(CH_3)_3$.

2.5.7 Preparation of t-butyl(diethylamido)zinc (8)

Bist-butylzinc (16 mmol) and diethylamine (16 mmol) were stirred in toluene (30 ml) at 80 °C for 12 hours. The mixture was allowed to cool down and the solvent was removed under *vacuo* to give a colourless liquid which was identified as tert-butyl(diethylamido)zinc. Yield 3.0 g.

$(CH_3)_3CZnN(C_2H_5)_2$ (**8**). ^{1}H NMR ($[^2H_6]C_6H_6$), 250 MHz) δ (ppm) 0.86 (3H, t, $^3JCH_3$-CH_2 = 7.1 Hz NCH_2CH_3), 1.32 [9H, s, $C(CH_3)_3$], 2.26 (2H, q, $^3JCH_2$-CH_3 = 7.1 Hz NCH_2). ^{13}C NMR ($[^2H_6]C_6H_6$), 250 MHz) δ (ppm) 1.37 $(CH_3)_3C$, 14.91 CH_2CH_3, 33.17 $C(CH_3)_3$, 44.44 NCH_2.

2.5.8 Preparation of t-butyl(di-iso-propylamido)zinc (9)

Bistert-butylzinc (18 mmol) and di-iso-propylamine (18 mmol) were stirred in toluene (30 ml) at 70-80 °C for 15 hours. The mixture was allowed to cool down to room temperature and the solvent was removed under *vacuo* to give a colourless liquid which was identified as tert-butyl(di-iso-propylamido)zinc. Yield 4.8 g.

$(CH_3)_3CZnN[CH(CH_3)_2]_2$ (**9**). ^{1}H NMR ($[^2H_6]C_6H_6$), 250 MHz) δ (ppm) 0.98 [6H, d, $^3JCH_3$-CH = 6.8 Hz $CH(CH_3)_2$], 1.15 [9H, s, $C(CH_3)_3$], 2.84 (1H, m, NCH). ^{13}C NMR ($[^2H_6]C_6H_6$), 250 MHz) δ (ppm) 2.06 $(CH_3)_3C$, 23.92 $CH(CH_3)_2$, 32.93 $C(CH_3)_3$, 46.60 NCH.

2.5.9 Preparation of t-butyl(di-iso-butylamido)zinc (10)

Bistert-butylzinc (18 mmol) and di-iso-butylamine (18 mmol) were stirred in toluene at 70-80 °C for 15 hours. The mixture was allowed to cool down to room temperature and the solvent was removed under *vacuo* to give a colourless liquid which was identified as tert-butyl(di-iso-butylamido)zinc. Yield 4.5 g.

$(CH_3)_3CZnN[CH_2CH(CH_3)_2]_2$ (**10**). ^1H NMR ($[^2H_6]C_6H_6$), 250 MHz) δ (ppm) 0.84 [6H, d, $^3JCH_2$-CH_2 = 6.8 Hz $CH(CH_3)_2$], 1.35 [9H, s, $C(CH_3)_3$], 1.65 (1H, m, CH_2CH) 2.33 (2H, m, NCH_2). ^{13}C NMR ($[^2H_6]C_6H_6$), 250 MHz) δ (ppm) 1.36 $(CH_3)_3C$, 28.52 $CH(CH_3)_2$, 33.59 $C(CH_3)_3$, 57.99 NCH_2.

2.5.10 Preparation of neopentylmagnesiumbromide

2,2-Dimethylpropylbromide (30 ml, 23.6 mmol) was added dropwise to magnesium turnings (5.76 g, 23.7 mmol), previously baked out with a crystal of iodine, stirring in (200 ml) of diethylether. After initation, the halide is added as to maintain a steady reflux. on complete addition, the reaction mixture was stirred until room temperature was reached then left to settle. After filteration the Grignard solution was standarised by titration of hydrolysed Grignard against dilute hydrochloric acid (0.79 M).

2.5.11 Preparation of bisneopentylzinc

Neopentylmagnesiumbromide (40 ml of 0.79 M solution) was added dropwise to zinc chloride (2.05 g, 15 mmol) in diethylether (50 ml) at 0 °C, giving an immediate white precipitates. On complete addition, the mixture was stirred for 2 hours and left to settle. The solvent was then removed in *vacuo* leaving a white residue from which bisneopentylzinc distills (10^{-2} Torr, 125 °C), is collected at -196 °C and is left to warm up revealing a colourless liquid. Yield 2.14 g.

2.5.12 Preparation of Neopentyl(dimethylamido)zinc (11)

Bisneopentylzinc (5 mmol) and dimethylamine (5 mmol) were reacted in toluene (30 ml) at 70-80 °C for 15 hours. On concentration under vaccum, a white insoluble solid product was obtained. Yield 1.2 g.

2.5.13 Preparation of Neopentyl(diethylamido)zinc (12)

Bisneopentylzinc (1.4 g, 7 mmol) and diethylamine (0.5 g, 7 mmol) were stirred in toluene at 80 °C for 12 hours. The mixture was allowed to cool down and the solvent was removed under *vacuo* to give a colourless liquid which was identified as neopentyl(diethylamido)zinc. Yield 1.27 g.

$(CH_3)_3CCH_2ZnN(C_2H_5)_2$ **(12).** ^{1}H NMR ($[^2H_6]C_6H_6$), 250 MHz) δ (ppm) 0.54 (2H, s, Zn*CH*$_2$), 0.89 (3H, t, $^3JCH_2$-CH_2 = 7.1 Hz NCH$_2$*CH*$_3$), 1.21 [9H, s, C(*CH*$_3$)$_3$], 2.30 (2H, q, $^3JCH_2$-CH_2 = 7.1 Hz N*CH*$_2$). ^{13}C NMR ($[^2H_6]C_6H_6$), 250 MHz) δ (ppm) 2.06 *CH*$_2$Zn, 15.57 CH$_2$*CH*$_3$, 32.96 $(CH_3)_3C$, 36.58 C(*CH*$_3$)$_3$, 44.38 N*CH*$_2$.

2.5.14 Preparation of Neopentyl(di-iso-propylamido)zinc (13)

Bisneopentylzinc (9 mmol) and di-iso-propylamine (9 mmol) were reacted in toluene (30 ml) at 70-80 °C for 15 hours. On concentration under vaccum, a white insoluble solid product was obtained. Yield 1.4 g.

2.5.15 Preparation of Neopentyl(di-iso-butylamido)zinc (14)

Bisneopentylzinc(16 mmol) and di-iso-butylamine (16 mmol) were stirred in toluene (30 ml) at 70-80 °C for 15 hours. The mixture was allowed to cool down to room temperature and the solvent was removed under *vacuo* to give a colourless liquid which was identified as tert-butyl(di-iso-butylamido)zinc. Yield 2.6 g.

$(CH_3)_3CCH_2ZnN[CH_2CH(CH_3)_2]_2$ **(14).** ^{1}H NMR ($[^2H_6]C_6H_6$), 250 MHz) δ (ppm) 0.58 (2H, s, Zn*CH*$_2$), 0.88 [6H, d, $^3JCH_3$-CH = 6.8 Hz CH(*CH*$_3$)$_2$], 1.26 [9H, s, C(*CH*$_3$)$_3$], 1.72 (1H, m, CH$_2$*CH*), 2.34 (2H, q, N*CH*$_2$). ^{13}C NMR ($[^2H_6]C_6H_6$), 250 MHz) δ (ppm) 2.06 *CH*$_2$Zn, 21.33 C*(CH*$_3$*)*$_3$, 28.81 *(CH*$_3$*)*$_2$C, 36.64 *C*H, 37.12 *C*(CH$_3$)$_3$, 58.63 N*CH*$_2$.

2.5.16 Deposition of thin films

Cadmium sulfide or zinc sulfide thin films were deposited onto glass microscope slides and GaAs by metal organic chemical vapour deposition. Samples (50 mg) were placed at one end of the Schlenck tube and lowered into the furnace. Glass slides or GaAs wafers were placed at the center of the furnace. The tube was continuously pumped (10^{-2} Torr). Cadmium sulfide deposition was carried out with the furnace at 350 °C whereas for zinc sulfide the furnace temperature was kept at 450 °C. The precursor itself was located slightly outside the furnace and therefore was at a lower temperature than that of the furnace, thin specular films were obtained in about 20 minutes. The films were characterised by elemental detection by analytical X-ray (EDAX) using electron microscopy, powder diffraction analysis and reflection high energy electron diffraction (RHEED) for CdS on GaAs.

References

1. Chemistry of The Elements, N. N. Greenwood, and A. Earnshaw, 1984, P 1412.

2. D. A. Langs, and C. R. Hare, J. Chem. Soc., Chem. Comm. 1967, 890.

3. E. C. Constable, Coord. Chem. Rev., 1984, 58, 1.

4. B. J. Aylett, in "Comprehensive Inorg. Chem.", Vol 3, Ed. A. F. Tretman-Dickenson, Pergamon, 1973.

5. B. J. Aylett, in "The Chemistry, Biochemistry, and Biology of Cadmium", Ed. M. Webb, Elseveir/North Holland 1979.

6. R. G. Prince, in "Comprehensive Coord. Chem.", Vol 5. Ed. G. Wilkinson, Pergamon Books Ltd. 1987.

7. Y. Takahasi, R. Yuki, M. Motojima, and K. Sugiyama, J. Crystal Growth, 1980, 50, 491.

8. M. A. H. Evans, and J. O. Williams, Thin Solid Films, 1982, 87, L1.

9. A. Saunders, A. Vecht, and G. Tyrell, Ternary Multiary Cmpd. Proc., Int. Conf. 7th. 1986, (Publ. 1987), (Chem Abs., 1988, 108, 66226h).

10. D. M. Frigo, O. F. Z. Khan, P. O'Brien, J. Crystal Growth, 1989, 96, 989.

11. M. B. Hursthouse, M. A. Malik, M. Motevalli, and P. O'Brien, Polyhedron, 1992, 11, 45.

12. K. Osaka, and T. Yamamoto, Inorg. Chem., 1991, 30, 2328.

13. M. Bochman, K. Webb, M. Harman, and M. B. Hursthouse, Angew. Chem. Int. Ed., 1990, 29, 638.

14. M. Bochman, K. Webb, M. B. Hursthouse, and M. Mazid, J. Chem. Soc. Dalton Trans., 1991, 2317.

15. B. O. Dabbousi, P. J. Bonasia, and J. Arnold, J. Am. Chem. Soc., 991, 113, 3186.

16. M. B. Hursthouse, M. A. Malik, M. Motevalli, and P. O'Brien, Organometallics, 1991, 10, 730.

17. M. A. Malik, and P. O'Brien, Mater. Chem., 1991, 3, 999.

18. M. B. Hursthouse, M. A. Malik, M. Motevalli, and P. O'Brien, J. Mater.Chem., 1992, 2, 949.

19. M. A. Malik, M. Motevalli, J. R. Walsh and P. O'Brien, Organometallics, 1992, 11, 136.

20. K. Osakada, and T. Yamamoto, J. Chem. Soc., Chem. Commun., 1987, 1117.

21. T. Yamamoto, A. Taniguchi, K. Kubota, and Y. Tominaga, Inorg. Chimica. Acta., 1985, 104, L1.

22. J. R. Walsh, P. O'Brien, A. C. Jones, and M. Motevalli, J. Organomet. Chem., 1993, 449, 1.

23. D. Oktavec, E. Beinrour, B. Siles, J. Slefanec, and J. Garaj, Collection Czechoslov., J. Chem. Soc., Chem. Commun., 1980, 45, 1495.

24. M. Bonamico, G. Mazzone, A. Vaciago and L. Zambonelli, Acta Cryst., 1965, 19, 898.

25. A. Domenicano, L. Torelli, A. Vaciago and L. Zambonelli, J. Chem. Soc. (A), 1968, 135.

26. M. Bonamico and G. Dessy, J. Chem. Soc. (A), 1971, 264.

27. H. P. Klug, Acta Cryst., 1966, 21, 536.

28. M. B. Hursthouse, M. A. Malik, M. Motevalli and P.O'Brien, J. R. Walsh and A. C. Jones, J. Mat. Chem., 1991, 1, 139.

29. M. B. Hursthouse, M. A. Malik, M. Motevalli and P.O'Brien, J. R. Walsh and A. C. Jones, Organometallics, 1991, 10, 3192.

30. M. B. Hursthouse, M. A. Malik, M. Motevalli and P.O'Brien, J. R. Walsh and A. C. Jones, J. Organomet. Chem., 1993, 1, 449.

31. J. Dekken, J. Boersma, L. Fernholt, A. Haaland and A. L. Spek, Organometallics, 1987, 6, 1202.

32. R. Baggio, A. Frigerio, E. B. Halac, D. Vega and M. Perec, J. Chem. Soc. Dalton Trans., 1992, 550.

33. K. A. Fraser and M. M. Harding, Acta Cryst. 1967, 22, 75.

34. M. J. Henderson, R. . Papasegio, C. L. Rasto, A. H. White and M. F. Lappert, J. Chem. Soc. Chem. Commun., 1986, 672.

35. G. W. Bushnell and S. R. Stobart, Can. J. Chem., 1980, 58, 574.

36. A. N. Benac, A. H. Cowley, R. A. Jones, C. M. Nunn and Wright, J. Amer. Chem. Soc., 1989, 11, 4986.

37. O. F. Z. Khan, D. M. Frigo, P. O'Brien, A. Howes and Hursthouse, J. Organomet. Chem., 1987, 334, C27.

38. M. Kamiyama, and E. Sugata, Eds. Handbook for thin layer engineering (Ohm, Tokyo, 1970).

39. G. M. Sheldrick, SHEL× 76, Program for Crystal Structure Determination, University of Cambridge, Cambridge U. K., 1979.

40. International Tables for X-ray Crystallography, Kynoch Press, Birmingham, U. K., 1974, Vol. 4.

Chapter 3

Electroless Deposition of II-VI Materials

3.1 Introduction

Electroless deposition also called chemical bath deposition (CBD) is a convenient and cheap method for depositing thin films of II-VI materials. This technique was first introduced by Bell, Hemmatt, and Wald [1], and since then has been used widely.

The CBD of films of sulfides or selenides usually involve the decomposition of alkaline solutions containing thiourea or sodium selenosulfate respectively, in the presence of a metal salt. In principle the process tries to use a controlled chemical reaction to effect deposition by precipitation. The substrates are immersed in an alkaline solution containing the chalcogen source, the metal ion, added base and a chelating agents, used to control the hydrolysis of the metal ion. The deposition rate can be controlled by altering the temperature, pH, and the relative concentration of the reactants in the solution (chalcogen source, chelating agent or metal ion). One particular advantage of CBD is that it is a low temperature technique and can be used for deposition onto a wide range of substrates.

Thin films of CdS, ZnS, PbS, CdZnS, CdSe, and PbSe have been deposited using such methods [2-5]. Triethanolamine (TEA) has been used as a complexing agent in depositing thin films of ZnS [6], CdZnS [7], ZnSe [8], CoSe [9], and MnS [10]. Ternary semiconductors such as $Cd_{1-x}Zn_xS$, $Cd_{1-x}Hg_xS$, $Cd_{1-x}Pb_xS$, and $Pb_{1-x}Hg_xS$ have also been prepared [2,11].

In the present work we have successfully deposited thin films of CdS, ZnS, $Cd_xZn_{1-x}S$ and ZnO onto glass microscope slides and tin oxide coated glass substrates by such a method. Thin films of comparable quality to those obtained in other work have been prepared and the effects of bath composition on the nature of the deposited films

have been considered in detail. The deposition of ZnO thin films on both glass and tin oxide coated glass substrates by using zinc acetate and ethylenediamine has been achieved. All these films have been characterized by scanning electron microscopy (including elemental detection by X ray analysis EDAX), transmission electron microscopy (including electron diffraction), X-ray diffraction, and the determination of band gaps by electronic spectroscopy. The composition of deposition baths has been studied by ^{113}Cd nmr and modelled using the known thermodynamic binding constants for the various species in solution.

3.2 Results and discussion

3.2.1 CdS Thin films

CdS is a wide band gap material, thin films of CdS have been used in solar cells [13], light emitting diodes [14], and ultrasonic transducers [15] as described in chapter 1. A simple solution growth method was employed to deposit CdS thin film.

Growth Rates

Initial investigations of the rate of growth of films from baths of [Cd]:[en]:[Th] were made by measuring the absorption of the films as a function of time at 45 and 50 °C, typical results are shown in figures 3.1a and 3.1b. In all cases, after an initial induction period, the rate of deposition is close to linear, which may support a rate determining step involving a constant (surface area) i.e. a surface controlled reaction. We sought to confirm the thicknesses of the films by a number of measurements using a profile stylus meter. Such measurements were only possible on films of good quality *vide*

infra, uneven films gave poor irreproducible results in such measurements. In figure 3.2 film thicknesses are plotted against time showing straight lines similar to those obtained for absorbance measurements and suggesting the growth rates to be linear. The thickness measurements can be used in combination with the absorbance measurements to establish an extinction coefficient for CdS at (300 nm) of 3.8 m^{-1}. This value can be used to convert all of the rate results into units of h^{-1}, these results are summarized in table 3.1. There is a good agreement between the rates as measured with the profile stylus meter and by absorbance. An activation energy for the deposition of CdS can be calculated, using the results in table 3.1, as 107 k J $mole^{-1}$, which can be compared to value of 85 k J $mole^{-1}$ as reported by Ortegaborges and Lincot for deposition from ammonia thiourea system onto gold substrate [16].

Table 3.1 Some Typical Growth Rates (μ h^{-1})

[Cd]:[en]	1:3	1:3.5	1:4
Temperature/ °C			
35	0.107		
40	0.212 (0.217)	0.189 (0.188)	0.117 -
45	(0.353) 0.291	(0.247) 0.296	- -
50	0.829	0.827	0.852
54	0.857		
60	2.88		

(rates determined by profile stylus meter measurements), other rates are extrapolated from absorbance measurements)

[Cd] = 0.018, mole dm^{-3}
[thiourea] = 0.018 mole dm^{-3}
pH 9.5 - 11

Growth at 45 °C

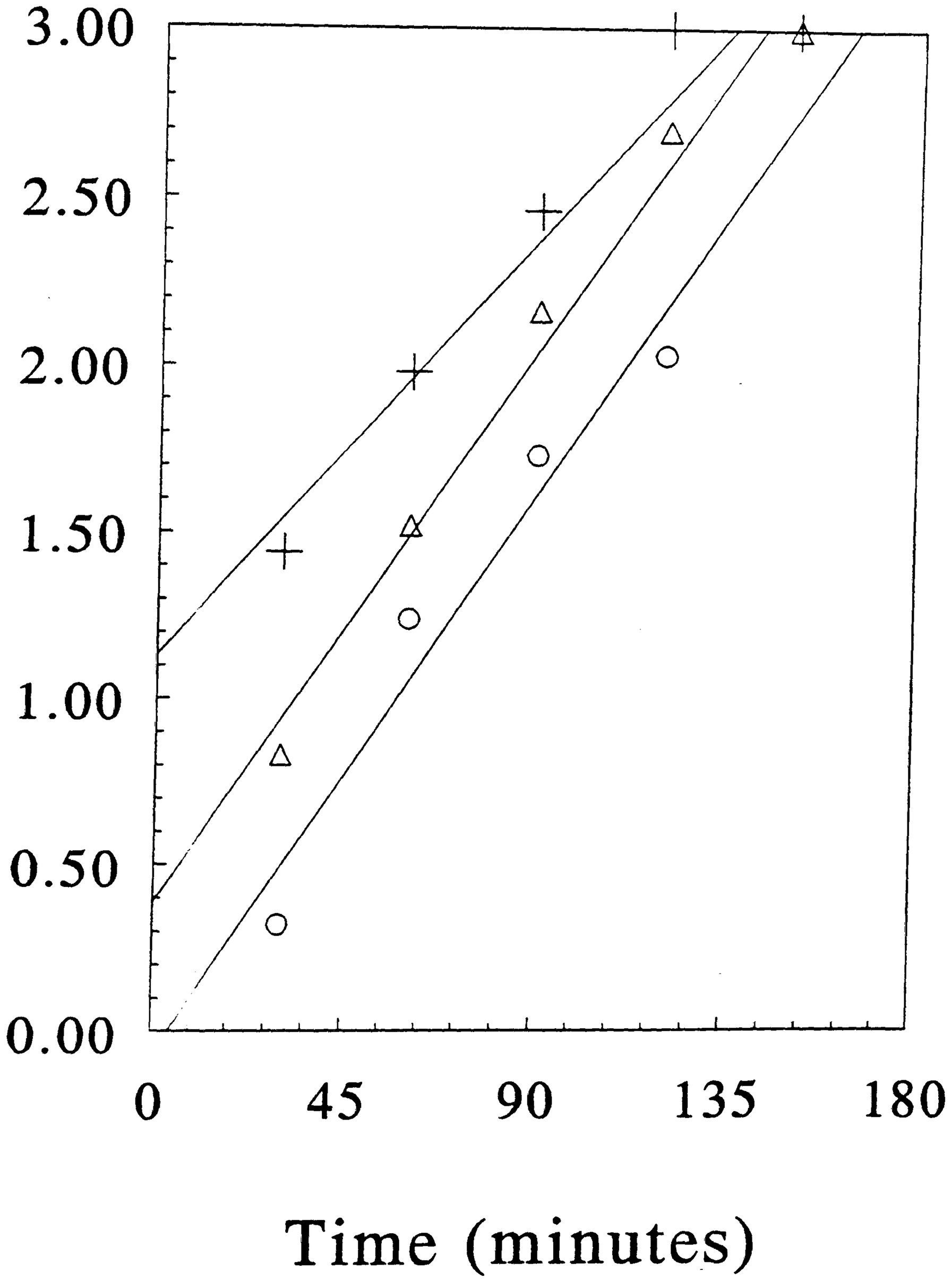

Figure 3.1a Typical rates as determined spectroscopically (300 nm) for various ratios of ethylenediamine to cadmium [Cd] = 0.018 mole dm^{-3}, [thiourea] = 0.018 mole dm^{-3}, 45 °C.

Growth at 50°C

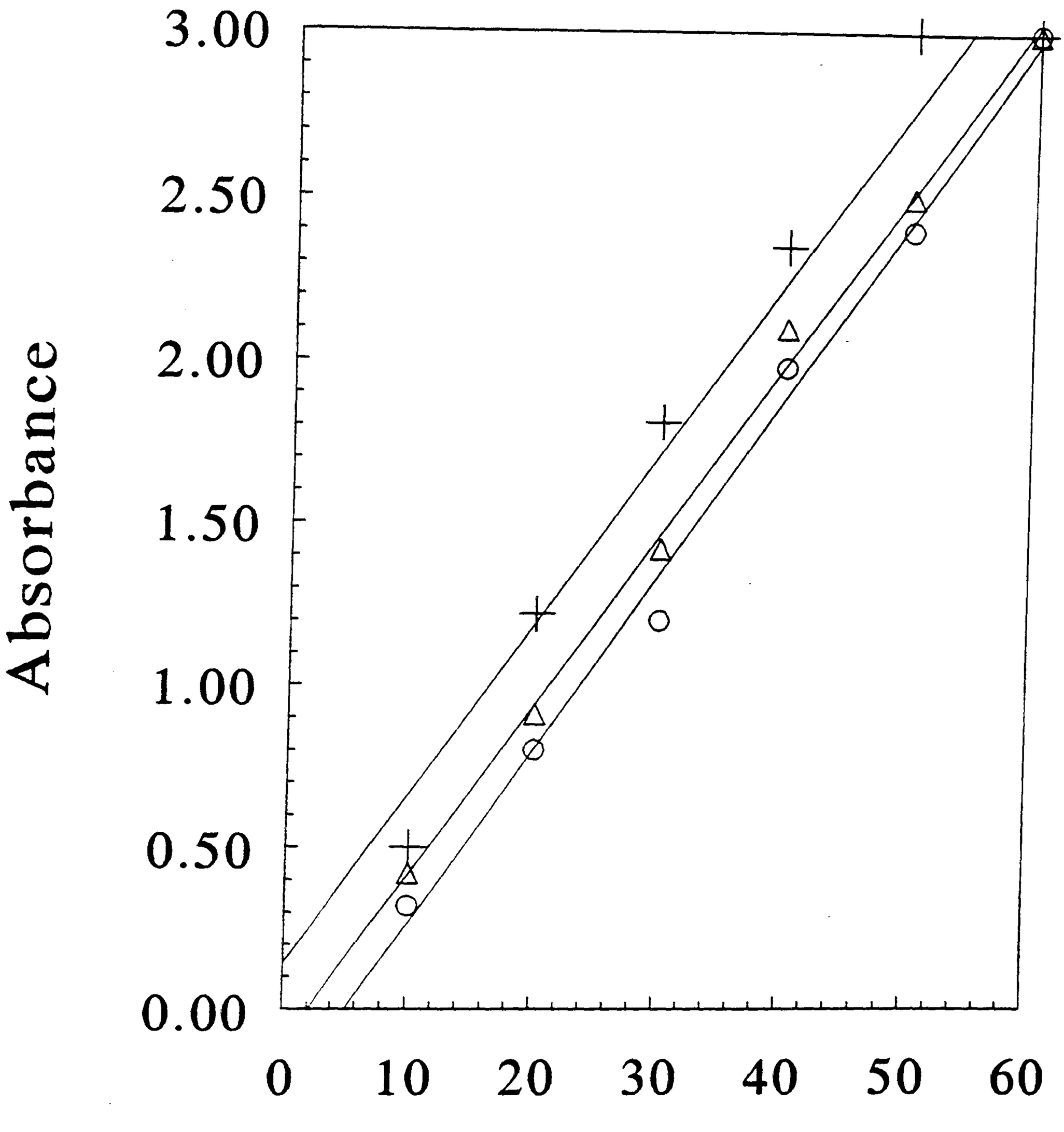

Figure 3.1b Typical rates as determined spectroscopically (300 nm) for various ratios of ethylenediamine to cadmium [Cd] = 0.018 mole dm^{-3}, [thiourea] = 0.018 mole dm^{-3}, 50 °C.

Various Growth Rates

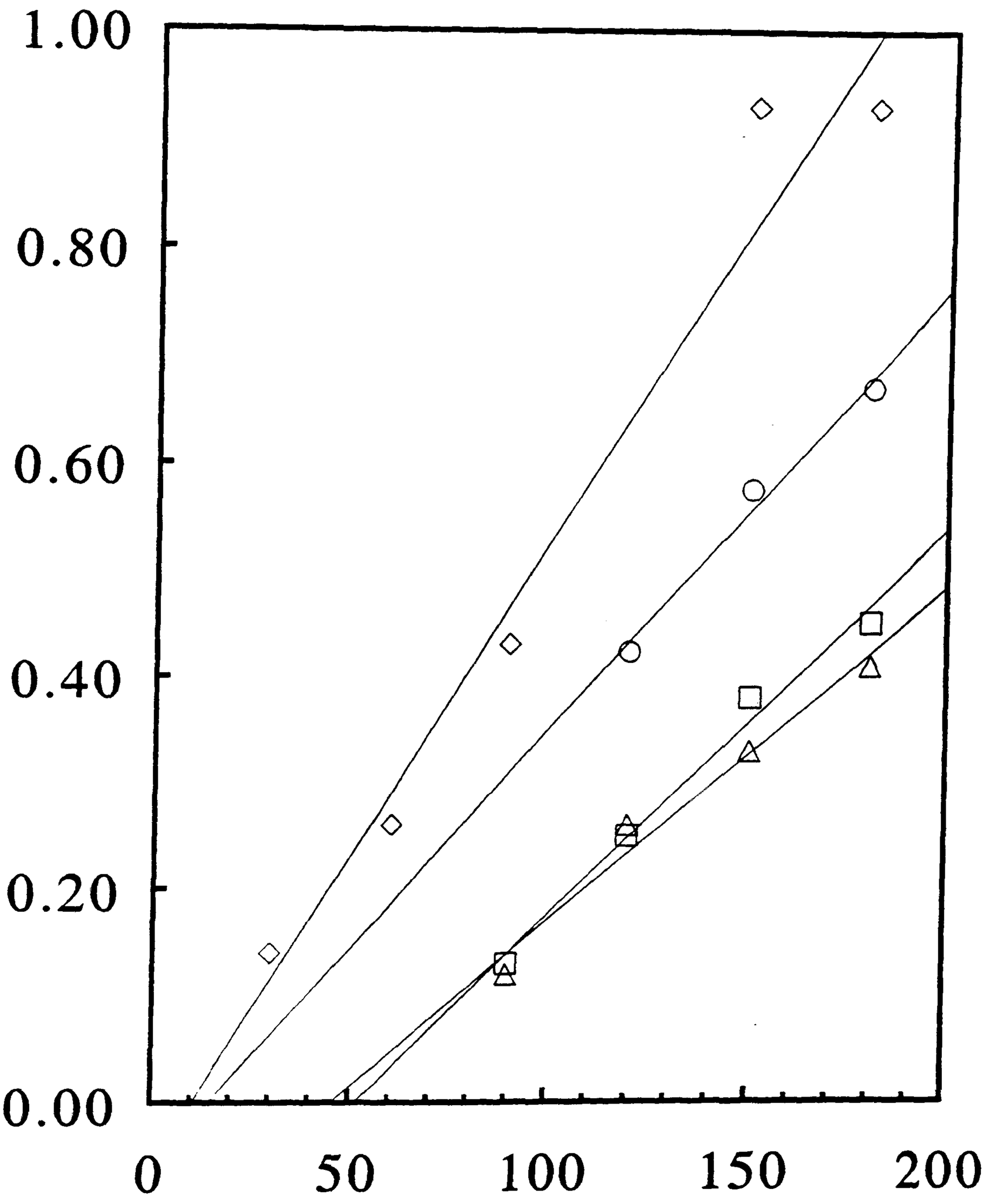

Figure 3.2 Thickness (microns) vs. time (minutes) for CdS grown on glass under various conditions in all cases [Cd] = 0.018 mole dm^{-3} , [thiourea] = 0.018 mole dm^{-3}, a. [Cd]:[en] = 1:3 , pH = 10.6, 40 °C, b. [Cd]:[en] = 1:3.5, pH = 11.0, 40 °C, c. [Cd]:[en] = 1:3.5, 45° C , pH = 11.0, d . [Cd]:[en] = 1:3 , pH = 10.5, 45 °C·

Film Quality

The experiments were usually terminated shortly after formation of the bulk precipitate and microscope glass slides or tin oxide coated glass were removed from the solution. The composition of cadmium and sulfur in the films have been confirmed by electron diffraction analytical X-ray (EDAX) using electron microscope as shown in figure 3.3.

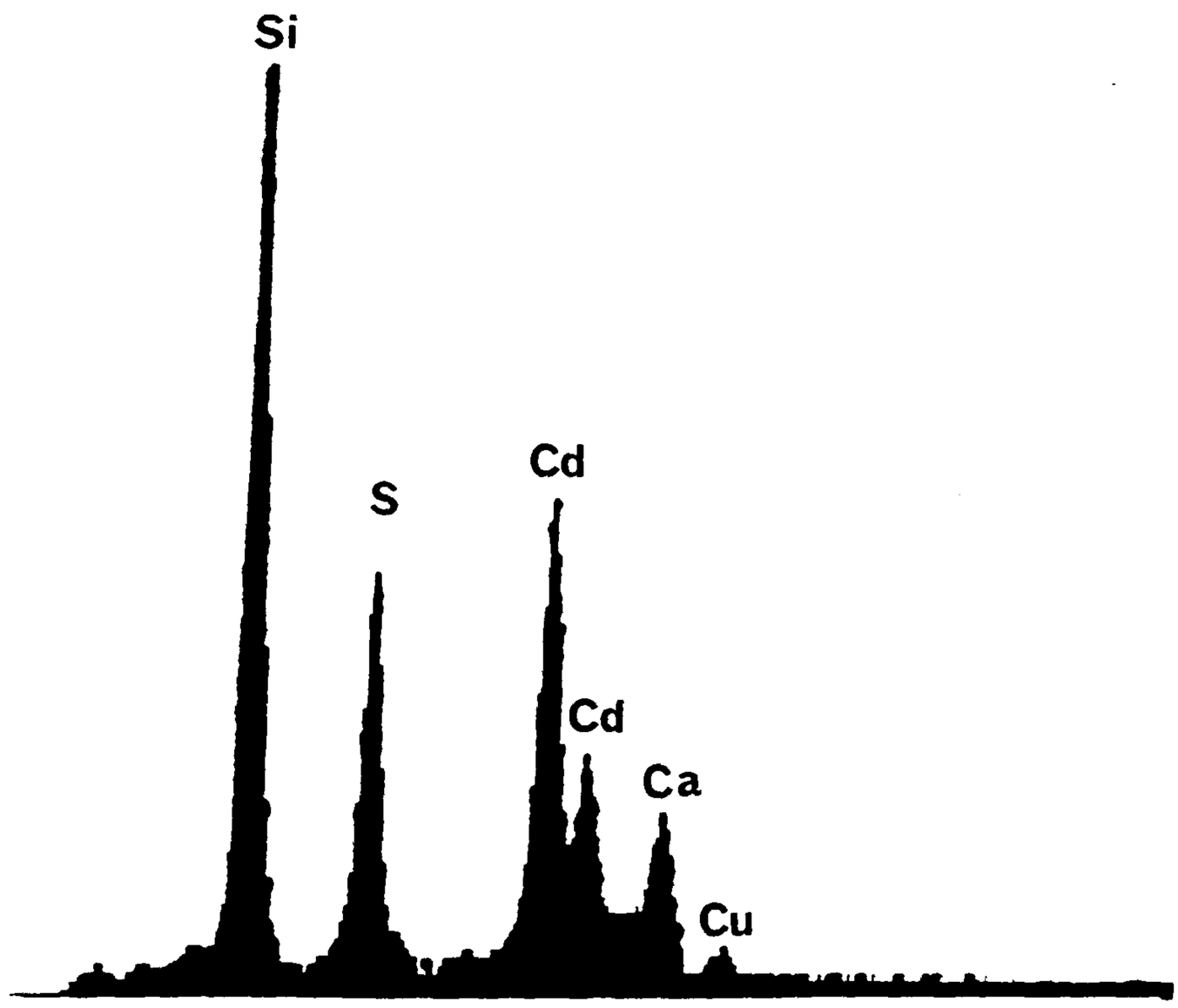

Figure 3.3 EDAX of CdS film deposited onto glass for 1 hour, [Cd] = 0.018 mole dm^{-3}, [thiourea] = 0.018 mole dm^{-3} at 40° C, pH = 11.0, [Cd]:[en] 1:3.5.

Adherent particles of bulk precipitate were removed by ultrasonication in distilled water. Some of these particles remained on the films and can be identified as scattered spherical particles that appear white in the micrographs because of charging. Two distinct morphologies of deposited CdS can be identified by scanning electron microscopy onto both substrates.

The most adherent and specular films deposited on glass slides at different period of time appear as in figure 3.4, these films consist of dense approximately 0.5 micron spherulites of cubic/hexagonal CdS. The size of the spherulites does not appear to increase with time in the deposition bath (figure 3.4 a-c). The pH values for the deposition of these films were in the range of 10.5 to 11.0. At higher values of pH (11.5 - 12.0), similar morphologies were observed but only very thin (ca 0.1μ) films were deposited. Such films were specularly reflecting and tightly adherent to the substrate surface and could not be removed by abrasion with a tissue. One important observation is that under these conditions there is little or no evidence for the growth of the particles forming the film figure 3.4 a-c. This observation is in contrast to those of Rieke and Bentjen [17] who for growth on silicon, at room temperature, over long periods of time, observed particulate growth in the CdS film.

The morphology of a typical film obtained at pH 9.0 to 10.5 is shown in figure 3.5. These films were thick uneven and powdery and could easily be removed by rubbing with a tissue; such films were deep in yellow colour and typically 1 to 2 microns thick with the distinctive morphology shown in figure 3.5.

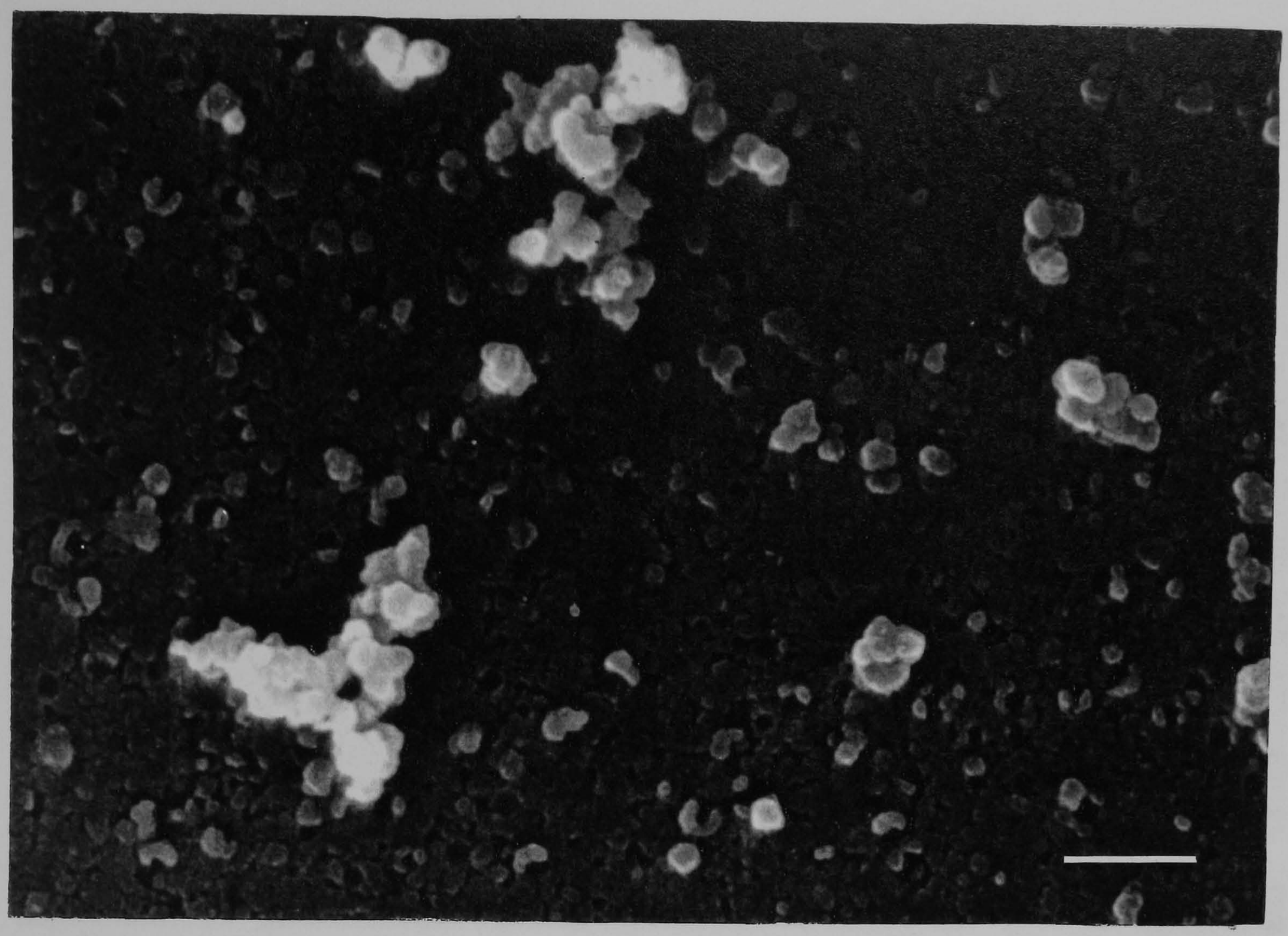

Figure 3.4a Scanning electron micrograph of specular CdS films deposited onto glass for 1 hour, [Cd] = 0.018 mole dm^{-3}, [thiourea] = 0.018 mole dm^{-3} at 40° C, pH = 11.0, [Cd]:[en] 1:3.5, ------ = 1 μ.

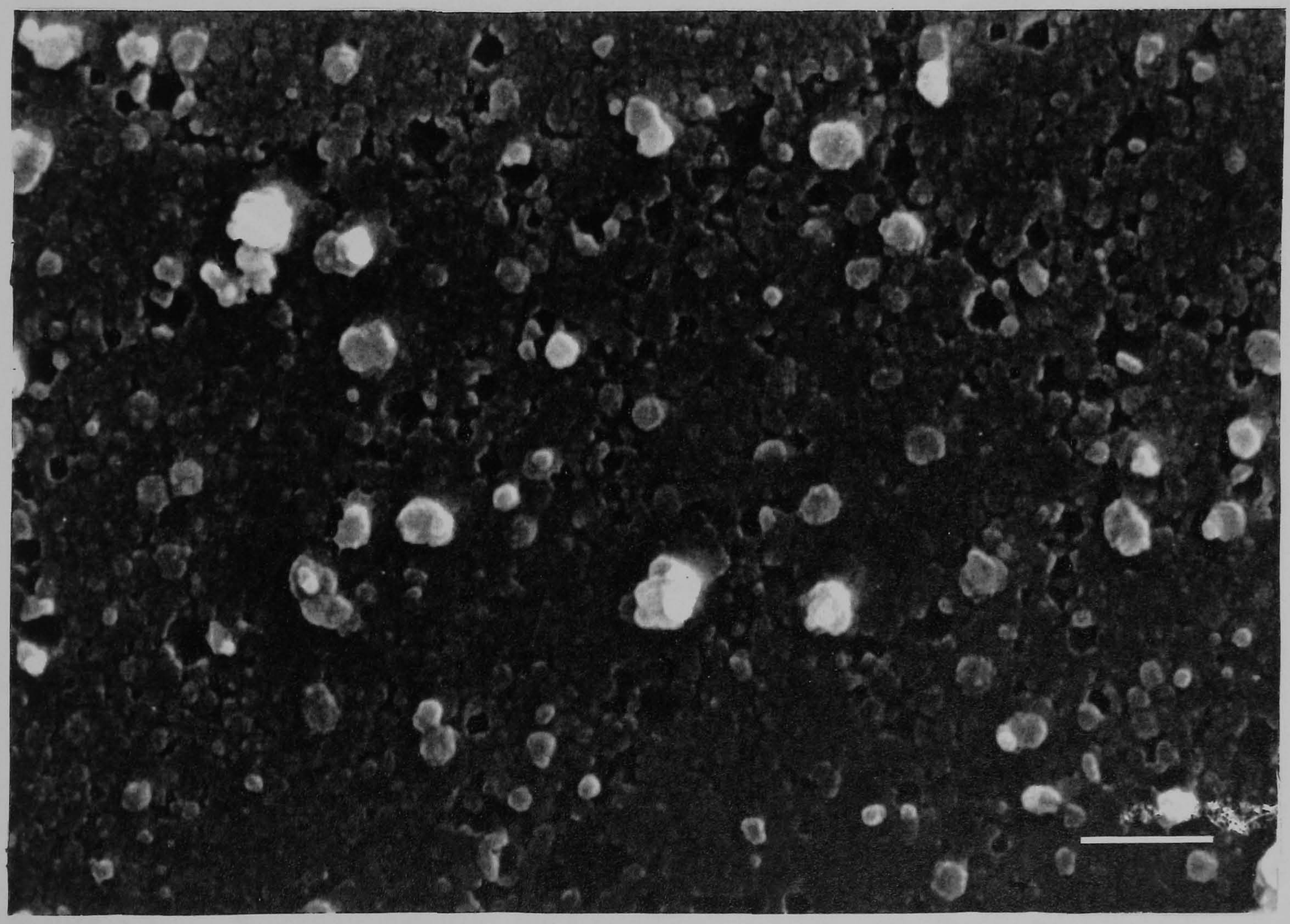

Figure 3.4b Scanning electron micrograph of specular CdS films deposited onto glass for 2 hours, [Cd] = 0.018 mole dm^{-3}, [thiourea] = 0.018 mole dm^{-3} at 40° C, pH = 11.0, [Cd]:[en] 1:3.5, ------ = 1 μ.

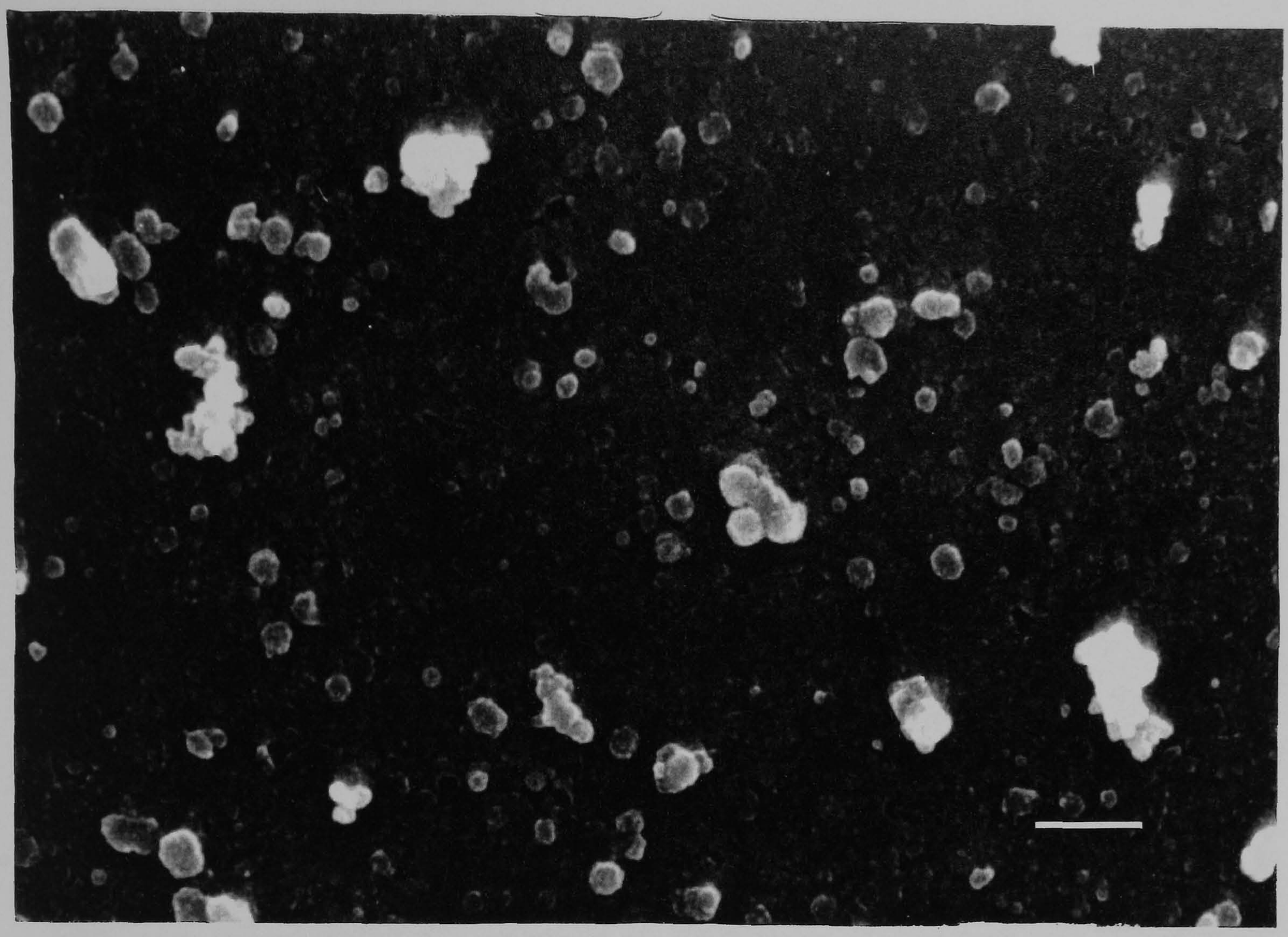

Figure 3.4c Scanning electron micrograph of specular CdS films deposited onto glass for 3 hours, [Cd] = 0.018 mole dm^{-3}, [thiourea] = 0.018 mole dm^{-3} at 40° C, pH = 11.0, [Cd]:[en] 1:3.5, ------ = 1 μ.

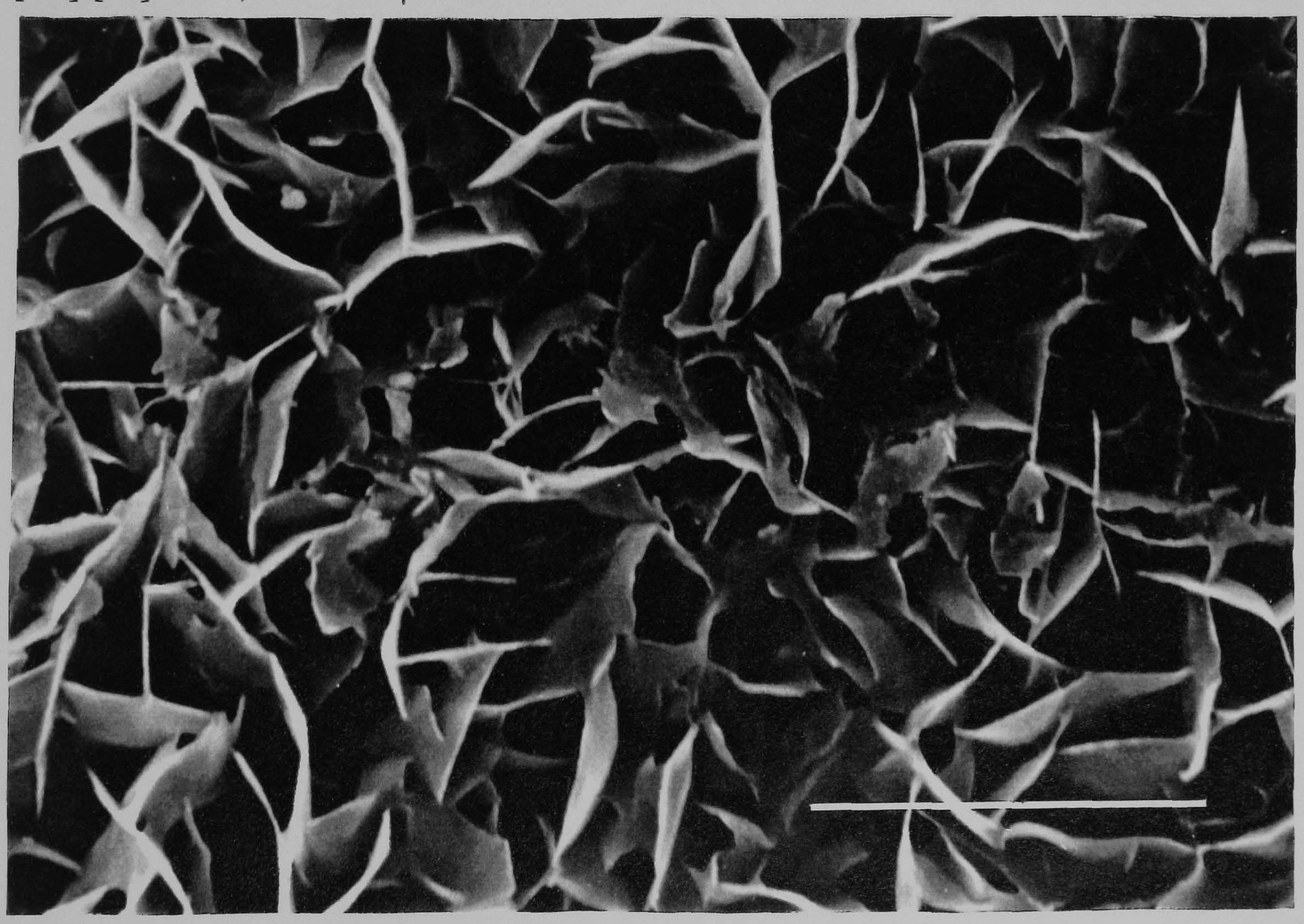

Figure 3.5 Scanning electron micrograph of a CdS film as grown on glass for 2 hours, [Cd] = 0.018 mole dm^{-3}, [thiourea] = 0.018 mole dm^{-3} at 40°C, pH = 10.2, [Cd]:[en] 1:2.5, ---------- = 1 μ.

At intermediate concentration of etylenediamine (pH 10.4 to 10.6) both types of morphologies were sometimes observed. A typical micrograph of such a film is shown in figure 3.6. The picture shows a secondary growth feature of the morphology typically seen at lower values of pH.

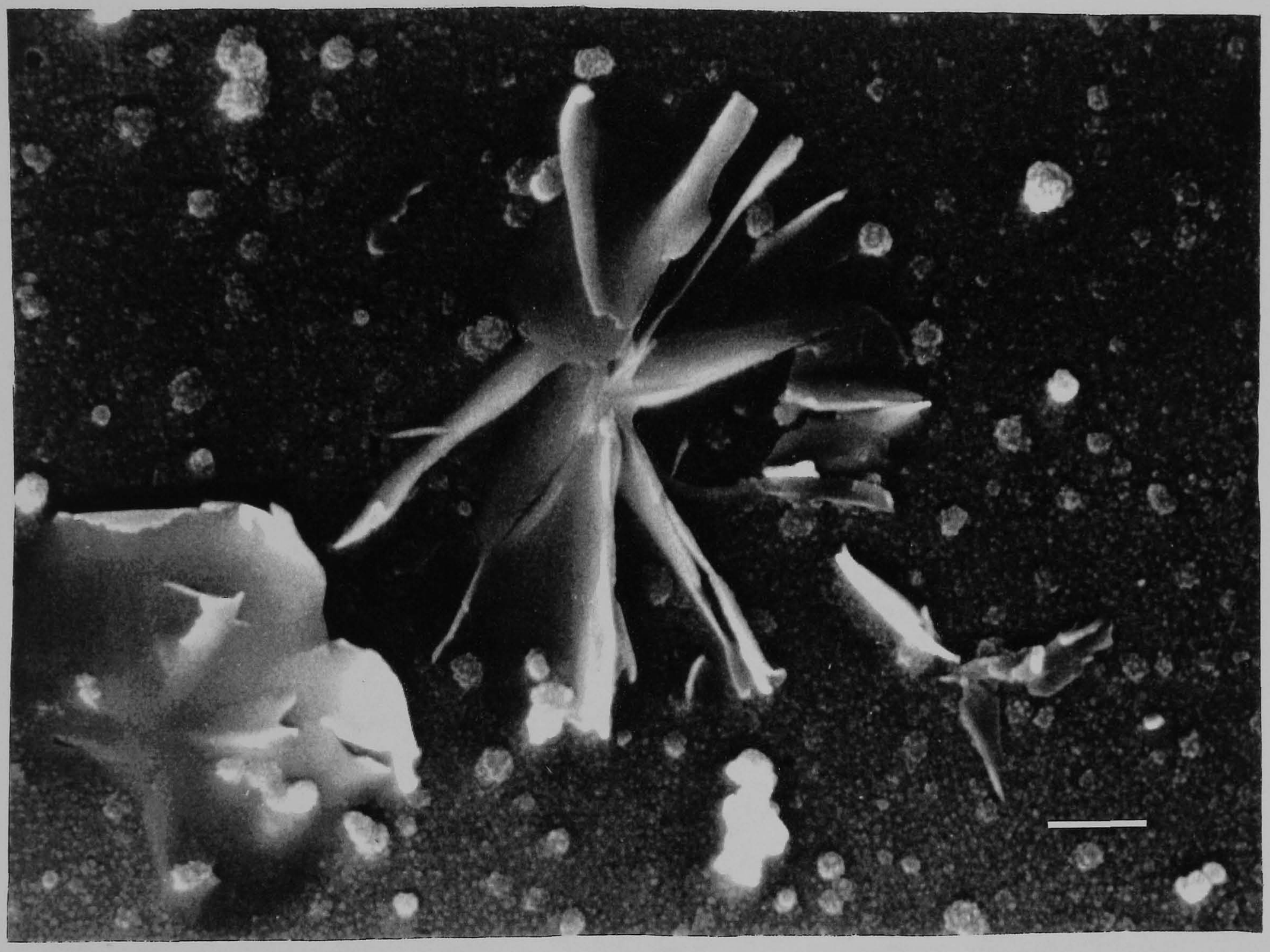

Figure 3.6 Scanning electron micrograph of a CdS film deposited onto glass for 2 hours at an intermediate value of pH = 10.5, [Cd] = 0.018 mole dm^{-3}, [thiourea] = 0.0.018 mole dm^{-3}, 50 °C, [Cd]:[en] 1:3, ------ = 1 μ.

Morphologies of CdS thin films on tin oxide coated glass were slightly different than on glass. A typical micrograph of specular and adherent CdS film on tin oxide is shown in figure 3.7. In comparison the films grown on glass were specular, adherent and uniform, whereas the films grown on tin oxide were cloudy and poorly reflecting.

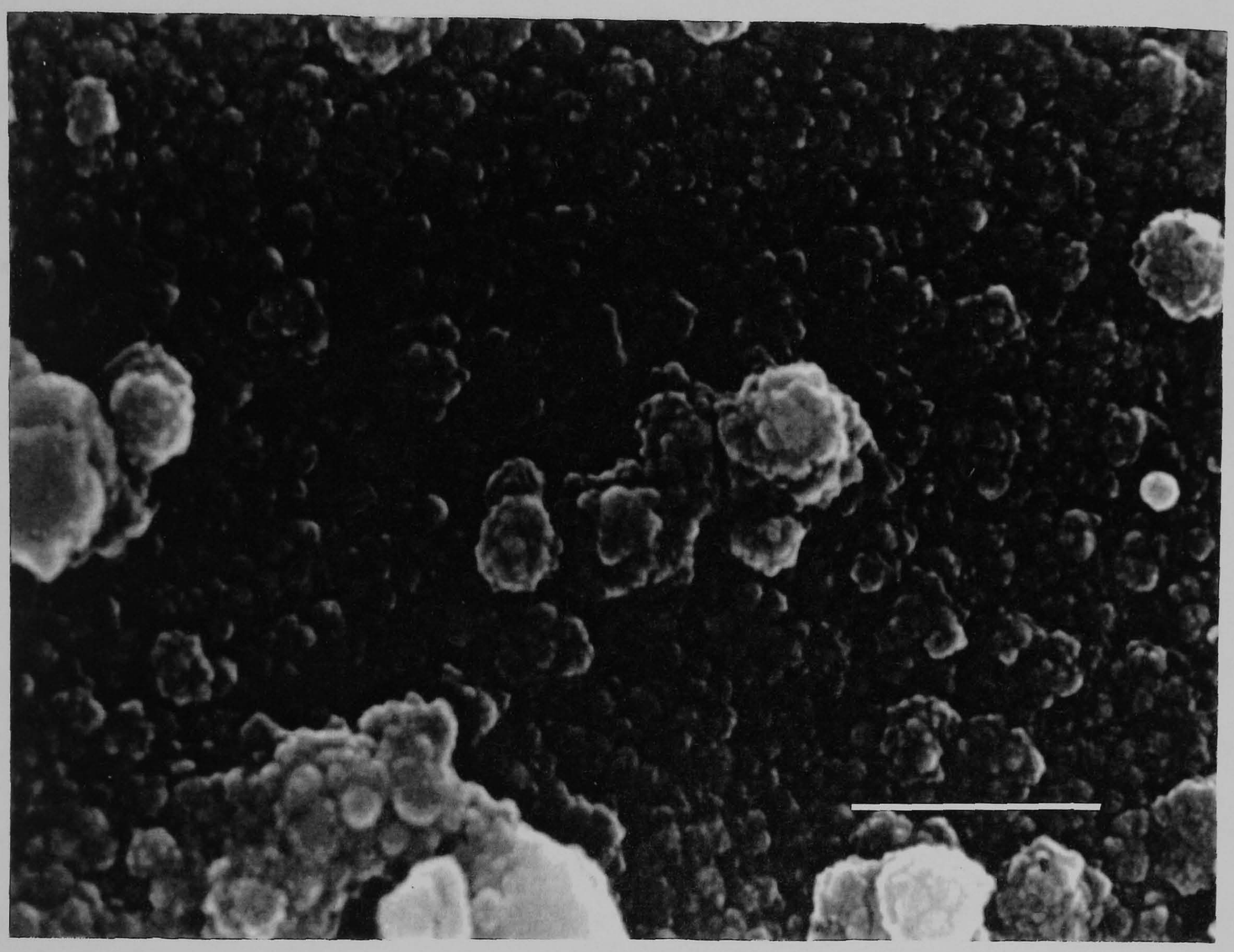

Figure 3.7 Scanning electron micrograph of specular CdS film deposited onto tin oxide coated glass for 3 hours, [Cd] = 0.018 mole dm^{-3}, [thiourea] = 0.018 mole dm^{-3} at 40 °C, pH = 11.0, [Cd]:[en] 1:3.5, ---------- = 1 μ.

Structural studies

Cadmium sulfide exists in both hexagonal (α-CdS, Greenokite) and cubic (β-CdS, Hawleyite) forms and polytypes are also known. There have been a number of studies of the phase deposited in chemical bath deposition (CBD) experiments. At room temperature, on silicon substrates using the ammonia thiourea system Rieke and Bentjen suggested that predominantly the cubic form was deposited [17]. In contrast Lincot et al, found that the initial layers formed from a similar system (but on carbon films supported on copper or gold grids at 60 °C) were composed of well defined crystallites of hexagonal CdS of the order of 10 nm in size [18]. However they also observed smaller colloidal particle formed in solution (3 - 6 nm) which had a mixed hexagonal/cubic structure. Similarly Chu et al. concluded that the films of CdS they deposited onto SnO_2 were polytypical and only poorly crystalline films were obtained on glass substrates [19].

In the present work some of the films were removed from the substrates and ground, which should obviate problems with preferred orientation. Powder X-ray diffraction patterns were also obtained for the bulk precipitates formed in the film deposition or by removing the thin films of CdS deposited onto glass are reported in table 3.2. The X-ray powder diffraction results for films removed from microscope slides under various condition are however equivocal as all the lines observed could be assigned to either the hexagonal or cubic form, table 3.2. X-ray diffraction pattern of a thick intact film grown on glass (3h, ca 1 micron thick, 50 °C, [Cd]:[en] = 1:3.5, pH = 11.0) is shown in figure 3.8 and there is some evidence for the hexagonal phase, but this identification depends on the very weak line 36.10° close to the expected position of the 102 reflection (2θ , 36.6°).

Table 3.2 Powder diffraction results for CdS grown at different temperature for 2 hours.

CdS[a] (50 °C)	CdS[a] (45 °C)	CdS[b] (40 °C)	ASTMS (Cubic)	CdS[c] (50 °C)	ASTMS (Hexagonal)
3.34 (m)	3.32 (m)	3.32 (w)	3.35	3.60	3.59
2.97 (m)	2.94 (w)	2.93 (m)	2.90	3.31	3.36
----	----	----	----	3.10	3.16
2.03 (m)	2.05 (w)	2.05 (m)	2.05	2.06	2.07
1.75 (s)	1.75 (s)	1.74 (s)	1.75	1.73	1.73
1.66 (w)	1.65 (m)	1.67 (m)	1.67	----	----
1.46 (w)	1.45 (w)	1.45 (w)	1.45	----	----
----	----	----	1.19	1.18	1.19

[Cd] = 0.018 mole dm^{-3}, [thiourea] = 0.018 mole dm^{-3}, pH = 11.00, [Cd]:[en], 1:3.5

w = weak, m = medium, s = strong

a. powder removed from substrate

b. powder collected from reaction bath

c. Calculated from electron diffraction pattern

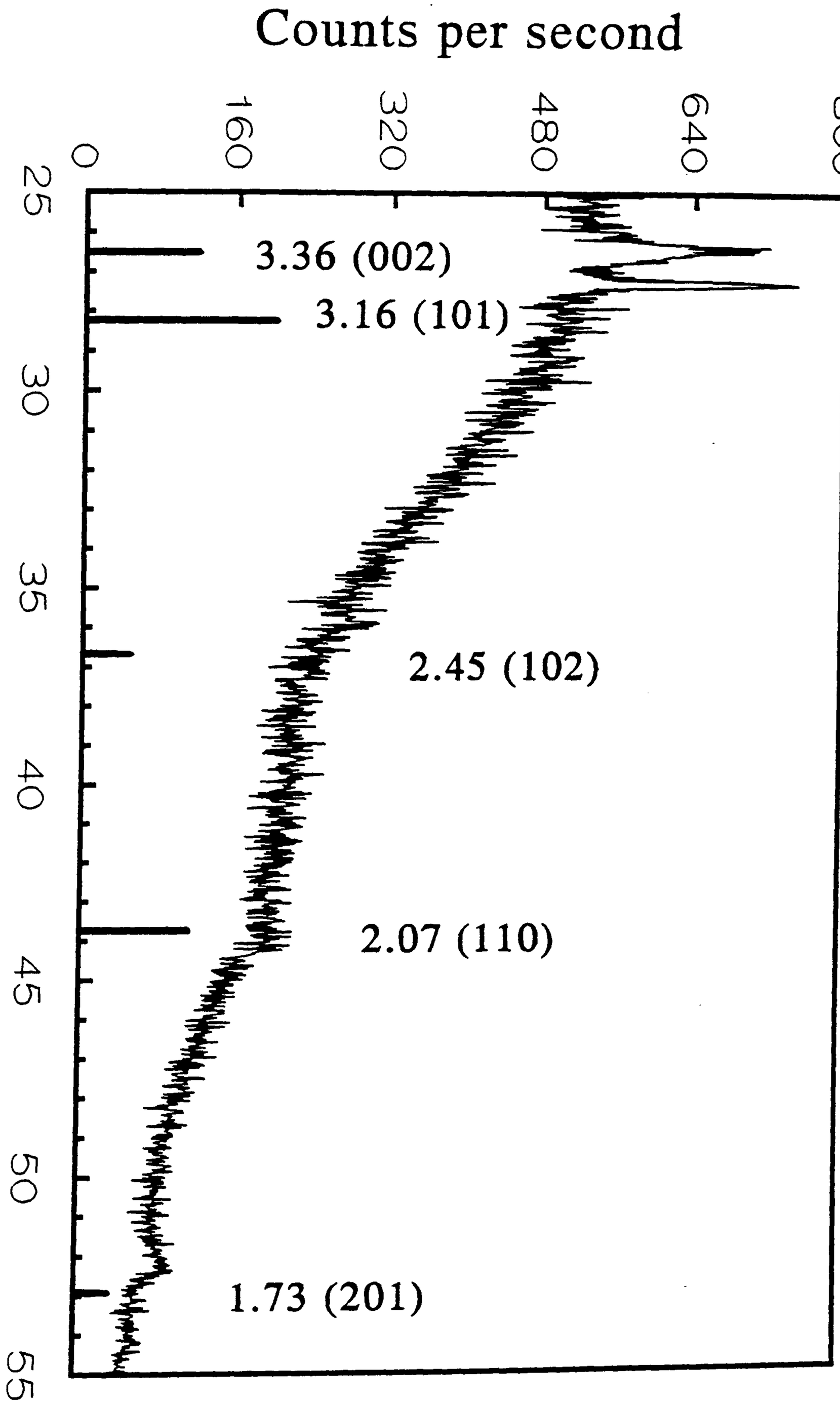

Figure 3.8 X-ray diffraction pattern of CdS film grown on glass for 1 hour, [Cd] = 0.018 mole dm^{-3}, [thiourea] = 0.018 mole dm^{-3} at 40 °C, pH = 11.0, [Cd]:[en] 1:3.5.

A more detailed study of the deposited cadmium sulfide was carried out by high resolution transmission electron microscopy (HR-TEM). A typical micrograph is shown in figure 3.9. Lattice fringes are continuous all over the micrograph with a spacing of 3.19 Å corresponding to the 101 reflection of hexagonal CdS (3.164 Å). This assignment is confirmed by the electron diffraction pattern of the same material as shown in figure 3.10. The principle diffractions closely correlate well with hexagonal CdS (table 3.2).

Figure 3.9 High-resolution transmission electron micrograph of CdS film removed from glass, growth conditions: [Cd] = 0.018 mole dm^{-3}, [thiourea] = 0.018 mole dm^{-3} at 50 °C, pH = 11.0, [Cd]:[en] 1:3.5, 3h.

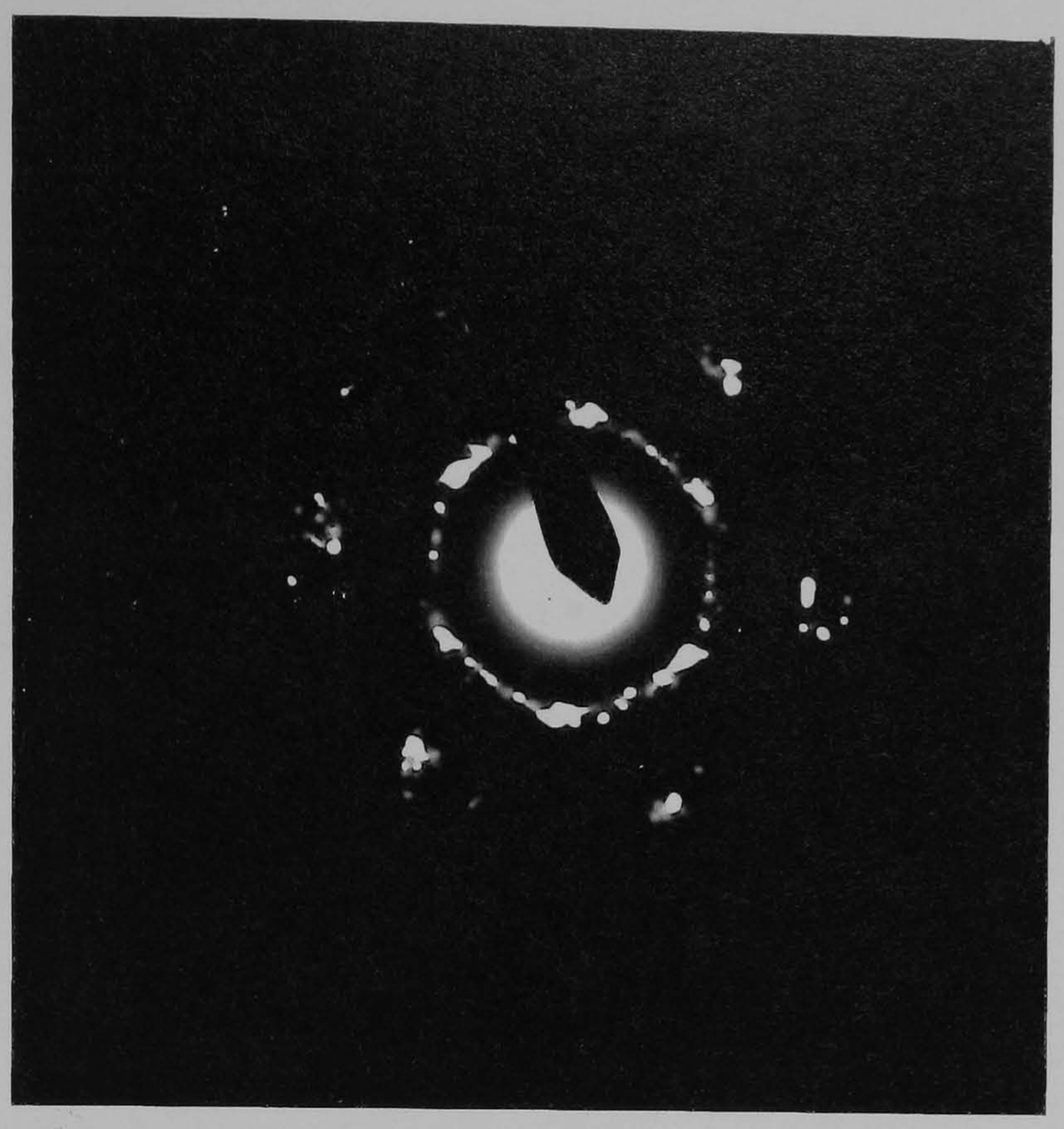

Figure 3.10 Electron diffraction pattern of CdS film removed from glass, growth conditions: [Cd] = 0.018 mole dm^{-3}, [thiourea] = 0.018 mole dm^{-3} at 50 °C, pH = 11.0, [Cd]:[en] 1:3.5, 3h.

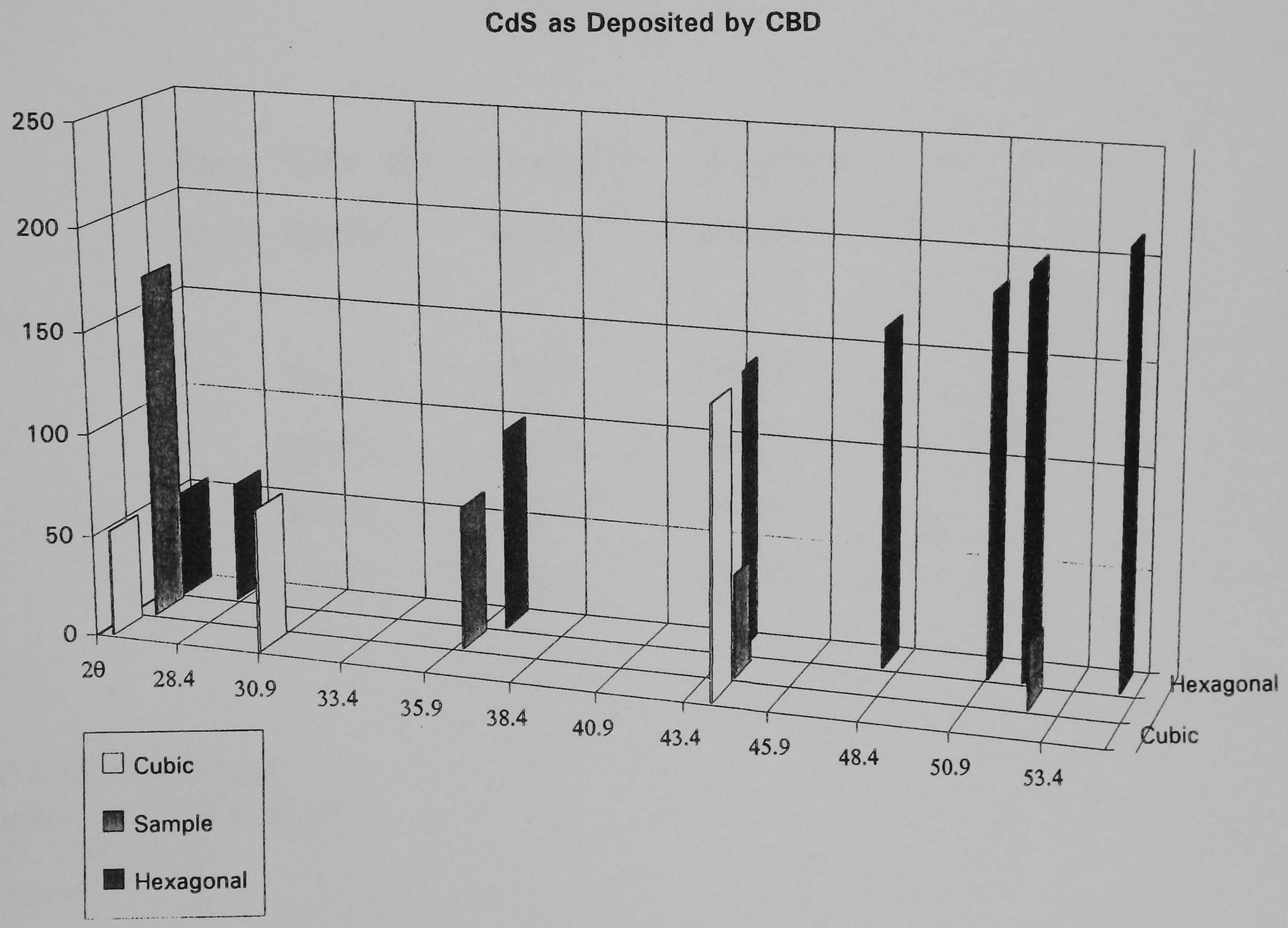

Figure 3.11 Phase of deposited CdS.

Factors Controlling Film Quality

During the deposition experiments growth was generally limited to the surface of the substrate and the walls of the reactor. The speciation of the bulk of the cadmium in the solution was assessed by measuring the ^{113}Cd nmr spectra. The chemical shift of cadmium in the deposition solution at different temperature showed little or no variation with time, the results are summarized in Table 3.3. Cadmium chemical shifts are remarkably sensitive to the chemical environment at the cadmium centre. It can be concluded that the bulk species in the solution is not varying due to the deposition.

Table 3.3 ^{113}Cd nmr data for deposition bath at various interval of time at different temperatures.

Time (hours)	Temp 50°C δ(ppm)	Temp 45°C δ(ppm)	Temp 40°C δ(ppm)
1	360.27	372.23	379.92
2	360.04	372.13	379.31
3	360.01	372.15	379.80
4	360.00	372.63	379.90

[Cd] = 0.018 mole dm^{-3}
[thiourea] = 0.018 mole dm^{-3}
[Cd] : [en] = 1:3.5
pH = 11.0

There have been several suggestions that the presence of a supersaturated concentration of hydroxy species in the deposition bath is essential for the production of high quality films [20]. We have tested this hypothesis by modelling the equilibrium in solution. The constant used were obtained from Martell et al. [12] and a typical set of input parameters are summarized in table 3.4. Speciation diagrams were calculated for several different composition, (ratios of [Cd] to [en]) as a function of pH . Using the output of the programme the point at which "$Cd(OH)_2$" would just precipitate was calculated using K_{sp} (2.44 x 10^{-14} at 50 °C) a typical speciation diagram is shown in figure 3.11. The solid line represents the point at which the hydroxide should precipitate or at which solutions are first likely to be supersaturated in a hydroxy species.

Table 3.4 Typical Input Parameters for Calculating Speciation

Species No.	Log B_{ijkl}	Stoichiometry i	j	k	l
1	1.180	0	1	0	1
2	1.330	1	1	0	0
3	2.180	1	2	0	0
4	2.700	1	3	0	0
5	3.300	1	4	0	0
6	9.160	0	0	1	1
7	15.560	0	0	1	2
8	5.080	1	0	1	0
9	9.160	1	0	2	0
10	10.520	1	0	3	0

Stoichiometric coefficients: i. cadmium, j. thiourea, k. ethylenediamine, l. H.

Values are from Reference [12], and correct to 50° C as described therein, the solubility product of '$Cd(OH)_2$' was taken as 2.44 x 10^{-14}.

Cadmium Speciation

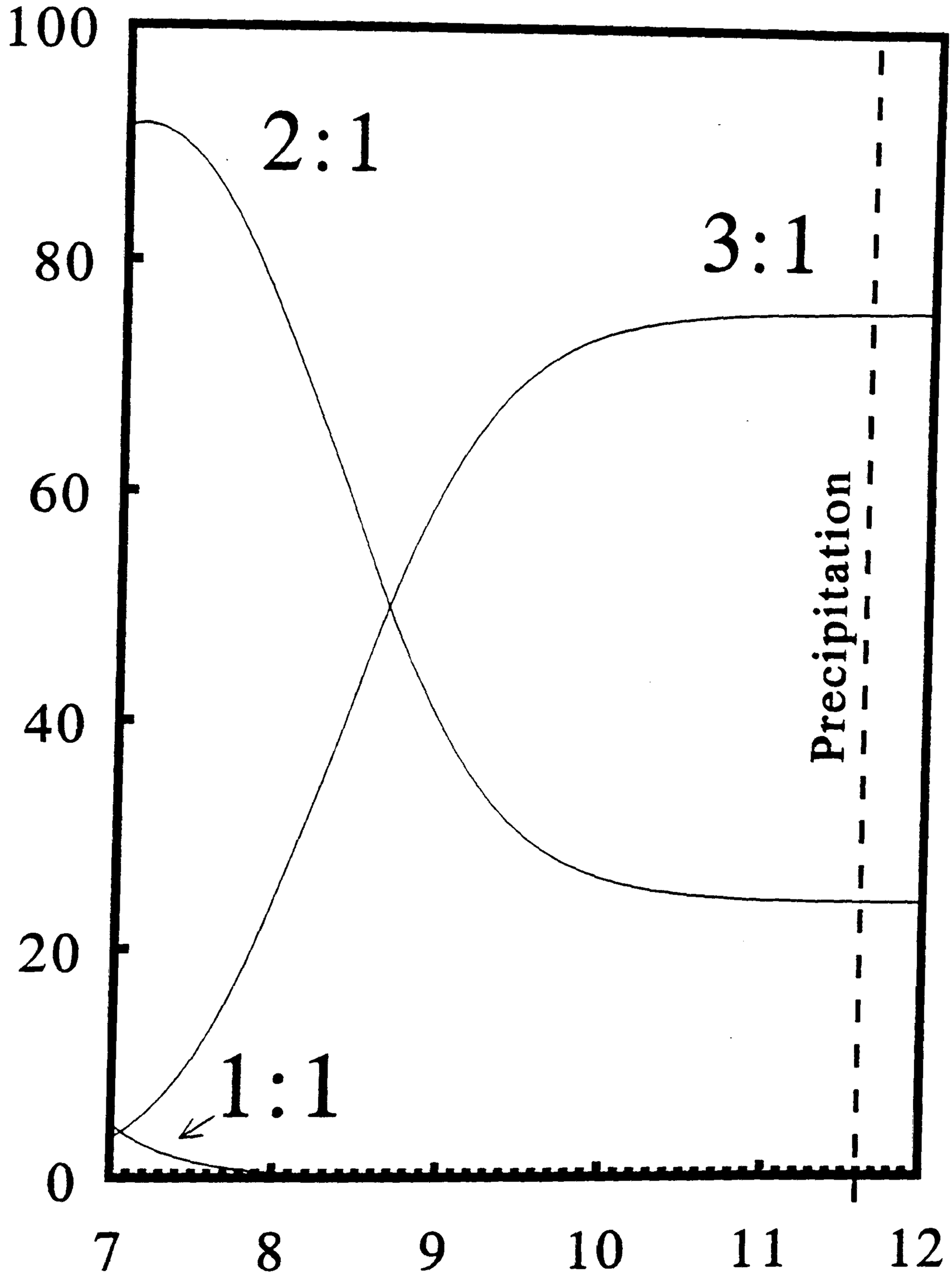

Figure 3.12 Typical Speciation Diagram
[Cd] = 0.018 mole dm^{-3}, [thiourea] = 0.018 mole dm^{-3}, [en] = 0.065 mole dm^{-3}.
Using the data in Table 3.4.

There is no simple relationship between pH and "$Cd(OH)_2$" supersaturation because pH controls the extent of hydrolysis of Cd (the hydroxide ion concentration) and the complexation by ethylenediamine. Cadmium forms a variety of complexes with hydroxide, and in moderately basic solution a "$Cd(OH)_2$" precipitate will form. The presence or absence of this precipitate was considered by Kaur et al. [20] and Kitaev et. al. [21] to be particularly important in the formation of good quality films. Because of the influence of pH on amine concentration and hence on free cadmium concentration, the cadmium hydroxide speciation and conditions for precipitation are not dependent on pH in similar manner. In addition, the formation of a precipitate is often dependent on kinetic factors influencing formation and resolution of the precipitate.

I have tried to establish by our modelling if the supersaturation of hydroxy species of cadmium is an important factor controlling the quality of the films of CdS formed. The results of these calculations and observations are summarized in figure 3.12, in which the solid line represents the point at which the solution becomes supersaturated with respect to "$Cd(OH)_2$". The different symbols represent specular good quality films (figure 3.4) and powdery low quality films (figure 3.5), the correlation with supersaturation of the hydroxy complexes is excellent. The ethylenediamine/thiourea/cadmium acetate system can be used to deposit polycrystalline films of CdS of good quality. The supersaturation of the solution with respect to hydroxy-complexes of cadmium appears to be the key factor controlling the quality of the films deposited. The mechanism of the deposition of the films must involve both the hydrolysis of thiourea to generate sulfide ions and their subsequent reaction with cadmium. The fact that the best films are deposited when "$Cd(OH)_2$" is supersaturated may suggest that the interaction of thiourea with a hydroxy complex of cadmium

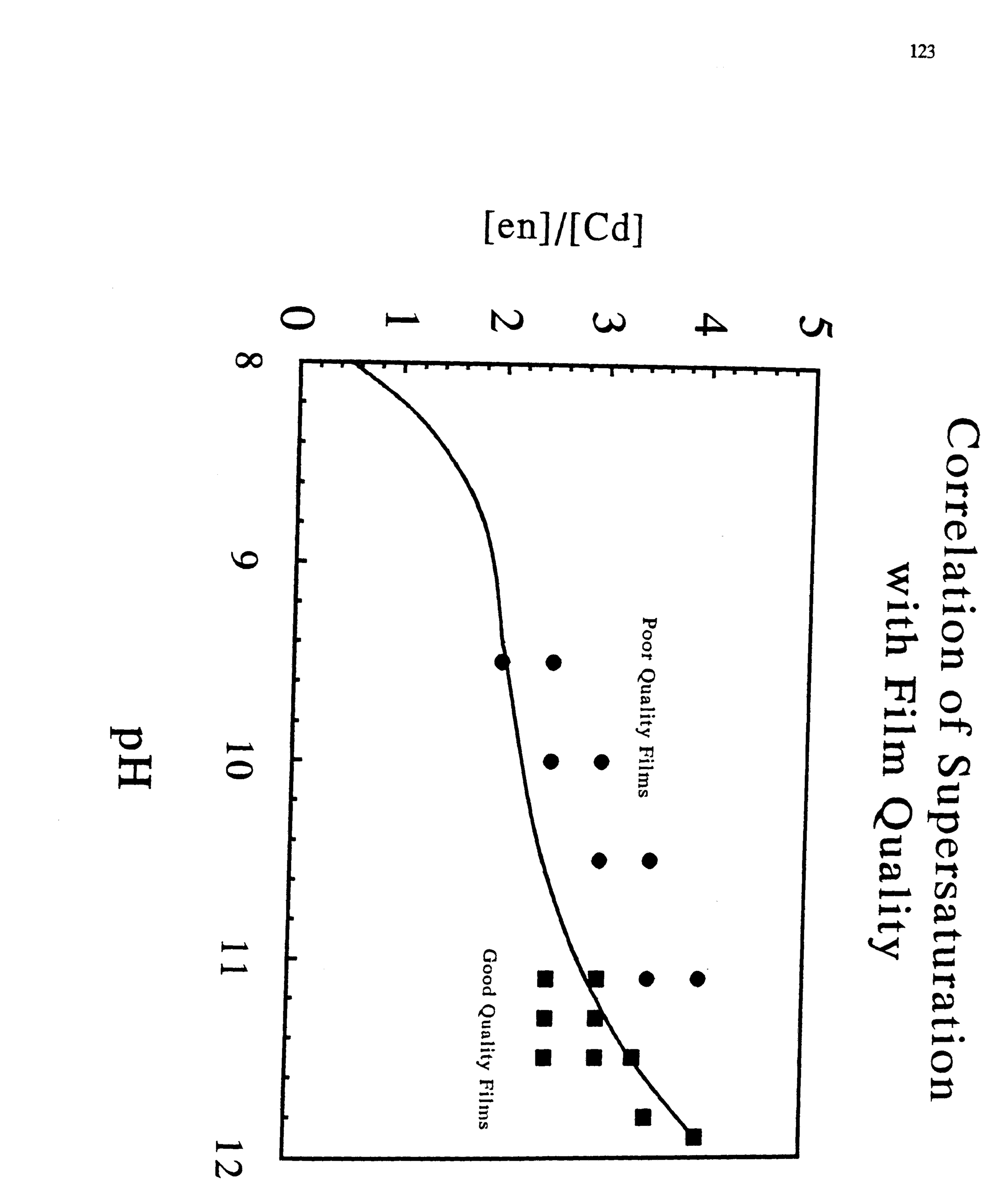

Figure 3.13 Speciation diagram, solid line theoretical limit for hydroxide precipitation, [■] adherent and specular films, [●] powdery films.

is an important step in the deposition. In contrast to the results of Reike we do not see any evidence for the growth of the microcrystals which form the thin film. There are significant differences between experimental conditions used. For example in the work by Reike, silicon substrates and elevated temperatures were used, where as in this work glass and tin oxide substrates and lower temperatures were used.

The absorption spectra of CdS films on both glass and tin oxide coated glass were recorded in the wave length range of 300 - 700 nm. The band gap values were found to be 2.42 eV (literature value 2.425 eV) [22] on both glass and tin oxide coated glass. In general uniform and good morphology films were grown onto glass substrate as compared to tin oxide coated glass.

The precise mechanism responsible for the deposition of good quality thin films of CdS is far from clear temperature, substrate and the chelating agent used, all play a role in controlling film quality. However supersaturation with hydroxy complexes is probably the most important factor controlling the quality of CdS films deposited.

3.3.2 ZnS thin films

Zinc sulfide is a wide band gap (3.65 eV) II-VI material. A substantial effort has been directed at the preparation of zinc sulfide thin films for use in electroluminescent displays [23,24], cathodluminescent displays and multilayer dielectric filters [25,26]. Zinc sulfide is transparent from the mid-infrared through the visible region, and films can be used in optical phase modulation, IR antireflection coating and as light guides and in integrated optics [27-29]. Thin films of zinc sulfide have been prepared by a wide range of methods including evaporation [30], sputtering [31], metal organic chemical vapour deposition (MOCVD) [32], molecular beam epitaxy (MBE) [33] and electrodeposition

[34]. Chemical bath deposition is an alternative method which is a simple, convenient and cheap. Thin films of zinc sulfide deposited by this method can be of reasonable quality and have been characterized by a number of techniques.

Factors Controlling Film Quality

During the deposition experiments the growth was generally limited to the surface of the substrate and the walls of the reactor. There are several factors which can effect the quality of the deposited ZnS films.

In all these experiments the concentration of zinc sulfate (0.025 M) and thiourea (0.035 M) was kept constant. Thin films of ZnS have been deposited at a wide range of ammonia (0.25 - 2.0 M) and hydrazine (1.0 - 4.0 M) concentration. Both ligands play an important role in controlling the nature of the phase deposition. The minimum amount of ammonia required, in the presence of hydrazine to deposit ZnS is 0.5 M. At ammonia concentration of 0.5 M, and with hydrazine less than 3.0 M in the deposition bath "$Zn(OH)_2$" precipitates to deposit "$ZnO/Zn(OH)_2$" (figure 3.14). EDAX showed only zinc as main species present with no evidence of sulfur. Similar results were obtained for all films grown at hydrazine concentration less than 1.0 M. The best films of ZnS were deposited with ammonia (1.0 M) and hydrazine (3.0 M). Such films were uniform and specular as shown in figure 3.16.

pH is another important parameter for chemical bath deposition. In the experiments carried out it was noticed that pH had no effect on ZnS deposition in the pH range 10.0 to 11.0 . The results are summarized in figure 3.14.

Nature of Phase Deposited
pH = 11.0 or 10.5

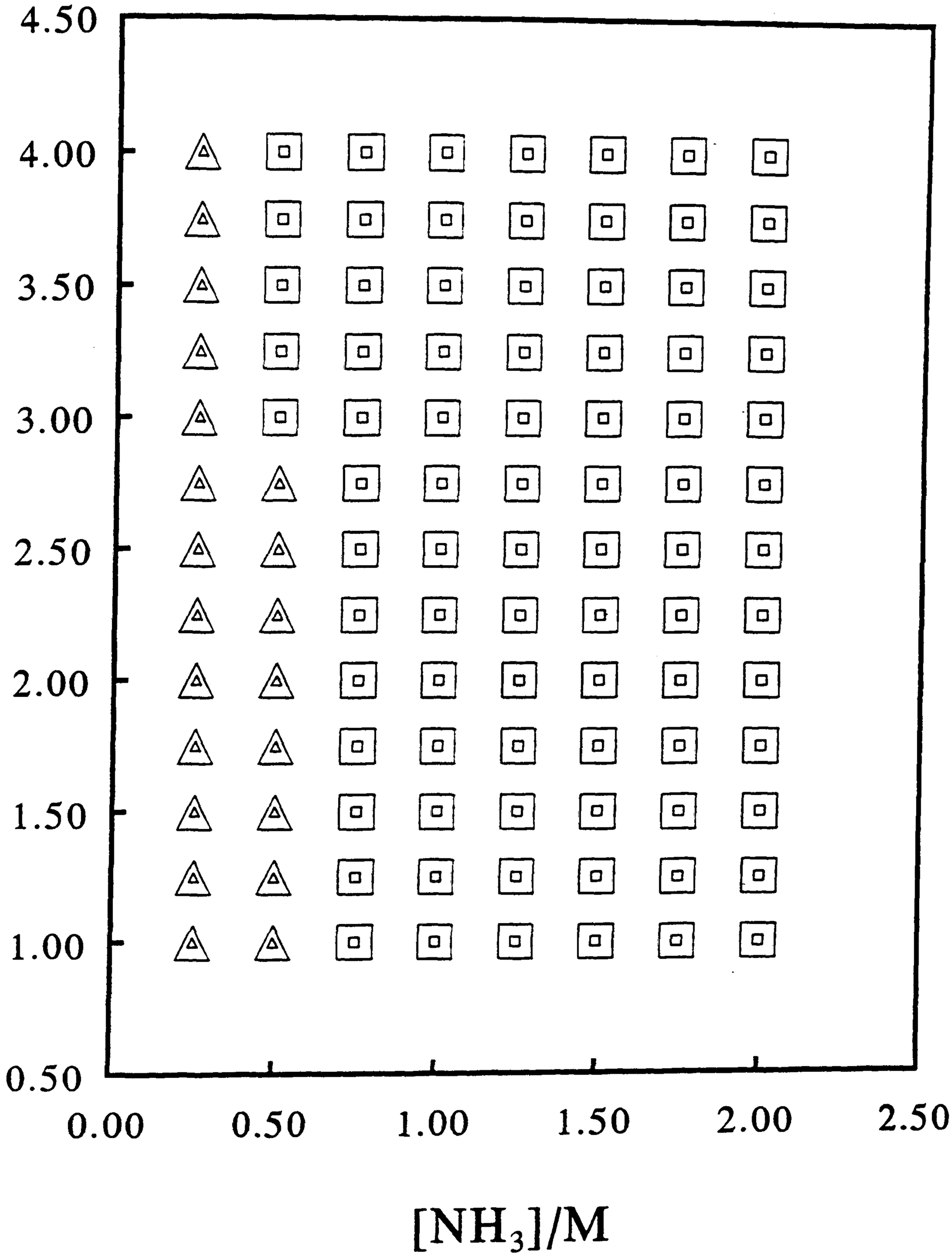

Figure 3.14 Nature of the Deposited Phase.

Film quality

Zinc sulfide films were grown on both glass microscope slides or tin oxide coated glass. The composition of zinc and sulfur in the deposited films have been confirmed by electron diffraction analytical X-ray (EDAX) using electron microscope as shown in figure 3.15. The bulk precipitates were removed by ultrasonication in distilled water. Some of these particles remained on the films and can be identified as scattered spherical particles that appear white in the micrographs because of charging.

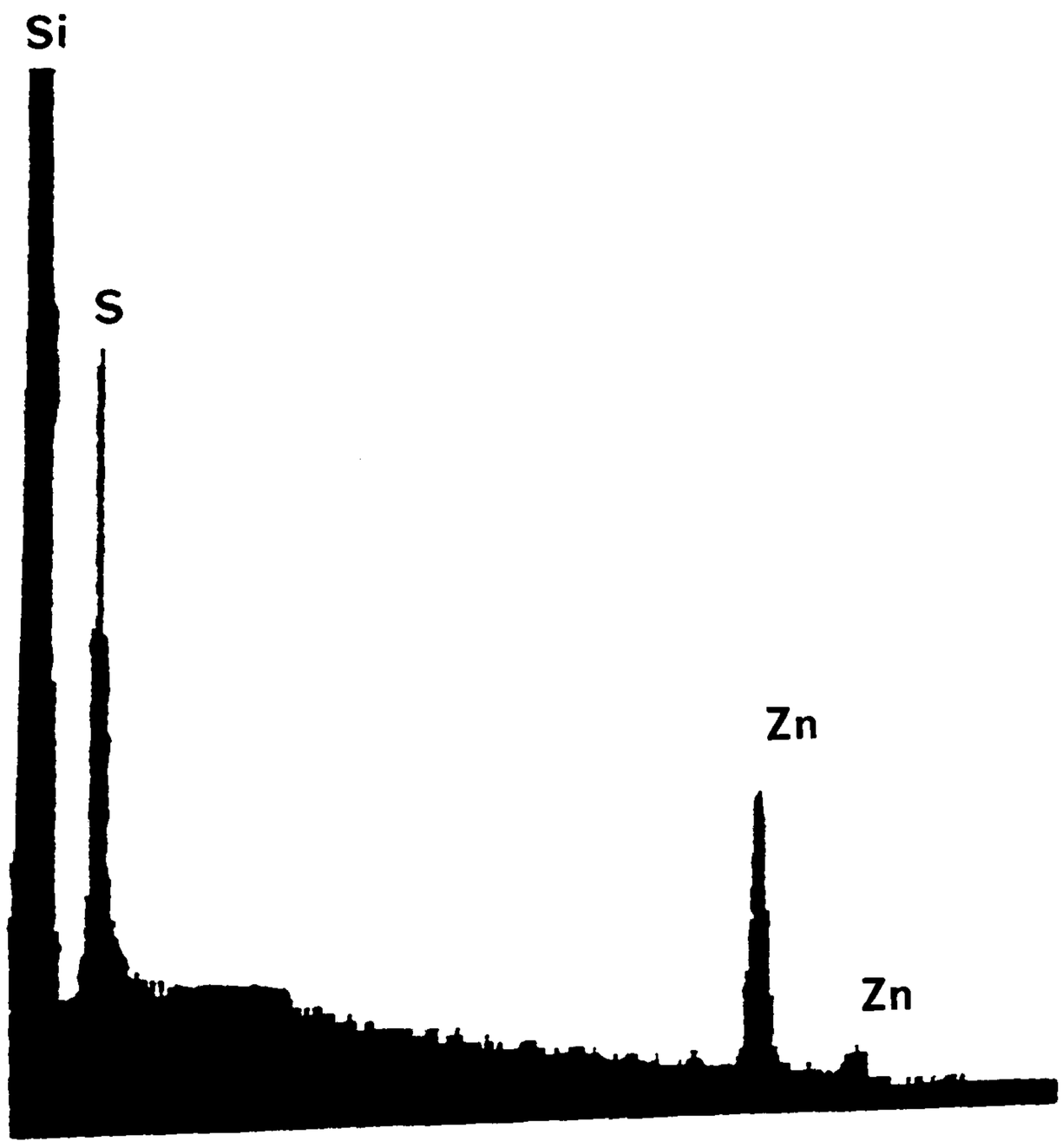

Figure 3.15 EDAX of ZnS film deposited onto glass for 1 hour, [Zn] = 0.025 mole dm^{-3}, $[NH_3]$ = 1.0 mole dm^{-3}, $[N_2H_4]$ = 3.0 mole dm^{-3}, [thiourea] = 0.035 mole dm^{-3} at 70 °C, pH = 10.2.

Scanning electron microscope has been used to study the morphology of the deposited films, only one type of morphology was observed using SEM. The most specular and adherent films were deposited at pH 10.0 - 10.5 with $[NH_3]$ = 1 mole dm^{-3}

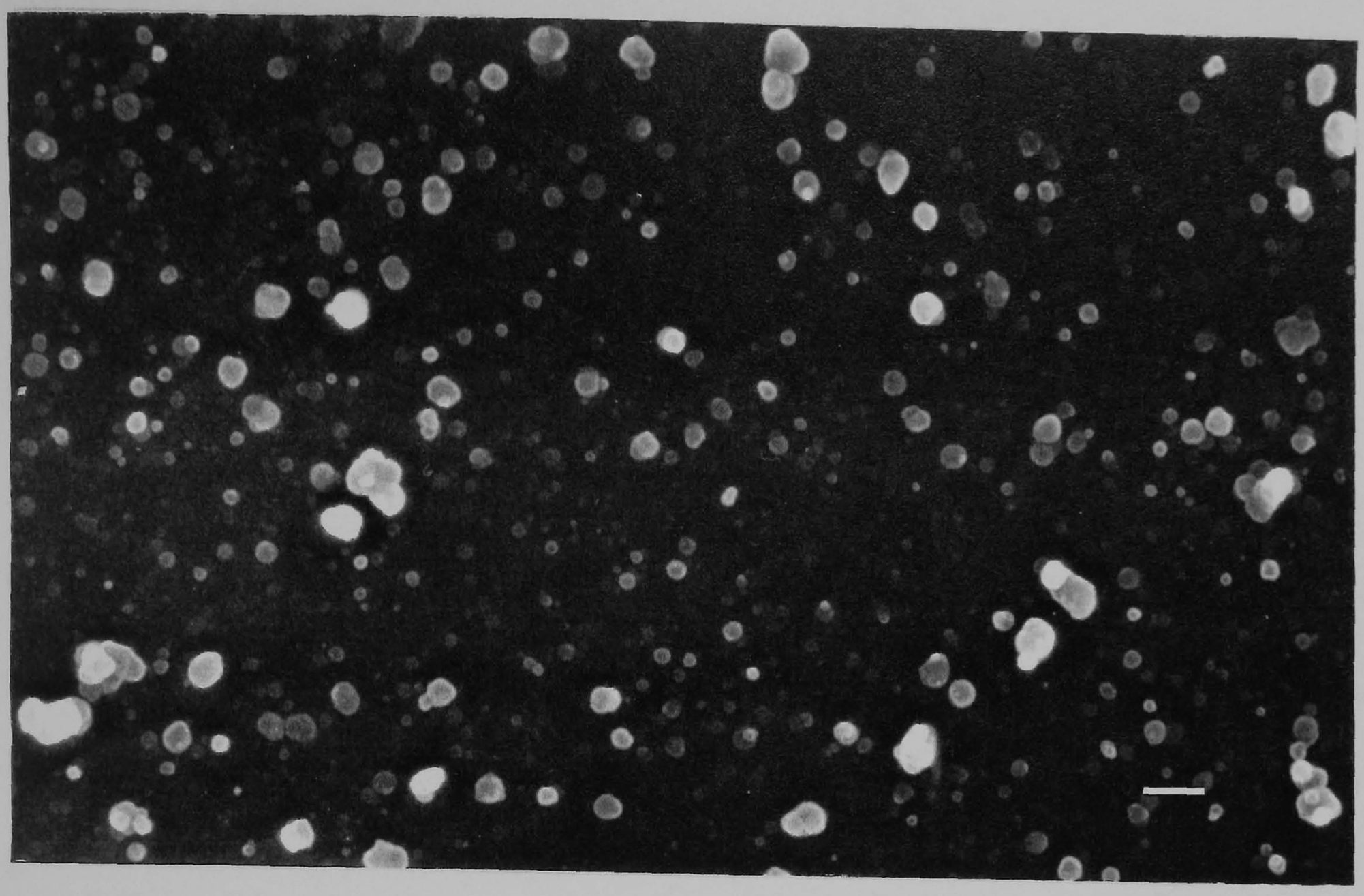

Figure 3.16a Scanning electron micrograph of ZnS film deposited onto glass for 1 hour, [Zn] = 0.025 mole dm^{-3}, $[NH_3]$ = 1.0 mole dm^{-3}, $[N_2H_4]$ = 3.0 mole dm^{-3}, [thiourea] = 0.035 mole dm^{-3} at 70 °C, pH = 10.2, ---- = 1 μ.

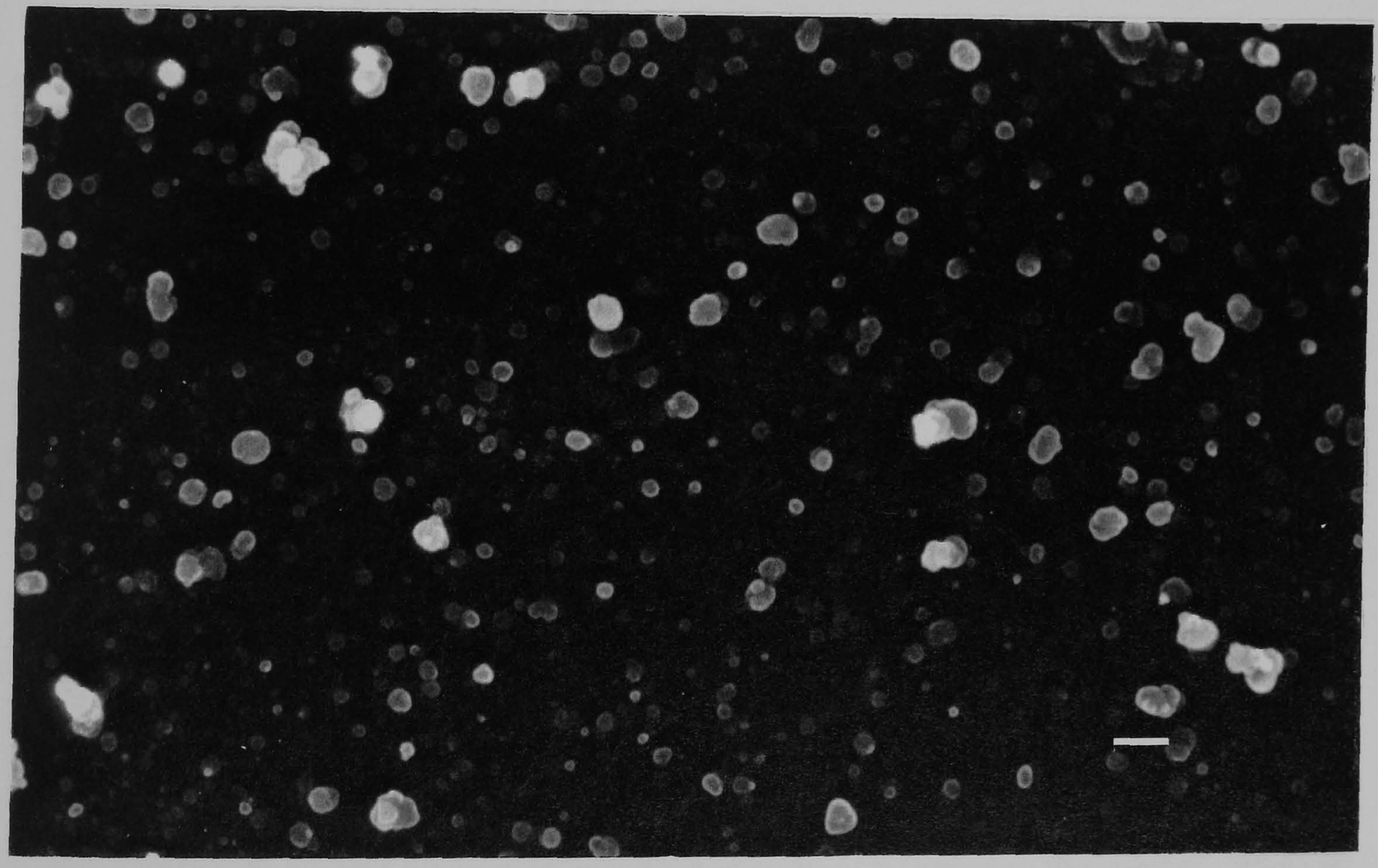

Figure 3.16b Scanning electron micrograph of ZnS film deposited onto glass for 2 hour, [Zn] = 0.025 mole dm^{-3}, $[NH_3]$ = 1.0 mole dm^{-3}, $[N_2H_4]$ = 3.0 mole dm^{-3}, [thiourea] = 0.035 mole dm^{-3} at 70° C, pH = 10.2, ---- = 1 μ.

and $[N_2H_4]$ = 3 mole dm^{-3} as reported by Dono and Herrero [35]. These films consist of small spherical particles of diameter ca 10 nm as shown in figure 3.16. Such film were uniform and adherent to the substrate surface. At higher pH values (11.0 - 11.5) non-uniform and very thin films were deposited. Similar features were observed at lower values of pH (9.0 - 9.8) and the films contained large quantity of ZnO or $Zn(OH)_2$.

Such films were powdery in nature and could be removed easily by rubbing with a tissue paper. The morphology of the deposited ZnS films were similar to those deposited by Dono et al. [35], using a bath containing $ZnSO_4/NH_3/N_2H_4/(NH_2)_2CS$. Films deposited on tin oxide were cloudy and less uniform than those deposited on the glass substrate. A typical micrograph is shown in figure 3.17.

The band gaps of ZnS films were estimated to be 3.66 eV (literature value 3.65 eV) [22] on both glass and tin oxide coated glass by electronic spectroscopy.

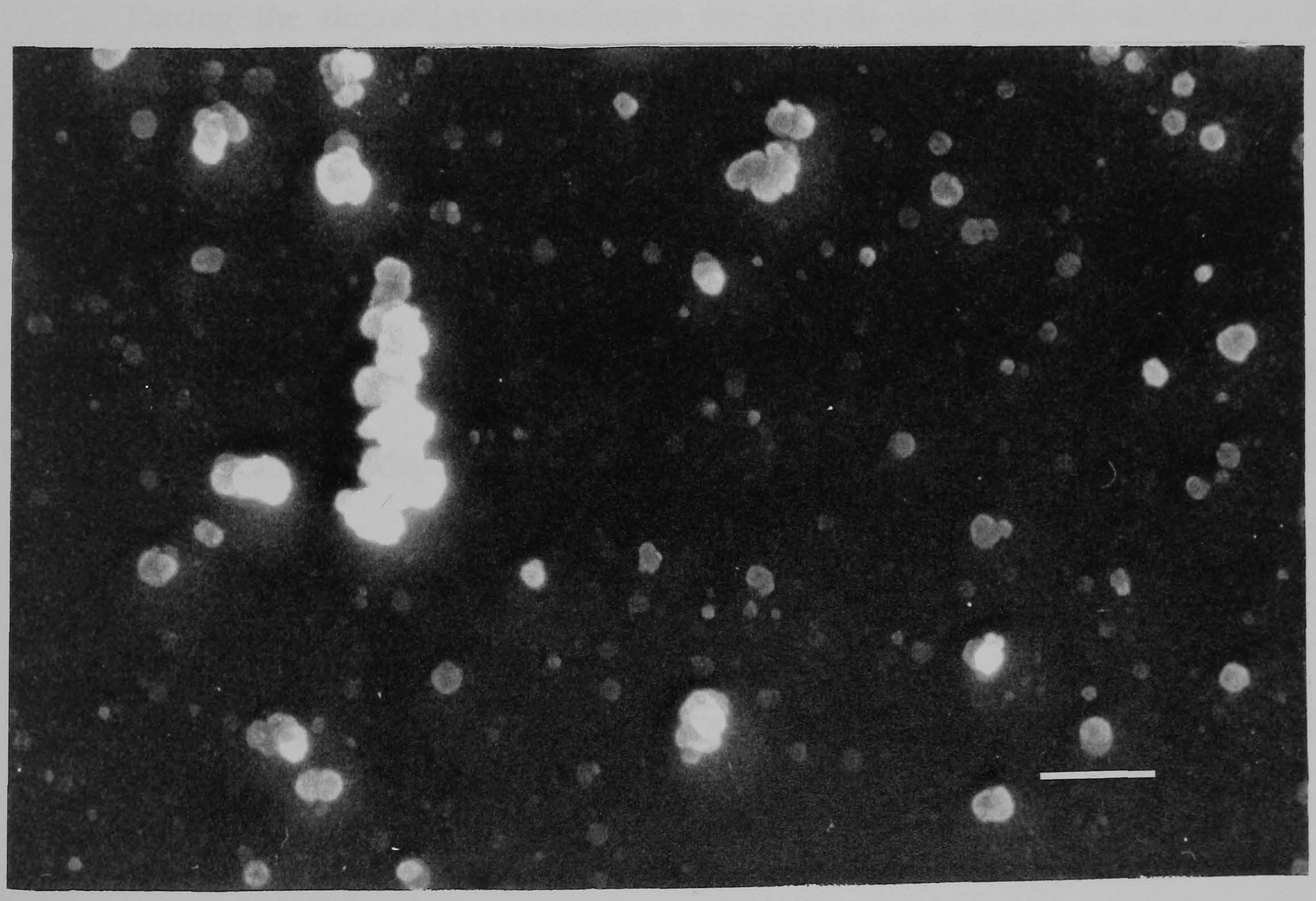

Figure 3.17 Scanning electron micrograph of ZnS film deposited onto tin oxide coated glass for 1 hour, [Zn] = 0.025 mole dm^{-3}, $[NH_3]$ = 1.0 mole dm^{-3}, $[N_2H_4]$ = 3.0 mole dm^{-3}, [thiourea] = 0.035 mole dm^{-3} at 70° C, pH = 10.2, ---- = 1 μ.

3.2.3 $Cd_xZn_{1-x}S$ thin films

The wide band gap II-VI alloy $Cd_xZn_{1-x}S$ is of interest as materials for electro-optical signal processing devices requiring energy gaps in the range 2.5 to 3.7 eV, beyond the range of III-V semiconductors [36,37]. $Cd_xZn_{1-x}S$ with x values in the range 1 - 0.4 has been used as window layers for solar cells.

In the present work we have attempted to deposit thin films of $Cd_xZn_{1-x}S$ onto both glass and tin oxide coated glass substrates using cadmium sulfate, zinc sulfate, ammonia, hydrazine and thiourea. Thin films are comparable in quality to those obtained in other work [38,39] and the effects of bath composition on the nature and morphology of the deposited films is considered.

Factors Controlling Film Quality

During the deposition experiments the growth was generally limited to the surface of the substrate and the walls of the reactor. There are several factors which can affect the quality and nature of the deposited $Cd_xZn_{1-x}S$ films.

Effect of pH on the deposited films

pH is an important parameter for the chemical bath deposition. The bath solution needs to be alkaline to deposit thin films but at the same time an excess of alkali could lead to the unwanted oxide or hydroxide deposition. It has been found that in CBD experiments pH is not the key factor which controls the deposition of $Cd_xZn_{1-x}S$ films. A number of films were deposited at a range of pH (10 - 11.0) (figure 3.18) and it has been found that in all deposited films Cd, Zn and S were the main species present depending on the concentrations used.

Effect of ammonia concentration on the deposited films

$Cd_xZn_{1-x}S$ films have been grown at a range of ammonia concentration (0.25 - 2.0 M). Most adherent and specular films were grown at ammonia concentration 1 M as shown in figure 3.20. At higher ammonia concentrations sometimes intermediate films were deposited. It was also found that at an ammonia concentration of 0.5 M or less only CdS films were deposited (figure 3.18) and the films had relatively poor morphology.

Effect of hydrazine concentration on the deposited films

Hydrazine also plays an important role in controlling the nature of the phase deposited. A number of experiments were carried at different concentration of hydrazine (1.0 - 4.0 M) and it was noticed that when hydrazine was less than 1 M in the solution no ternary films were formed. The films were non-uniform and deep in yellow colour. EDAX showed the presence of only cadmium and sulfur in the films. At higher concentration of hydrazine cadmium and zinc were present together with sulfur in the films.

Effect of cadmium sulfate, zinc sulfate and thiourea on the deposited films

In all these experiments the concentration of thiourea was kept constant (0.035M). Cadmium sulfate and zinc sulfate concentrations were varied in the range (0.005 - 0.025 M) and films with different x values were obtained at different concentration of ammonia and hydrazine. The composition of such films were determined by EDAX measurements. The band gap of $Cd_xZn_{1-x}S$ films were estimated by electreonic spectroscopy in the range of 2.44 - 3.3 eV by altering the concentrations of cadmium sulfate and zinc sulfate in the bath.

Nature of Phase Deposited
pH = 11.0 or 10.5

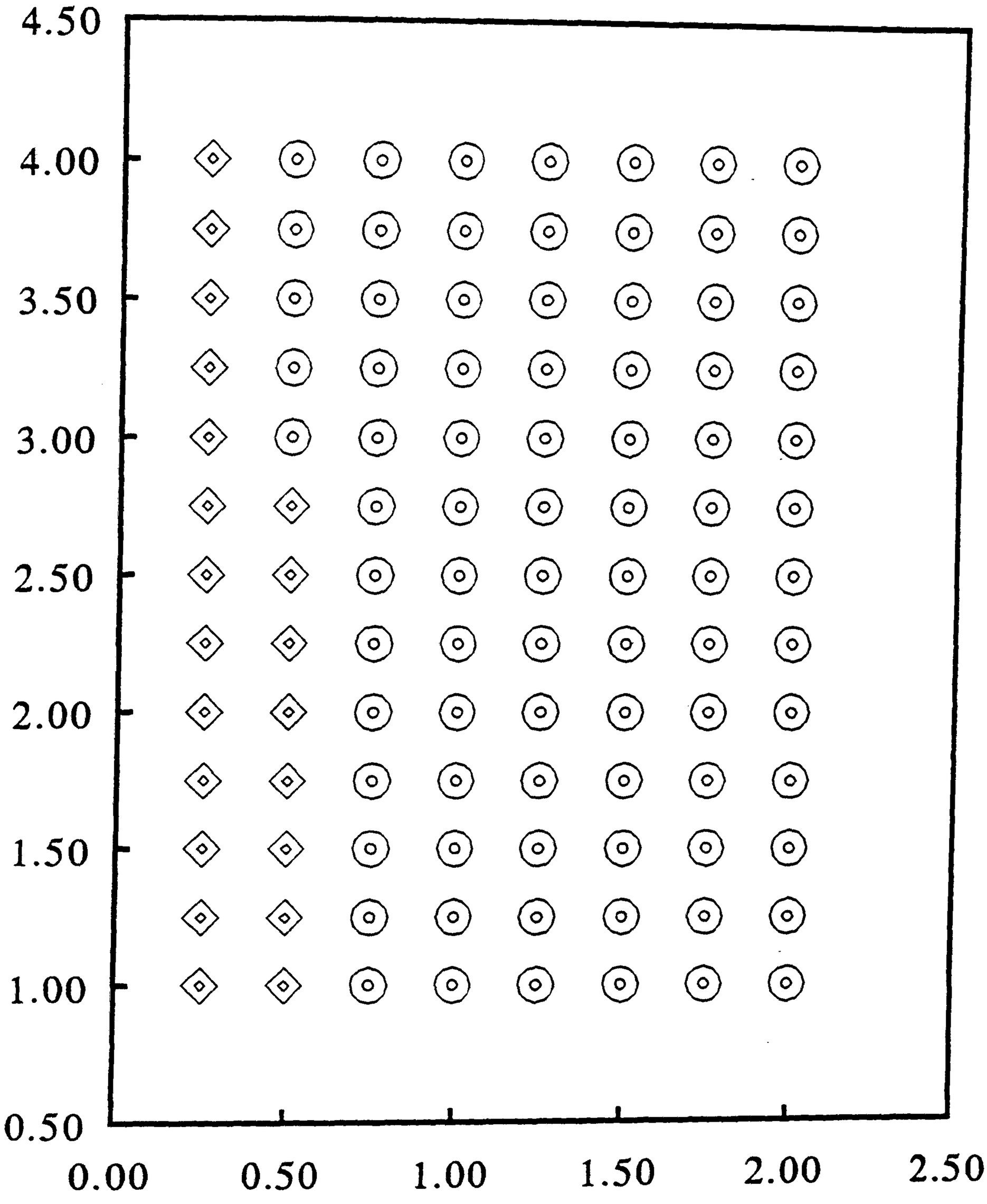

Phase deposited ○ CdZnS ◇ CdS ○ CdZnS ◇ CdS

Large markers pH = 10.5, small markers pH = 11.0

Figure 3.18 Nature of the Deposited Phase.

Film Quality

The experiments were usually terminated shortly after formation of the bulk precipitate and the glass slides or tin oxide coated glass were removed from the solution. The composition of cadmium, zinc and sulfur in the films have been confirmed by electron diffraction analytical X-ray (EDAX) using electron microscope as shown in figure 3.19. Adherent particles of bulk precipitate were removed by ultrasonication in distilled water. Some of these particles remained on the films and can be identified as scattered spherical particles that appear white in the micrographs because of charging. Scanning electron micrograph of $Cd_xZn_{1-x}S$ films grown at different concentration of reactant and various pH are shown in figures. Two distinct morphologies of deposited $Cd_xZn_{1-x}S$ can be identified in these micrographs.

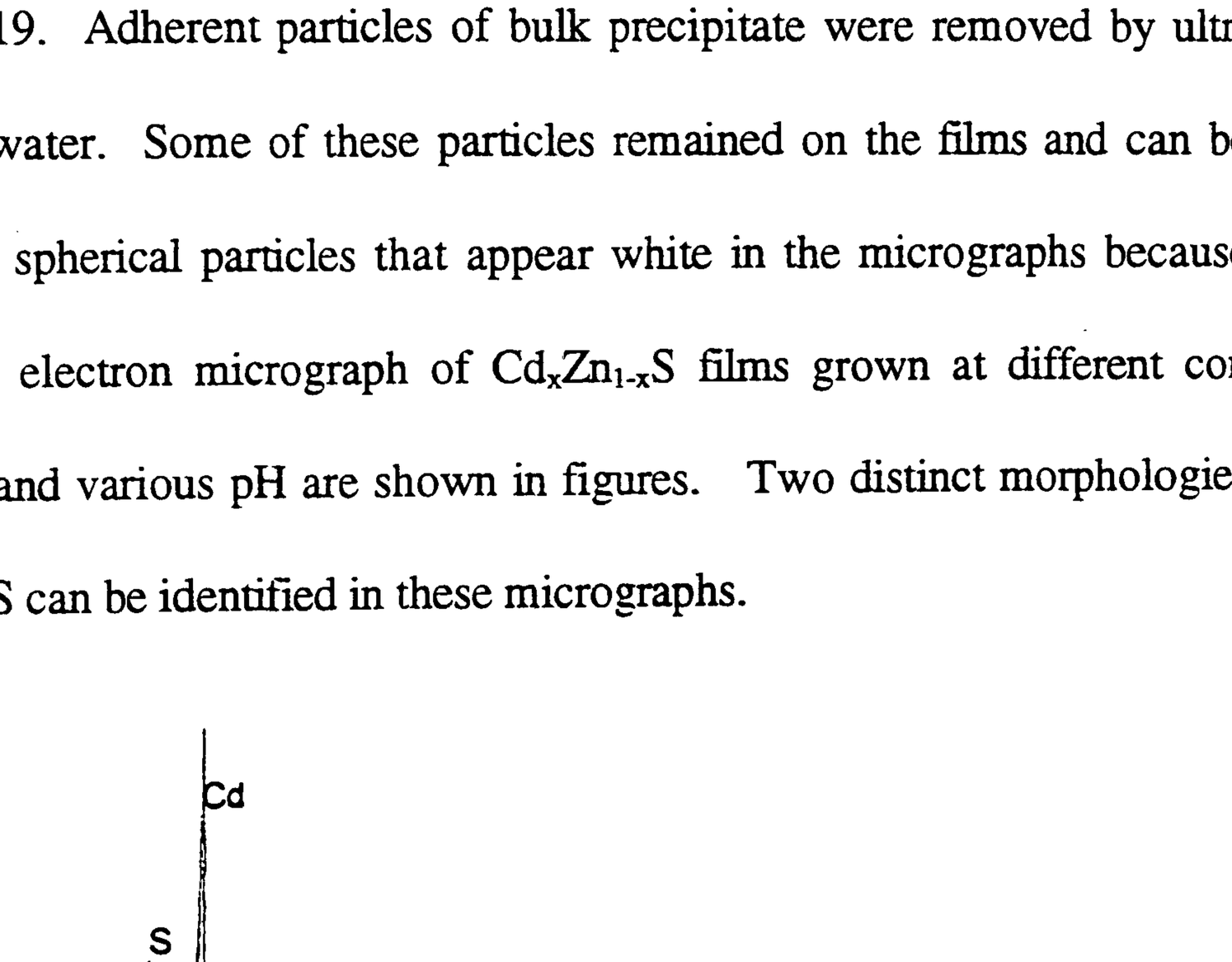

Figure 3.19 EDAX of $Cd_xZn_{1-x}S$ film as grown on glass [Cd] = 0.015 mole dm^{-3}, [Zn] = = 0.013 mole dm^{-3}, [NH_3] = 1.0 mole dm^{-3}, [N_2H_4] = 2.0 mole dm^{-3} and [thiourea] = 0.035 mole dm^{-3}, 70 °C, pH 10.2, 1h.

The most adherent and specular films appear as in figures 3.20 and 3.21, these films consist of dense approximately 0.2 μ micron spherulites of $Cd_xZn_{1-x}S$. The size of the spherulites does not appear to increase with time in the deposition bath (figure 3.20). The pH values for the deposition of these films were in the range of 10.5 to 11.0. At higher values of pH, similar morphologies were observed but only very thin (ca 0.1 m) films were deposited. Such films were specularly reflecting and tightly adherent to the substrate surface and could not be removed by abrasion with a tissue. Similar morphologies of deposited chalcogenides films were observed on tin oxide coated glass. Such films were comparatively less specular and uniform as shown in figure 3.21. One important observation is that under these conditions there is little or no evidence for the growth of the particles forming the film figures 3.20 and 3.21.

The morphology of a typical film as grown on glass at pH 9.0 to 10.5 is shown in figure 3.22. These films were thick uneven and powdery and could easily be removed by rubbing with a tissue; such films were deep in yellow colour and typically 1 to 2 microns thick with particles of irregular shapes of ca 5 - 10 microns, the distinctive morphology shown in figure 3.22. On both substrates at intermediate concentration of ammonia and hydrazine both types of morphologies were sometime observed figure 3.23.

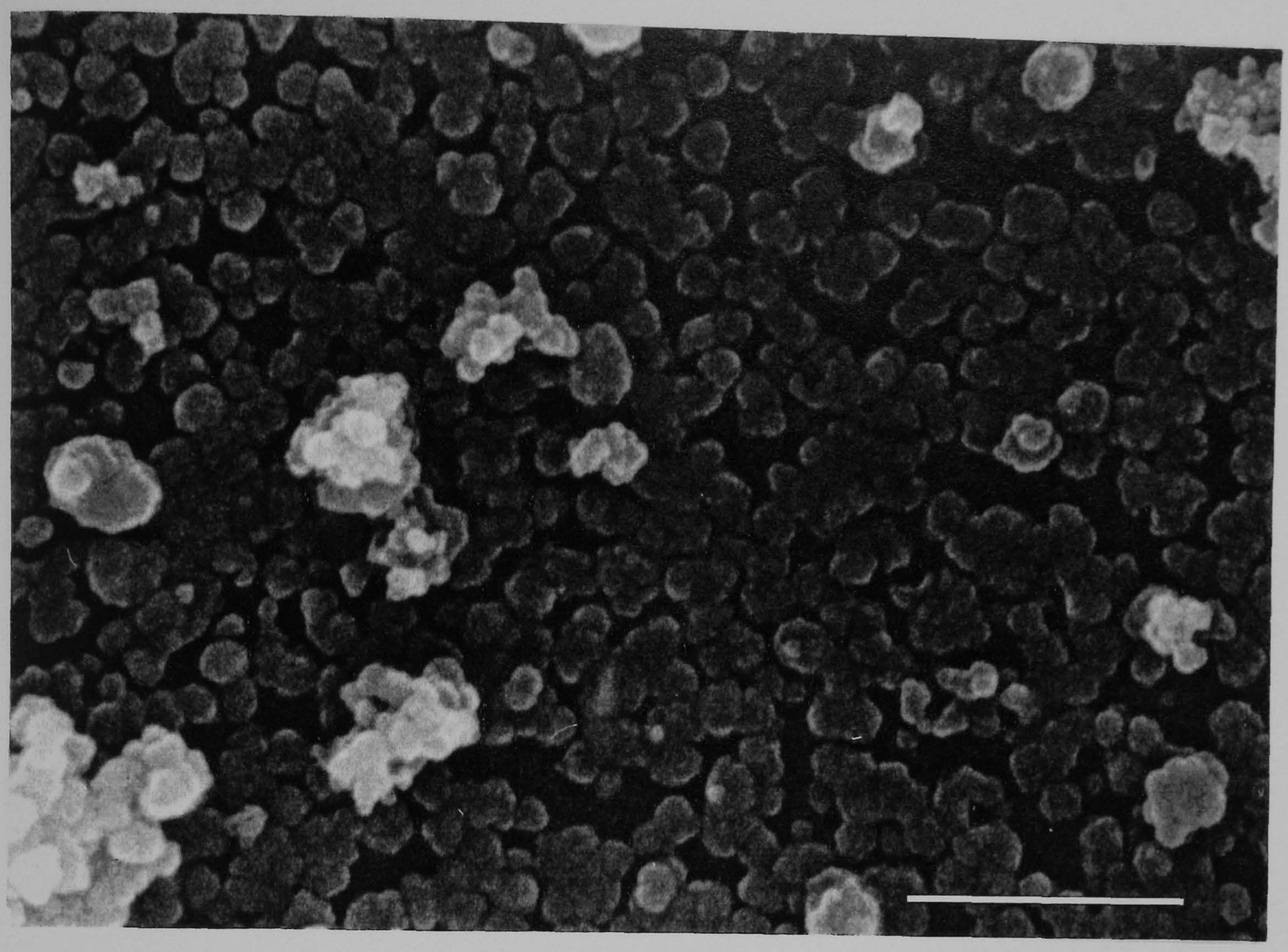

Figure 3.20a Scanning electron micrograph of $Cd_xZn_{1-x}S$ film as grown on glass [Cd] = 0.015 mole dm^{-3}, [Zn] = 0.013 mole dm^{-3}, [NH_3] = 1.0 mole dm^{-3}, [N_2H_4] = 2.0 mole dm^{-3} and [thiourea] = 0.035 mole dm^{-3}, 70 °C, pH 10.2, 1h, ---------- = 1 μ.

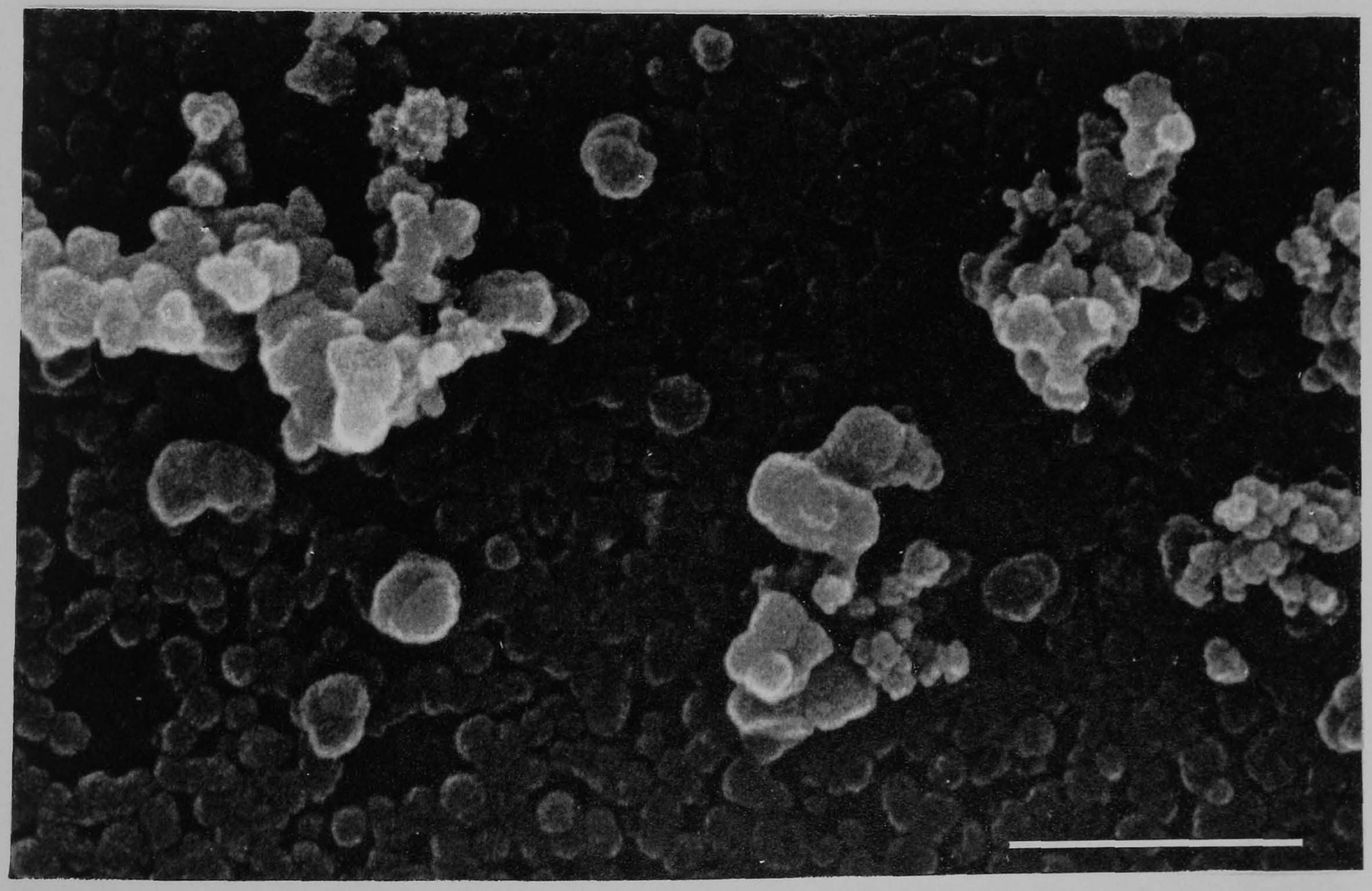

Figure 3.20b Scanning electron micrograph of $Cd_xZn_{1-x}S$ film as grown on glass [Cd] = 0.015 mole dm^{-3}, [Zn] = 0.013 mole dm^{-3}, [NH_3] = 1.0 mole dm^{-3}, [N_2H_4] = 2.0 mole dm^{-3} and [thiourea] = 0.035 mole dm^{-3}, 70 °C, pH 10.2, 2h, ---------- = 1 μ.

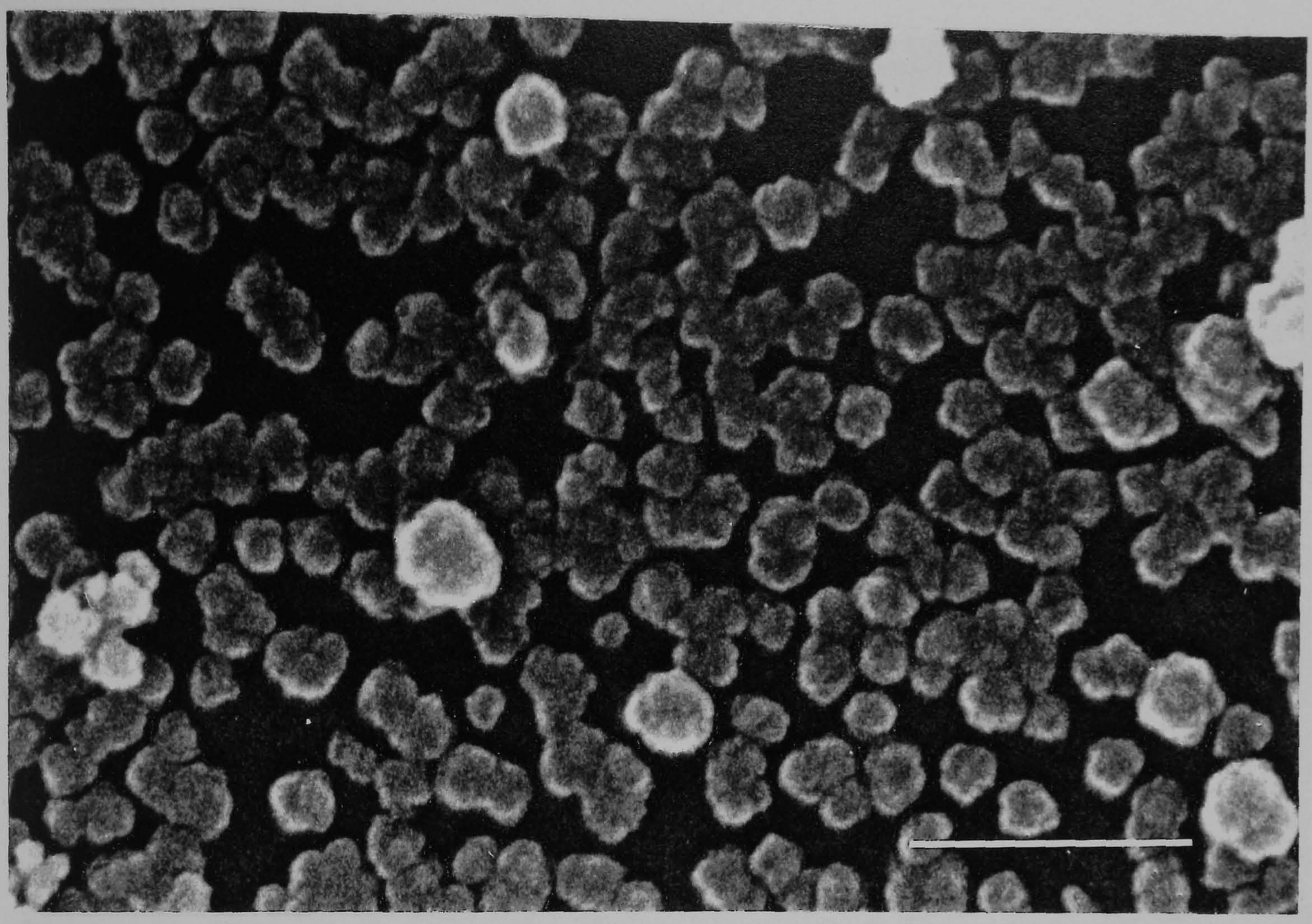

Figure 3.21 Scanning electron micrograph of $Cd_xZn_{1-x}S$ film as grown on tin oxide [Cd] = 0.013 mole dm^{-3}, [Zn] = 0.013 mole dm^{-3}, $[NH_3]$ = 1.0 mole dm^{-3}, $[N_2H_4]$ = 2.0 mole dm^{-3} and [thiourea] = 0.035 mole dm^{-3}, 70 °C, pH 10.5, 1h, ---------- = 1 μ.

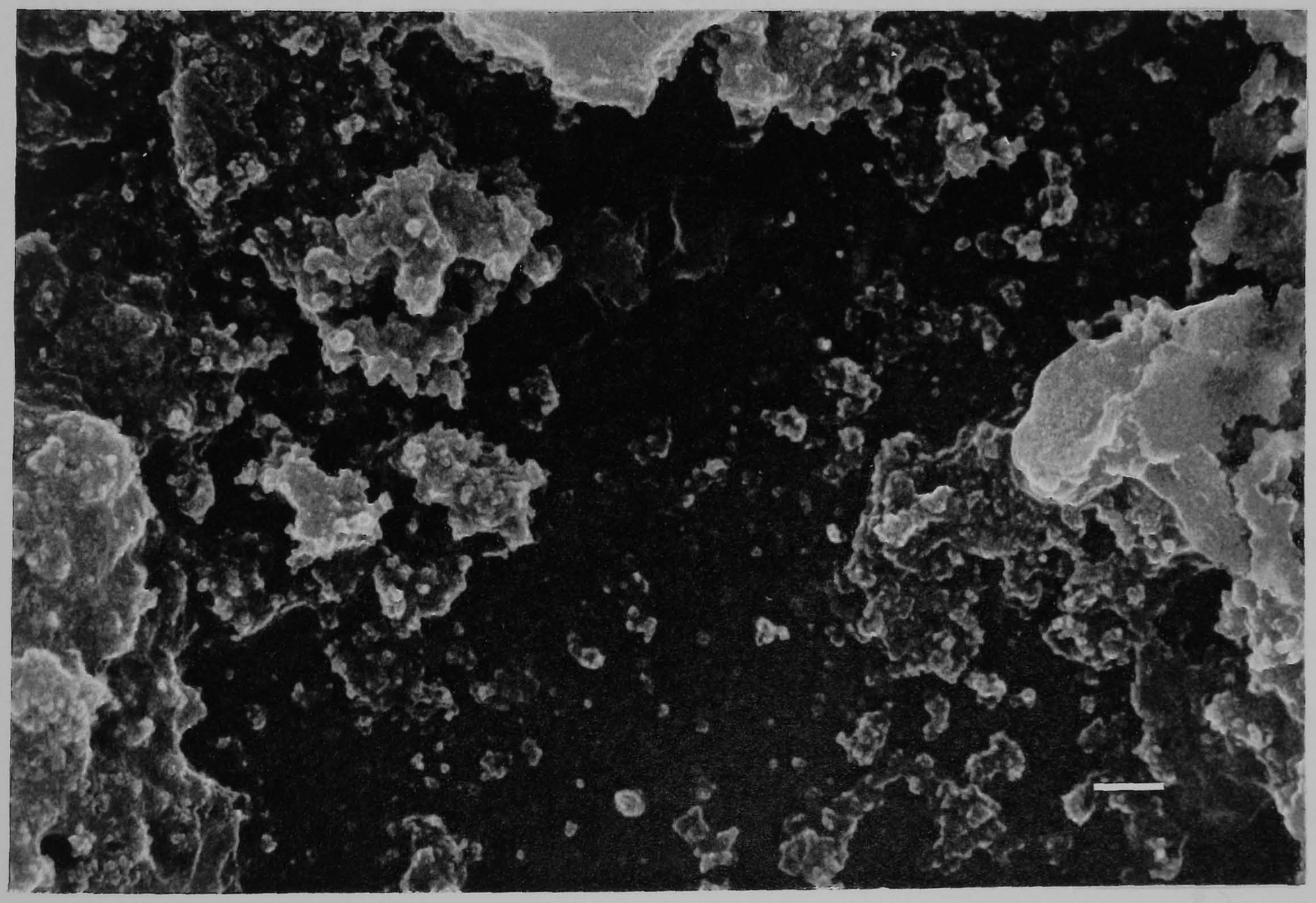

Figure 3.22 Scanning electron micrograph of $Cd_xZn_{1-x}S$ film as grown on glass [Cd] = 0.013 mole dm^{-3}, [Zn] = 0.013 mole dm^{-3}, $[NH_3]$ = 0.5 mole dm^{-3}, $[N_2H_4]$ = 1.0 mole dm^{-3} and [thiourea] = 0.035 mole dm^{-3}, 70 °C, pH 9.5, 1h, ---- = 1 μ.

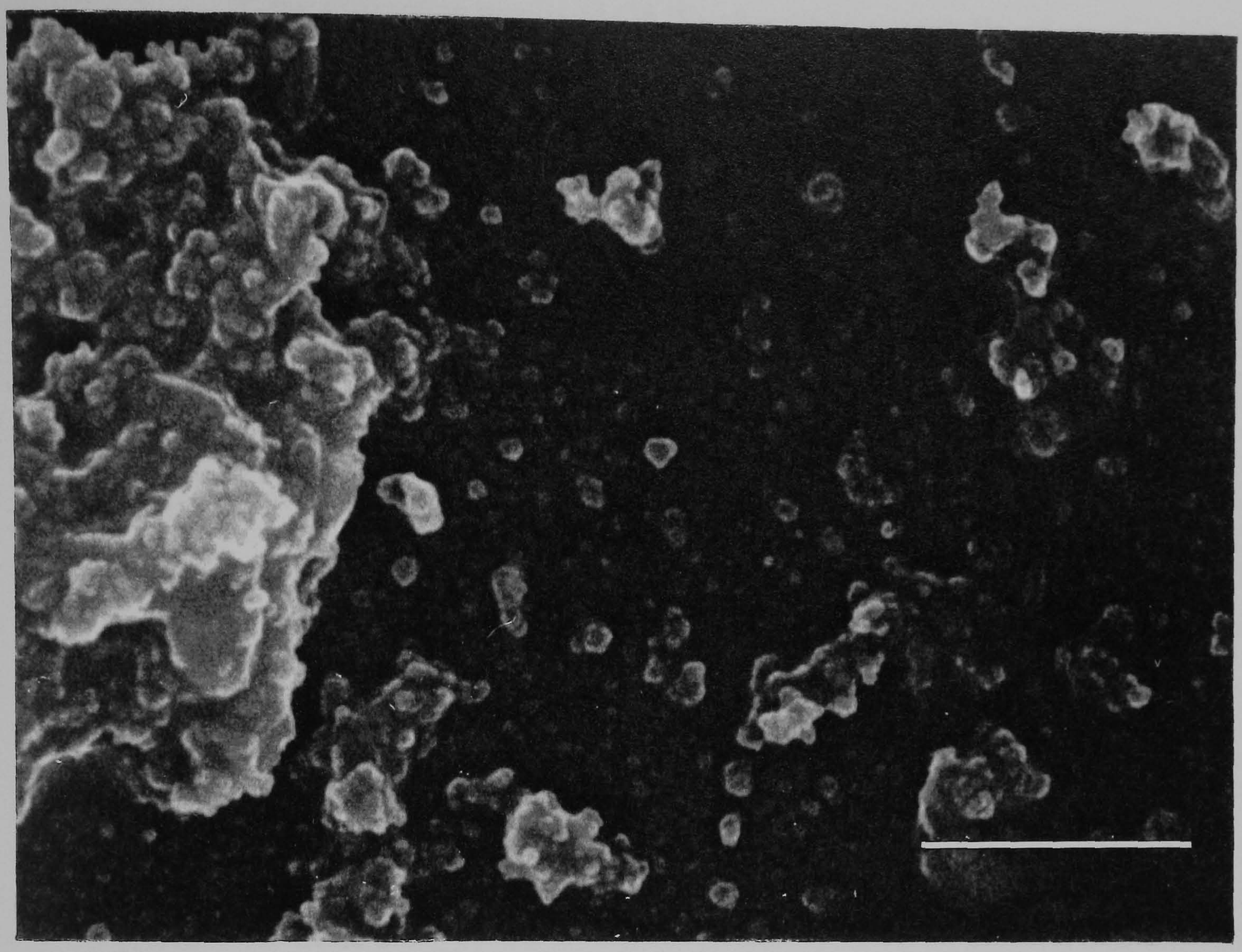

Figure 3.23 Scanning electron micrograph of $Cd_xZn_{1-x}S$ film as grown on glass [Cd] = 0.013 mole dm^{-3}, [Zn] = 0.013 mole dm^{-3}, [NH_3] = 0.75 mole dm^{-3}, [N_2H_4] = 2.0 mole dm^{-3} and [thiourea] = 0.035 mole dm^{-3}, 70 °C, pH 10.2, 1h, ---------- = 1 μ.

Structural studies

X-ray diffraction patterns (XRD) were recorded on both glass and tin oxide coated glass. The d-spacing were calculated and compared to the standard values of cadmium sulfide (both hexagonal and cubic phase) and zinc sulfide (hexagonal phase), and are given in table 3.5. It was noticed that the deposited films were polycrystalline having mixed cadmium sulfide and zinc sulfide phase. The film grown on glass substrate predominantly consists of hexagonal (Greenokite) cadmium sulfide and the reflection for hexagonal (Wurtizte) zinc sulfide also present. $Cd_xZn_{1-x}S$ grown on tin oxide showed similar structure but a number of peaks were absent.

Table 3.5 X-ray diffraction results of $Cd_xZn_{1-x}S$ as grown on both microscope glass slides and tin oxide coated glass

CdS[a]	CdS[b]	CdS (H)	h	k	l	ZnS (H)	$Cd_xZn_{1-x}S$[c]
3.58	3.58	3.58	1	0	0	3.32	3.58
3.36	3.35	3.36	0	0	2	3.13	3.36
3.16	3.19	3.16	1	0	1	2.93	3.10
2.45	2.44	2.45	1	0	2	-----	-----
2.07	-----	2.07	1	1	0	1.91	2.12
1.90	-----	1.90	1	0	3	1.77	-----
1.79	-----	1.79	2	0	0	1.67	-----
1.76	-----	1.76	1	1	2	-----	-----
1.73	-----	1.73	2	0	1	-----	-----
1.68	-----	1.68	0	0	4	-----	-----

[Cd] = 0.013 mole dm^{-3}
[Zn] = 0.013 mole dm^{-3}
[Th] = 0.035 mole dm^{-3}
[NH_3] = 1.0 mole dm^{-3}
[N_2H_4] = 2.0 mole dm^{-3}
a = Glass, b = Tin oxide, c = calculated from lattice fringes

Transmission electron microscopy (TEM)

It has been found that the particles of the powder prepared by dispersion and direct deposition onto the TEM grids were electron beam transparent. Figure 3.24 shows the microstructure of the crystal and the selected area diffraction pattern. The sample was composed of small particles forming an agglomerate. The particles were well crystallized and reflected by strong diffraction rings and spots. The very strong rings were found to be (100), (002) and (101) lattices of hexagonal CdS.

High-resolution lattice plane images of the particles were obtained by placing the objective in such a way around the main (000) transmitted beam that the diffraction spots of small lattice spacing were eliminated from the image formation. The addition of the

specimen was tilted against the transmitted beam as to produce many diffraction conditions of the lattices which spacing were larger than resolution of the microscope.

Figure 3.25 shows the lattice plane images of the particle represented by five fringe pattern. The direction of the lattice fringes vary over the whole area indicating different orientation between the crystals. Some area which did not show any lattices were not fulfilling the Bragg's diffraction conditions for the lattice planes to be resolved. The thicker fringes observed in the micrograph were noise fringes formed as a result of crystals overlapping and those must not be confused with the real fine lattice pattern. The measurements from the negatives correspond to the lattice spacing of 3.58 Å, 3.36 Å, 3.10 Å and 2.12 Å. In the case of CdS sample as discussed earlier in this chapter the lattice spacing were continuos all over the micrograph and correspond to 3.19 Å (101) hexagonal phase. In the $Cd_xZn_{1-x}S$ sample the fringe spacings were different all over the micrograph. The fringe spacing of 3.10 Å and 2.12 Å lies in between (101) and (110) spacings of hexagonal CdS and hexagonal ZnS indicating the presence of $Cd_xZn_{1-x}S$ with hexagonal CdS (110). Similar results were observed by Hampden-Smith et al. [40] for CdS and $Cd_xZn_{1-x}S$ thin films deposited by MOCVD.

The EDS performed on the same selected area of the shown film in TEM using 10 nm diameter electron beam also confirmed the presence of zinc in cadmium sulfide.

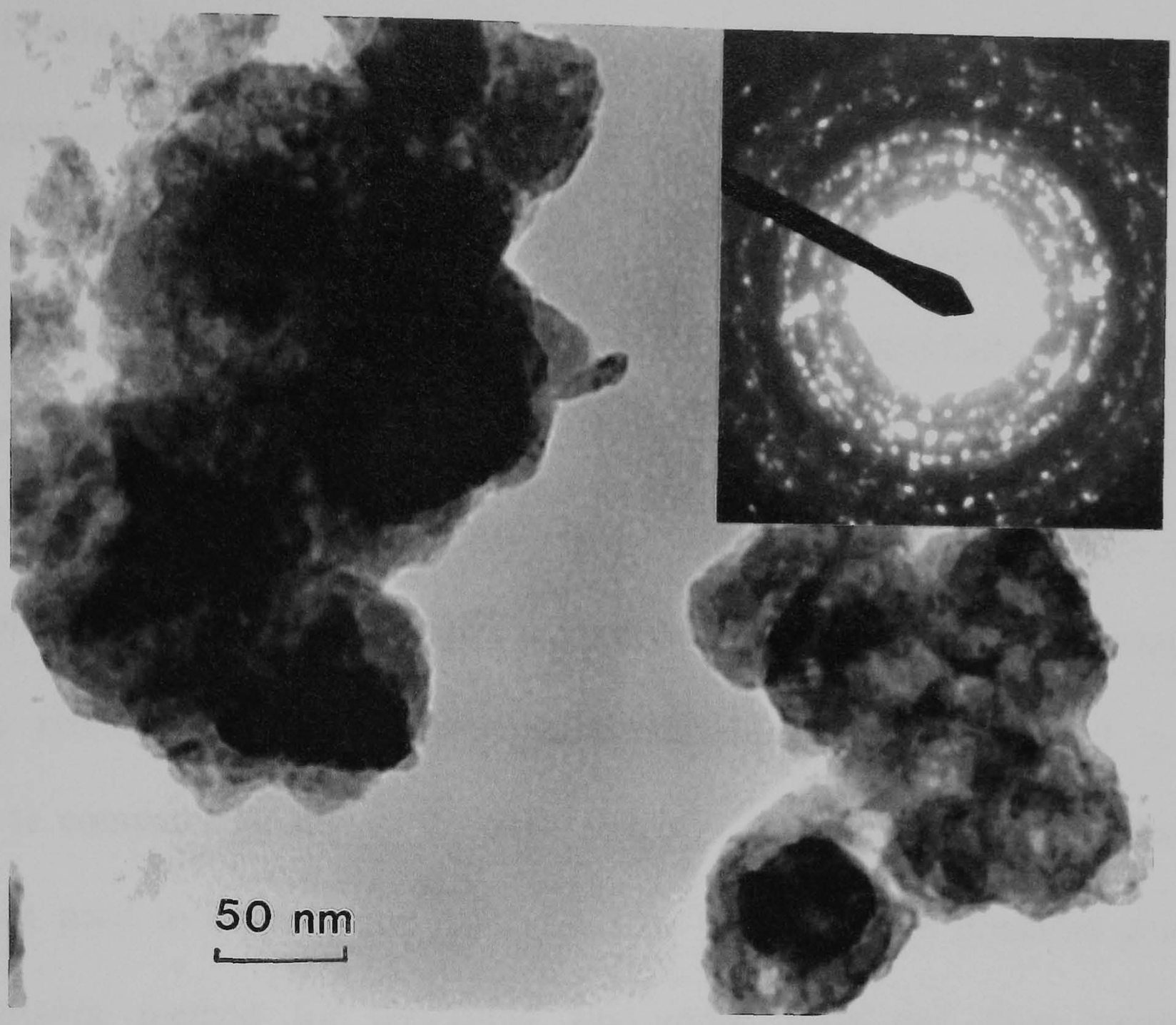

Figure 3.24 Transmission electron micrograph and electron diffraction pattern of $Cd_xZn_{1-x}S$ film as grown on glass [Cd] = 0.013 mole dm^{-3}, [Zn] = 0.013 mole dm^{-3}, [NH_3] = 1.0 mole dm^{-3}, [N_2H_4] = 2.0 mole dm^{-3} and [thiourea] = 0.035 mole dm^{-3}, 70 °C, pH 10.2, 2h.

Figure 3.25 Transmission electron micrograph of $Cd_xZn_{1-x}S$ film as grown on glass [Cd] = 0.013 mole dm^{-3}, [Zn] = 0.013 mole dm^{-3}, [NH_3] = 1.0 mole dm^{-3}, [N_2H_4] = 2.0 mole dm^{-3} and [thiourea] = 0.035 mole dm^{-3}, 70 °C, pH 10.2, 2h.

3.2.4 ZnO thin films

Transparent conductive oxide (TCO) layers have been studied extensively because of their broad range of applications, including: as transparent electrodes in photovoltaic and display devices [41,42]. It has also been reported that conductive ZnO thin films with carrier concentration of 10^{20}-10^{21} cm^{-3} are useful as a coating materials for transparent IR shields because of their low cost [43-46]. Zinc oxide is used for a wide variety of applications (ceramics, paints, catalysis, etc.) [47], and has attracted interest as transparent electrode material in photovoltaic cells because of its good material properties as compared to indium tin oxide [48,49]. A number of techniques have already been used to deposit zinc oxide [50-53]. This section describes a simple solution growth method for depositing zinc oxide films and their subsequent characterization.

Film Quality

ZnO films were deposited with [Zn] = 0.018 M and for a range of ethylenediamine concentrations ([en] = 0.03 - 0.042 M). The best films were deposited with [Zn] = 0.018 M, [en] = 0.042 M. The starting pH of the bath was around 9.0 or 9.1, which was raised to 10.0 - 11.0 by adding NaOH. The addition of base to the bath plays an important role in the deposition of good quality ZnO films as only poor quality films were grown without the addition of NaOH. The reaction bath was slightly turbid before the addition of the NaOH, on the addition of NaOH, zinc hydroxides precipitate and ZnO is formed. The films grown at pH 10.5 or 11 were uniform, adherent and specular whereas films grown at pH 10 or less were powdery, spotted and non-uniform easily removed by abrasion with a tissue.

A scanning electron micrograph of ZnO films grown at different ethylenediamine concentrations and various pH values are shown in figures 3.26 and 3.27. At least two distinct morphologies of deposited ZnO can be identified in these micrographs. Adherent and specular film (figure 3.26a), which consists of flowers of approximately 1-2 μ micron diameter with well formed triangle features around a central spheres. The pH values for the deposition of these films were in the range of 10.5 - 11.0 (ethylenediamine concentration of 0.042 M and zinc concentration of 0.018 M). Such films were specularly reflecting and tightly adherent to the substrate and could not be removed by abrasion with a tissue. The morphology of a typical film obtained at ethylenediamine concentration less than 0.037 M and pH 10 or less is shown in figure 3.26b. These films were non-uniform, powdery, and spotted and can be removed by rubbing with a tissue. Electron microscopy showed random rod shaped particles of up to 1 μ micron in length. At pH (11.5 - 12.0) the morphology was again somewhat different with clumps of sub micron particles, similar to the spherulites in the good films but with no secondary features (figure 3.26c). The morphology of ZnO film deposited onto tin oxide coated glass was slightly different than those grown on glass. A typical micrograph of ZnO film on tin oxide coated glass is shown in figure 3.15. These films were not usually uniform and had a poorer morphology with very thin random rod shaped particles of ca 1 μ micron. The ZnO particle morphologies observed in related work [54,55] were similar to those in the present study (figure 3.26). However, Trindade et al. associated the different morphologies of ZnO particles with the use of different ligands [54], whereas in the present work a single ligand metal combination has been used. It seems likely that supersaturation is an important factor controlling the morphology of the zinc oxide.

Table 3.6 Some Typical Deposition Results for ZnO as grown onto glass slides and tin oxide coated glass at 50° C for 1 hour.

Ratio [Zn]:[en]	pH Starting	pH Final	Film quality
1:2	9	9	No deposition
1:2	9.1	9.5	No deposition
1:2	9	10	Uneven and non-uniform film with poor morphology
1:2	9	10.5	Uneven and non-uniform film
1:2	9.1	11	Specular and adherent film
1:2	8.5	11.5	Uneven and non-uniform film
1:2	8.5	11.8	Uneven and non-uniform film
1:2.25	9.5	9.5	No deposition
1:2.25	9.4	10	No deposition
1:2.25	9.4	10.5	Uniform, adherent and specular film
1:2.25	9.5	11	Uniform even growth
1:2.25	9.5	12	Good films showing both morphologies

[Zn] = 0.018 mole dm^{-3}
[en] = 0.036 or 0.041 mole dm^{-3}

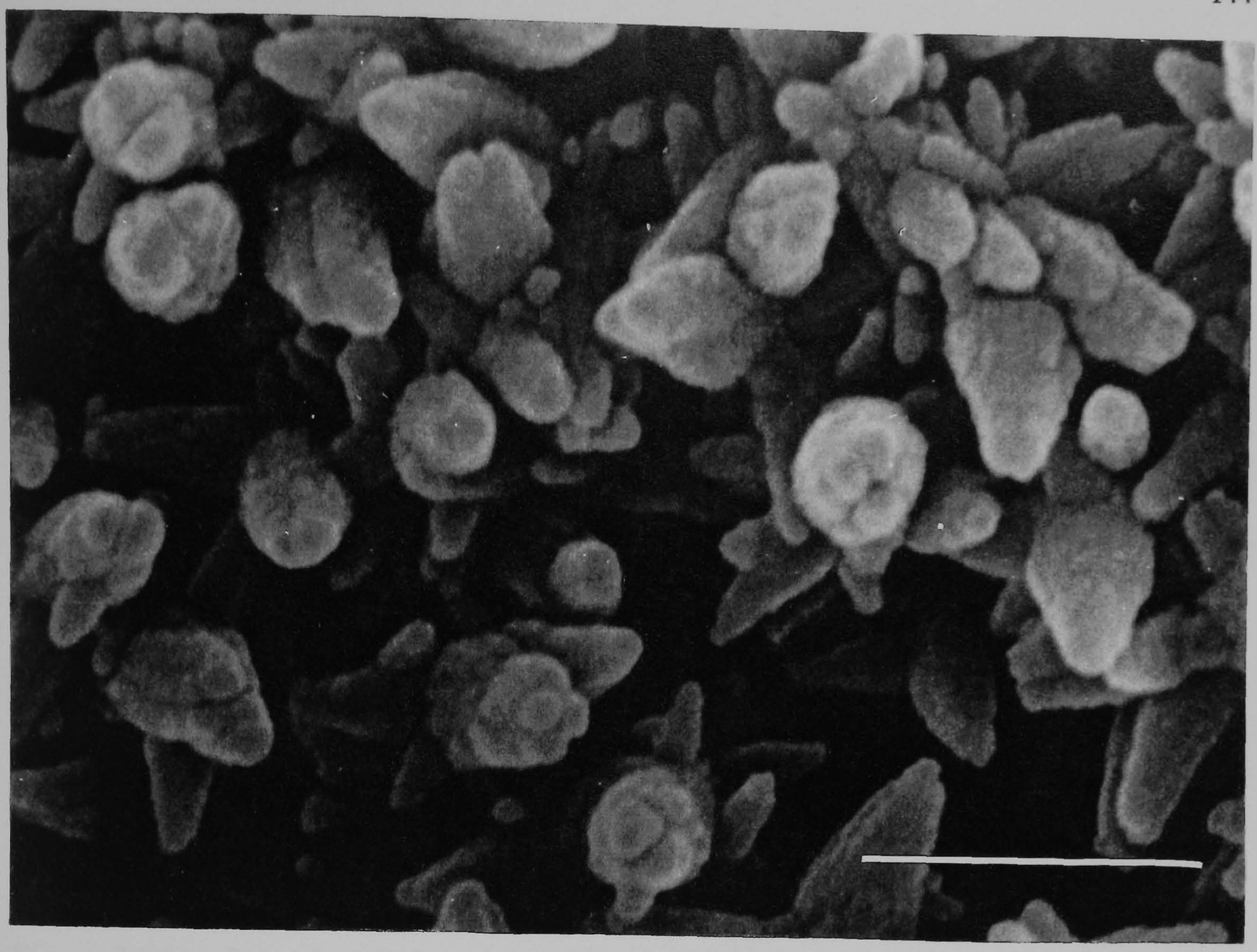

Figure 3.26a Scanning electron micrograph of ZnO film grown on glass [Zn] = 0.018 mole dm^{-3}, [Zn] : [en] = 1 : 2.25, at 50 °C, pH = 11.0, 1h, ---------- = 1 μ.

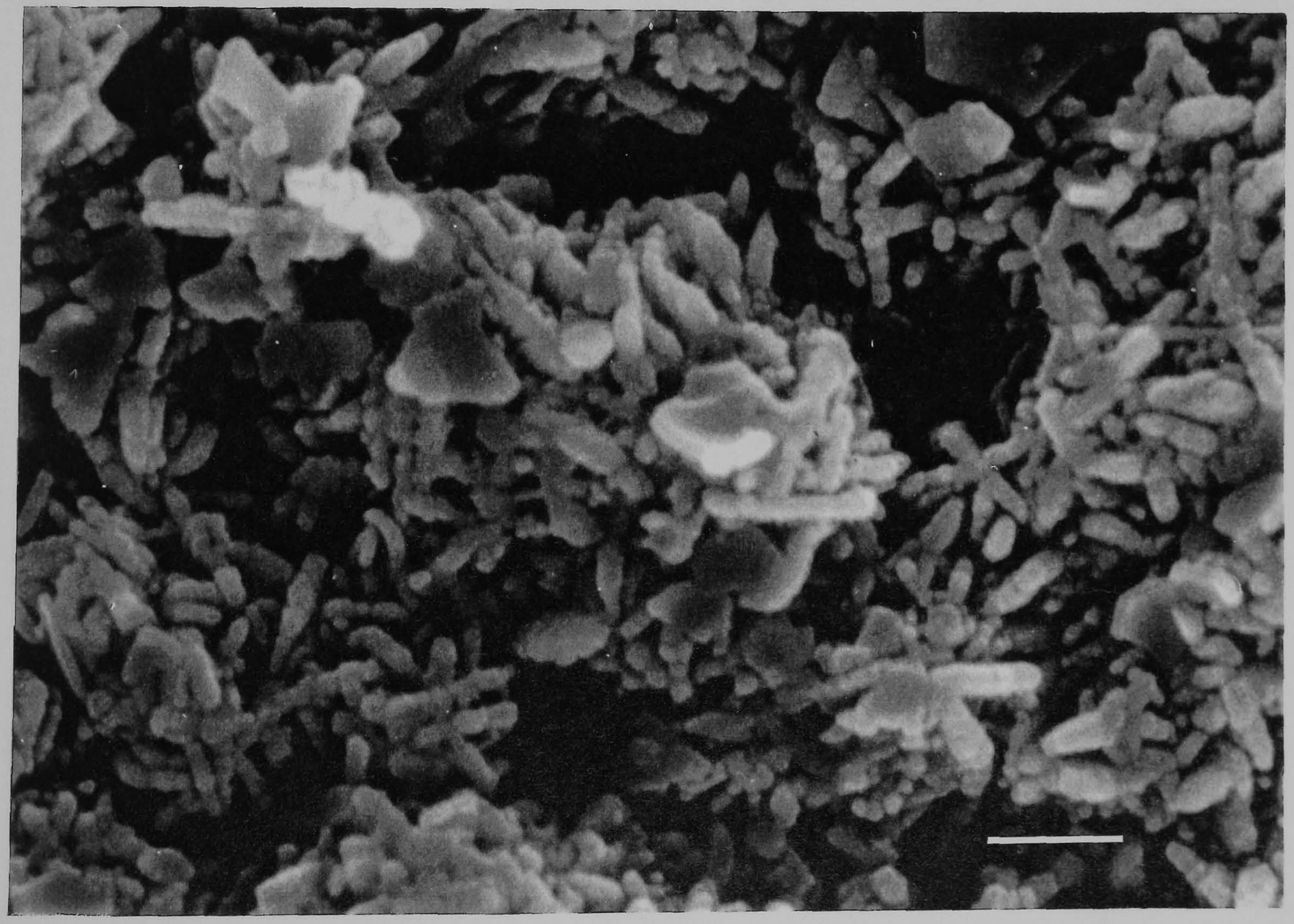

Figure 3.26b Scanning electron micrograph of ZnO film grown on glass [Zn] = 0.018 mole dm^{-3}, [Zn] : [en] = 1 : 2, at 50° C, pH = 10.0, 1h, -------- = 1 μ.

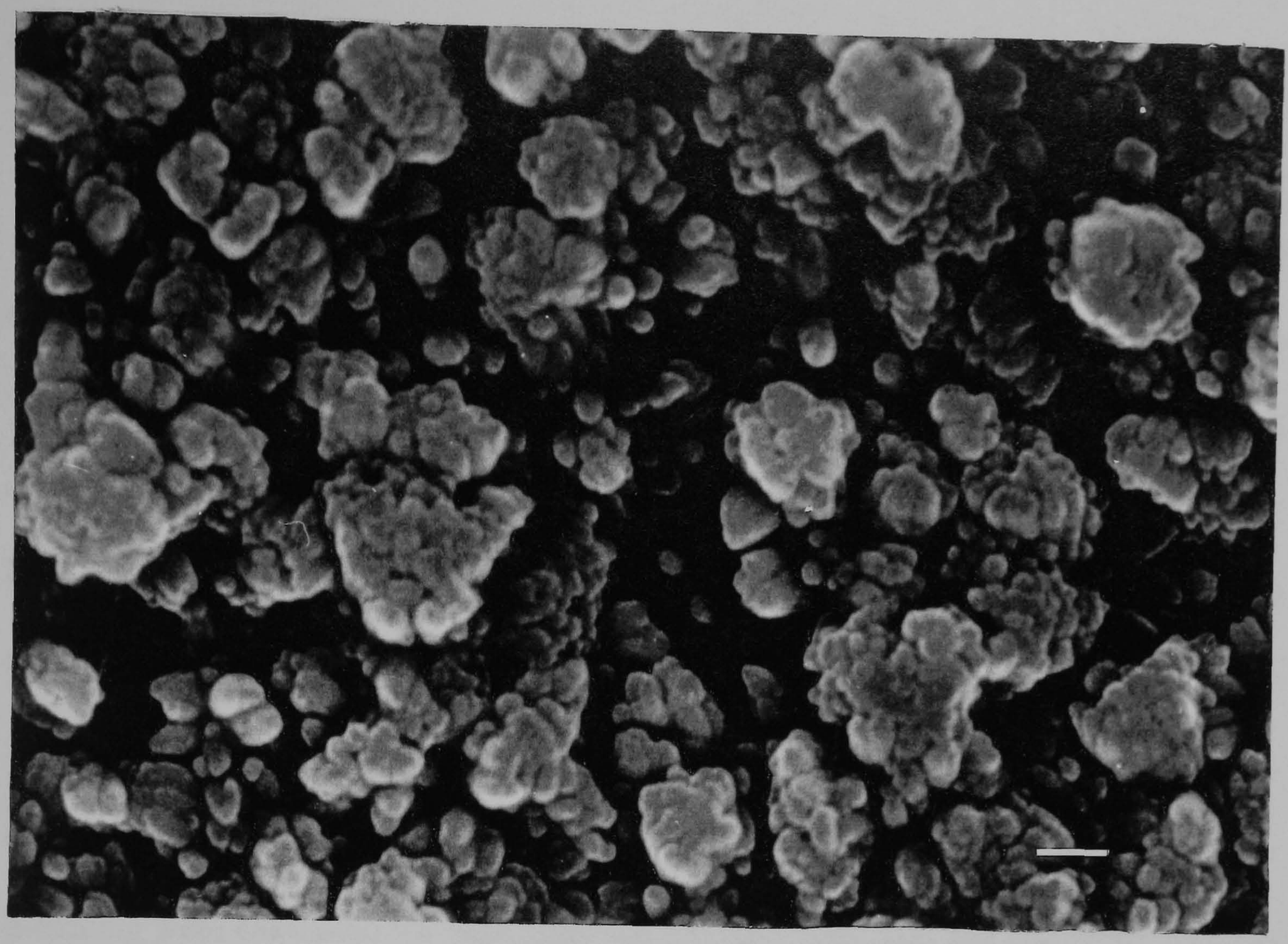

Figure 3.26c Scanning electron micrograph of ZnO film grown on glass [Zn] = 0.018 mole dm^{-3}, [Zn] : [en] = 1 : 2.25, at 50° C, pH = 12.0, 1h, ---- = 1 μ.

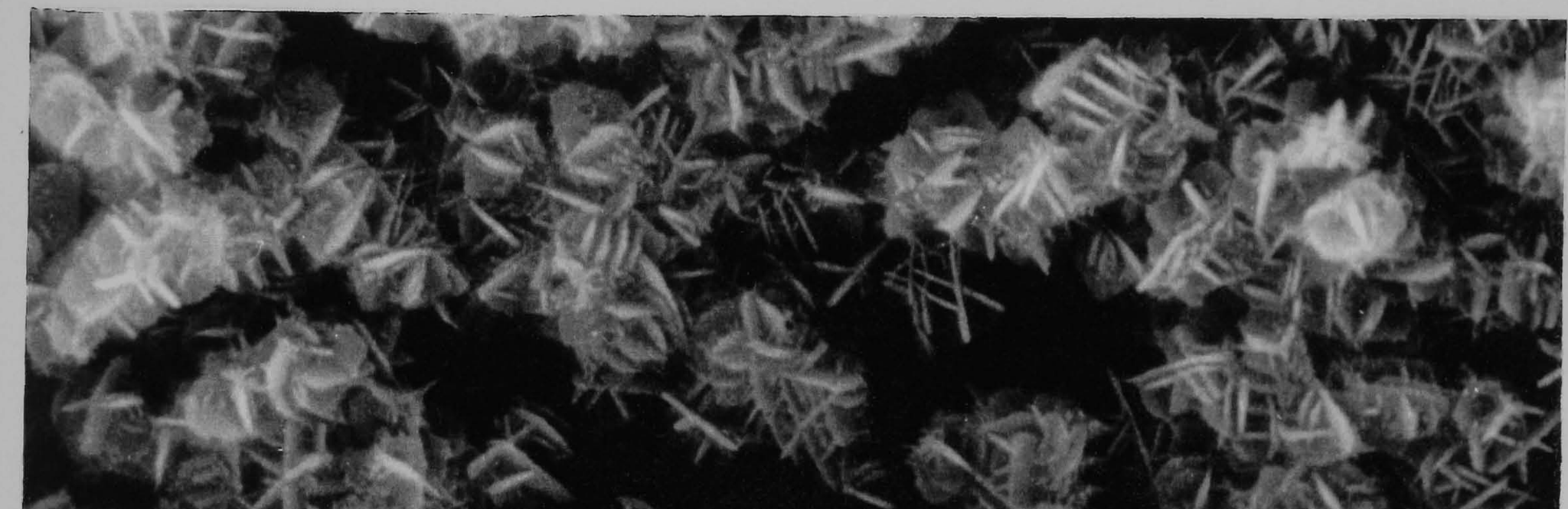

Figure 3.27 Scanning electron micrograph of ZnO film grown on tin oxide [Zn] = 0.018 mole dm^{-3}, [Zn] : [en] = 1 : 2.25, at 50 °C, pH = 11.0, 1h, ---- = 1 μ.

Structural studies

Zinc oxide commonly exists in the hexagonal (Wurtzite) form. In CBD experiments carried on glass substrate Raviendra and Sharma [56] reported that the films were polycrystalline in nature having Wurtzite structure with no sign of preferred orientation. In contrast O'Brien et al [50], found that the ZnO films as grown by MOCVD on glass substrate were hexagonal but the crystals were oriented in the 110 direction.

In present work the crystal structure has been identified by X-ray diffraction studies using Cu K_α radiation of wavelength 1.5418 Å and a LiF monochromater. The d-spacing were calculated for both glass and tin oxide substrates and compared with the standard values table 3.7. The data indicate that the ZnO has crystallized in the hexagonal form, with a space group P63/mc; a = 3.253Å; b = 3.253Å; c= 5.213Å; α = 90°; ß = 90°; γ = 120°. A comparison with standard ASTMS data for ZnO shows that almost all the reflections are present for good quality film (figure 3.28a), whereas a number of reflections are absent in poor morphology films and film grown on tin oxide coated glass (figure 3.28b). The X-ray diffraction patterns indicate the absence of preferred orientation of ZnO in the deposited films which is in good agreement with previous work [57].

Table 3.7 X-ray diffraction results for ZnO (Hexagonal) grown at 50 °C on glass and tin oxide coated glass for 1 hour.

ZnO[a] d/A; I(%) Glass, pH=11.0	ZnO[b] d/A; I(%) Glass, pH=10.5	ZnO[c] d/A; I(%) Glass, pH=12.0	ZnO[d] d/A; I(%) SnO_2, pH=11.0	ASTMS d/A; I(%)	h	k	l
2.81(67.4)	2.81(62.5)	2.81(58.3)	2.81(52.3)	2.82(55)	1	0	0
2.60(93.9)	2.60(100)	2.60(94.5)	2.60(100)	2.60(40)	0	0	2
2.47(100)	2.47(98.6)	2.47(100)	2.47(81)	2.48(100)	1	0	1
1.91(25.9)	1.91(25.7)	1.91(26.1)	1.91(22.5)	1.91(23)	1	0	2
1.62(31.1)	1.62(23.2)	1.62(28.1)	1.62(28.3)	1.62(32)	1	1	0
1.48(32.2)	1.48(37.8)	1.48(36.4)	1.48(31.5)	1.48(29)	1	0	3
1.41(9.4)	1.43(7.1)	-----	-----	1.41(4)	2	0	0
1.38(23.2)	1.37(20.7)	1.38(24.5)	1.38(19.6)	1.38(23)	1	1	2
1.36(13.5)	-----	-----	1.36(11.4)	1.36(11)	2	0	1
1.30(7)	-----	-----	-----	1.30(2)	0	0	4
1.24(6)	-----	-----	-----	1.24(4)	2	0	2
1.18(4.4)	-----	-----	-----	1.18(3)	1	0	4
1.09(7.9)	-----	-----	-----	1.09(11)	2	0	3
1.06(4.6)	-----	-----	-----	1.06(4)	2	1	0
1.04(7.1)	-----	-----	-----	1.04(12)	2	1	1
1.01(5.3)	-----	-----	-----	1.02(7)	1	1	4

[Zn] = 0.018 mole dm^{-3}

a. [Zn] : [en] = 1:2.25

b. [Zn] : [en] = 1:2

c. [Zn] : [en] = 1:1.75

d. [Zn] : [en] = 1:2.25

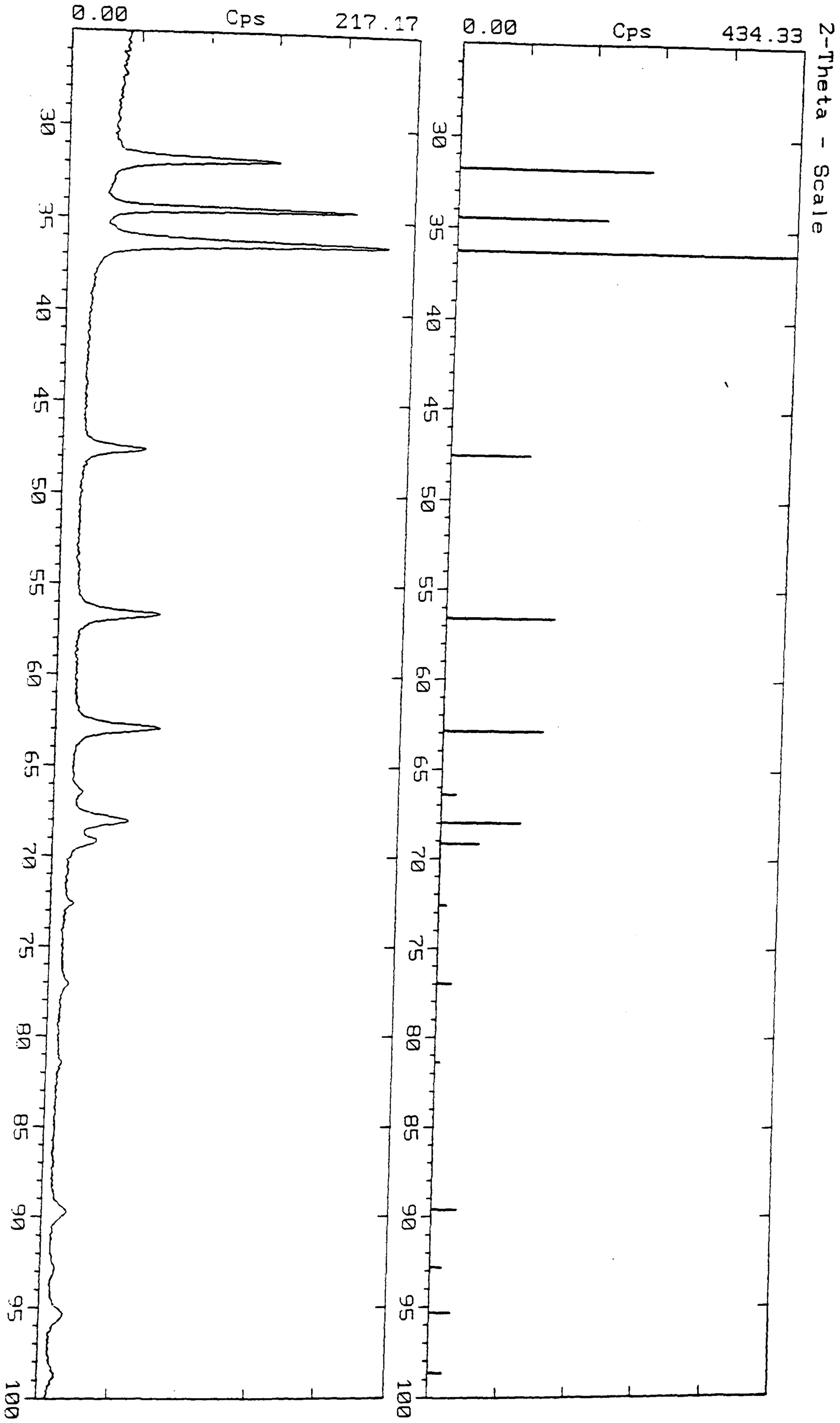

Figure 3.28a XRD pattern for ZnO film grown on glass [Zn] = 0.018 mole dm^{-3}, [Zn] : [en] = 1 : 2.25, at 50 °C, pH = 11.0, 1h.

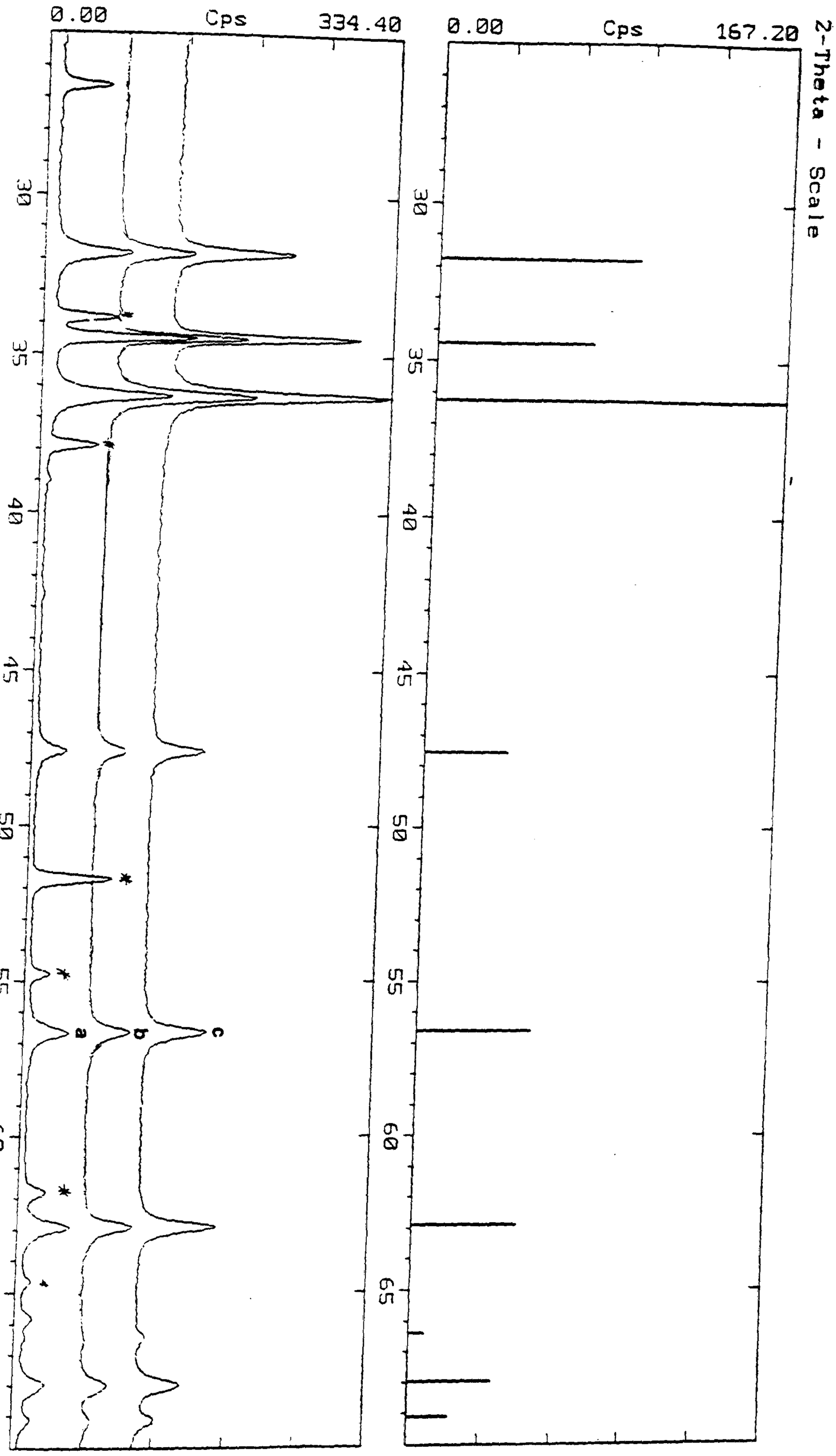

Figure 3.28b XRD patterns for ZnO films, [Zn] = 0.018 mole dm^{-3}, at 50° C, 1h.

a, [Zn] : [en] = 1 : 2.25, pH = 11.0, Tin oxide
b, [Zn] : [en] = 1 : 1.75, pH = 10.5, Glass
c, [Zn] : [en] = 1 : 2, pH = 12, Glass
*, Tin oxide from the substrate

Factors Controlling Film Deposition

The equilibrium in the bath solution has been modelled and the stability constants used were obtained from Martell et al. [12] and a typical set of input parameters are summarized in table 3.8. Speciation diagram were calculated for several different composition, (ratios of [Zn] to [en]) as a function of pH. Using the output of the programme the point at which "$Zn(OH)_2$" would just precipitate was calculated using K_{sp} 1.0 x 10^{-15} (50 °C) a typical speciation diagram is shown in figure 3.29. The solid line represents the point at which the hydroxide should precipitate or at which solutions are first likely to be supersaturated in a hydroxy species. There is no simple relationship between pH and "$Zn(OH)_2$" supersaturation because pH controls the extent of hydrolysis of Zn (the hydroxide ion concentration) and the complexation by ethylenediamine. Zinc forms a variety of complexes with hydroxide, and in moderately basic solution a "$Zn(OH)_2$" precipitate will form.

I have tried to establish by our modelling if the supersaturation of hydroxy species of zinc is an important factor controlling the deposition of ZnO films formed. The results of these calculations and observations are summarized in figure 3.30, in which the solid line represents the point at which the solution becomes supersaturated with respect to "$Zn(OH)_2$". The different symbols represent good quality films and low quality films, the correlation of supersaturation with the formation of films is excellent. Clearly the supersaturation line predicts the region in which ZnO can be deposited. However unlike related studies on deposition of CdS discussed earlier in this chapter, there is no simple correlation with the quality of the film deposited. The best quality films were deposited close to supersaturation line. Good quality films were grew more slowly than the poor quality films. The degree of supersaturation of the solution with

respect to hydroxy-complexes of zinc appears to be the key factor controlling ZnO deposition.

Table 3.8 Typical Input Parameters for Calculating Speciation

Species No.	Log B_{ijk}	Stoichiometry i	j	k
1.	9.13	0	1	1
2.	16.27	0	1	2
3.	5.25	1	1	0
4.	9.86	1	2	0
5.	12.14	1	3	0

Stoichiometric coefficients: i. Zn, j. ethylenediamine, k. H.

Values are from reference [12], and correct to 50 °C as described therein.

The precise mechanism responsible for the deposition of good quality thin films of ZnO is far from clear temperature, substrate and the chelating agent used all play a role in controlling film quality. However supersaturation with hydroxy complexes is probably the most important factor controlling ZnO deposition.

The absorption spectra of ZnO films on both glass and tin oxide were recorded in the wave length range of 300 - 700 nm. From the absorption spectra, it can be concluded that the material is wide band gap. The band gap values were found to be 3.15 eV (literature value 3.2 eV) [39] on both glass and tin oxide coated glass.

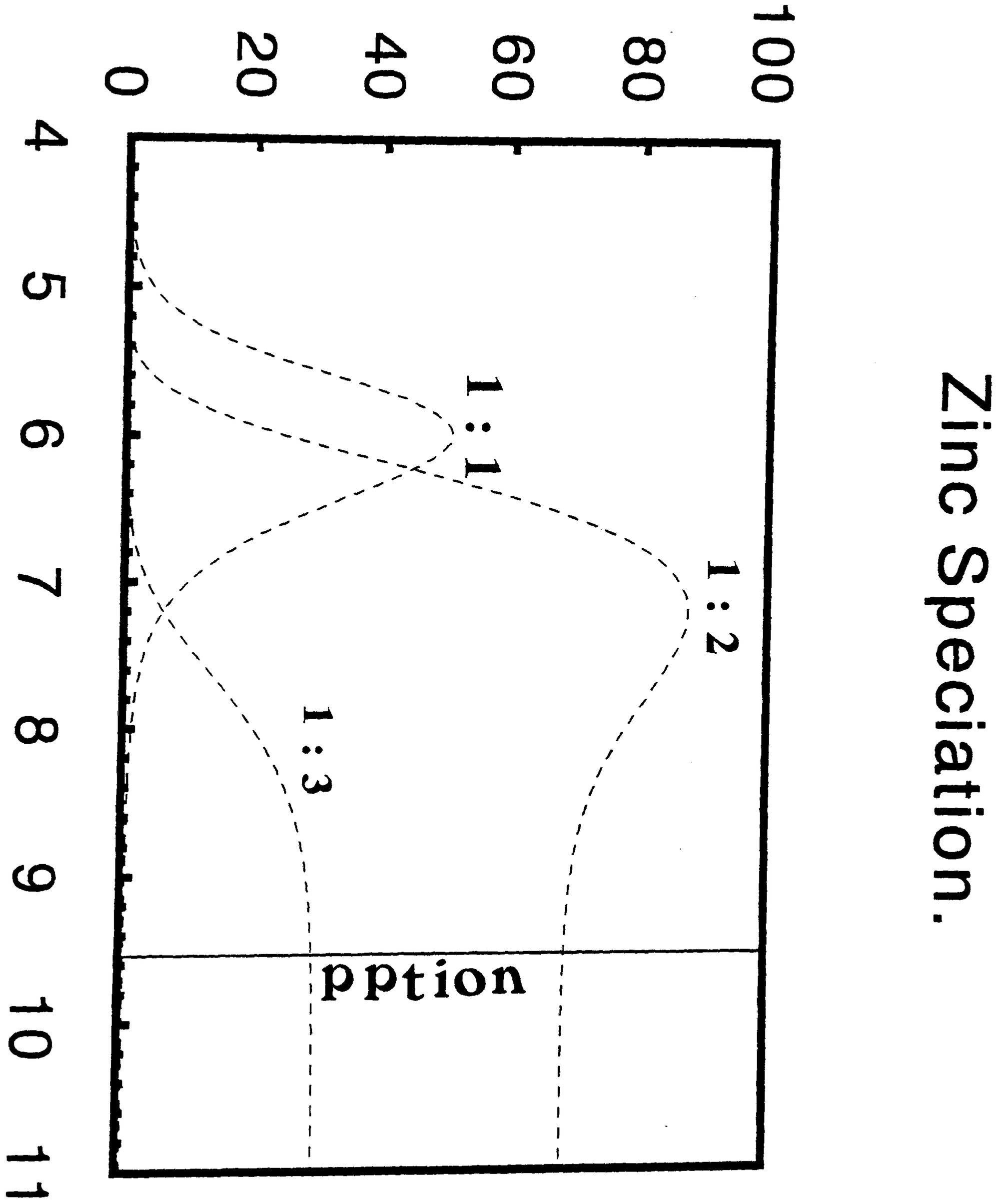

Figure 3.29 Typical Speciation Diagram
[Zn] = 0.018 mole dm^{-3}, [Zn] : [en] = 1 : 2.25. Using the data in table 3.8.

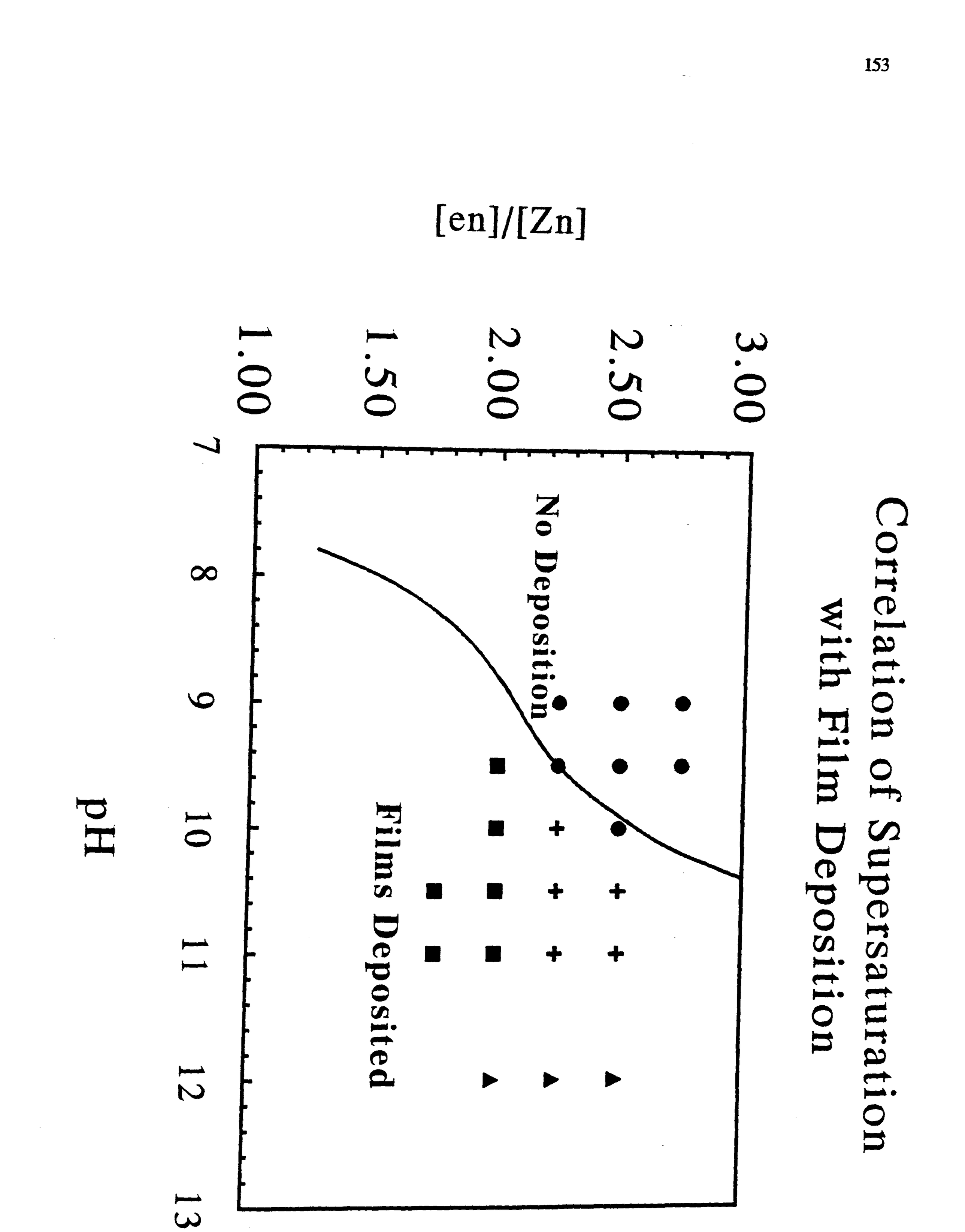

Figure 3.30 Speciation diagram, solid line theoretical limit for hydroxide precipitation, [+] Good morphology films, [■] Poor morphology films, [▲] Mixed morphology films, [●] no deposition.

3.3 Experimental

3.3.1 Deposition of CdS

Thin films of CdS were grown onto glass microscope slides and tin oxide coated glass from solutions containing cadmium acetate (0.5-1 M), ethylenediamine (2-4 M), and thiourea (0.5-1 M). If required the pH of the final bath was adjusted by the addition of a small quantity of acid (0.5 M HCl) or base (0.5 M NaOH). The reaction mixture was maintained at the desired temperature for deposition with continuous stirring. Thoroughly clean (washed with trichloroethylene, rinsed with water and acetone) glass microscope slides or tin oxide coated glass were immersed into the reaction bath. Substrates were taken out after different intervals of time, washed with distilled water, dried and the thin films deposited analyzed.

3.3.2 Deposition of ZnS

ZnS thin films were grown onto glass microscope slides and tin oxide coated glass from solutions containing zinc sulfate (0.005 - 0.025 M), ammonia (0.5 - 2.0 M), hydrazine (1.0 - 4.0 M) and thiourea (0.035 M). When required the pH of the final bath was adjusted by the addition of a small quantity of acid (0.5 M HCl) or base (0.5 M NaOH). The reaction mixture was maintained at the desired temperature for deposition with continuous stirring. Thoroughly clean (washed with trichloroethylene, rinsed with water and acetone) glass microscope slides or tin oxide coated glass were immersed into the reaction bath. Substrates were taken out after different intervals of time, washed with distilled water, dried and the thin films deposited analyzed.

3.3.3 Deposition of $Cd_xZn_{1-x}S$

The $Cd_xZn_{1-x}S$ thin films were grown onto glass microscope slides and tin oxide coated glass from solutions containing cadmium sulfate (0.005 - 0.025 M), zinc sulfate (0.005 - 0.025 M), ammonia (0.5 - 2.0 M), hydrazine (1.0 - 4.0 M) and thiourea (0.035 M). When required the pH of the final bath was adjusted by the addition of a small quantity of acid (0.5 M HCl) or base (0.5 M NaOH). The reaction mixture was maintained at the desired temperature for deposition with continuous stirring. Thoroughly clean (washed with trichloroethylene, rinsed with water and acetone) glass microscope slides or tin oxide coated glass were immersed into the reaction bath. Substrates were taken out after different intervals of time, washed with distilled water, dried and the thin films deposited analyzed.

3.3.4 Deposition of ZnO

Thin films of ZnO were grown onto glass microscope slides and tin oxide coated glass from solutions containing zinc acetate (0.0188 M), and ethylenediamine (0.3 - 0.425 M). The pH of the final bath was adjusted by the addition of a small quantity of base (0.5 M NaOH). The reaction mixture was maintained at the desired temperature for deposition with continuous stirring. Thoroughly clean (washed with trichloroethylene, rinsed with water and acetone) glass microscope slides or tin oxide coated glass were immersed into the reaction bath. Substrates were taken out after different intervals of time, washed with distilled water dried, and the thin films deposited were analyzed.

3.3.5 Modelling

The speciation of the solutions was modelled using a programme SPECIES (from L.D. Petit, University of Leeds). The input parameters for the programme are the

equilibrium constants for the various processes being modelled. Only homogeneous equilibria are modelled. The constants used were obtained from Martell et al [12]. As the programme only models homogenous equilibria the approach taken was to run the model for a given set of conditions (temperature and bath composition) as a function of pH. The output of the programme includes the free metal ion concentration, the pH is an input parameter; consequently by inspection of the output the point at which the solubility product of the first insoluble phase '$M(OH)_2$' (M = Cd) was exceeded could be calculated i.e. the point at which aseemingly homogenous solution is super-saturated with respect to insoluble hydroxy species.

3.3.6 Characterization techniques

Deposited films of II-VI materials were characterized by several techniques. The absorbance of films at (300 nm) was measured with a Philips PU 8710 Spectrophotometer, a Corning pH meter model 7 was used for pH measurements. Scanning Electron Microscopy (SEM), including Electron Diffraction Analytical X-ray (EDAX), was recorded with a JEOL 1200 EX II TEMSCAN microscope. X-ray powder diffraction was measured using Philiph X-ray Generator PW1130 and X-ray diffraction pattern were recorded using a Siemens D5000 diffractrometer using CuK_α radiation and a LiF monochromator. The sample was mounted at 1° and scanned from 10-90° in steps of 0.02 with a count time of 2 seconds. Transmission Electron Microscopy (TEM) with Electron Diffraction (EDS) was recorded on JEOL JEM 2010-200 KV. ^{113}Cd nmr spectra were recorded with a Bruker AM 250 pulsed Fourier-transform NMR instrument.

References

1. R. O. Bells, M. Hammatt, and F. Wald, Phys. Stat. Sol., 1970, 1, 375.
2. N. C. Sharma, R. C. Kainthla, D. K. Pandya, and K. L. Chopra, Thin Solid Films, 1979, 60, 55.
3. I. Kaur, D. K. Pandya, and K. L. Chopra, J. Electrochem. Soc., 1980, 127, 943.
4. G. A. Kitaev, A. A. Uritskaya, and S. G. Mokrushin, Russian J. Physical Chem., 1965, 39, 1101.
5. R. C. Kainthla, D. K. Pandya, and K. L. Chopra, J. Electrochem. Soc., 1980, 127, 277.
6. S. Biswas, P. Pramanik, and P. K. Basu, Mat. Lett., 1986, 4, 81.
7. G. K. Padam, G. L. Malhotra, and S. U. M. Rao, J. Appl. Phys., 1988, 63, 770.
8. P. Pramanik, and S. Biswas, J. Electrochem. Soc., 1986, 133 ,350.
9. P. Pramanik, S. Bhattacharya, and P. K. Basu, Thin Solid Films, 1987, 149, L81.
10. P. Pramanik, M. A. Akhter, and P. K. Basu, Thin Solid Films, 1988, 158, 271.
11. M. Skyllas-Kazacos, J. F. McCann, and R. Arruzza, Appl. Sur. Sci., 1985, 22, 1091.
12. A. E. Martell and R. M. Smith, Critical Stability Constants Vol 2, page 36.
13. M. Tsuiki, H. Minoura, T. Nakamura, and Y. Ueno, J. Appl. Electrochem., 1978, 8, 523.
14. H. Katayama, S. Oda, and H. Kukimoto, Appl. Phys. Letters, 1975, 27, 697
15. H. J. Rohde, Thin Solid Films, 1983, 100, L125.
16. D. Lincot, R. Ortegaborges and M. Fromet, Phil. Mag. B-Physics of Condensed Matter Structural Optical and Magnetic Properties, 1993, 68, 185.

17. P. C. Rieke and S. B. Bentjen, Chem. Mater., 1993, 5, 43.

18. D. Lincot and R. Ortegaborges, J. Electrochem. Soc., 1993, 140, 3464.

19. T.L.Chu, S.S.Chu, N.Schultz, C.Wang and C.Q.Wu, J. Electrochem. Soc., 1992, 139, 2443.

20. I. Kaur, D. K. Pandya, and K. L. Chopra, J.Electochem. Soc., 1980, 127, 943.

21. G. A. Kitaev, A. A. Uritakaya and S. G. Mokrushin, Russ. J. Phys. Chem., 1965, 39, 1101.

22. M. Kamiyama, and E. Sugata, Eds. Handbook for thin layer engineering (Ohm, Tokyo, 1970).

23. R. Mach and G. O., Phys. Status Solidi A,1982, 69, 11.

24. T. Emma and M. McDonough, J. Vac. Sci. Technol., 1984, A2, 362.

25. A. Preisinger and H. K. Pulker, Jpn. J. Appl. Phys., 1974, Suppl. 2, Part 1, 769.

26. A. M. Ledger, Appl. Opt., 1979, 18, 2979.

27. P. L. Jones, D. Moore and D. C. Smith, J. Phys., 1976, E9, 312.

28. P. L. Jones, D. R. Cotton and D. Moore, Thin Solid Films, 1982, 88, 163.

29. J. A. Aguilera, J. Aguilera, P. Baumeister, A. Bloom, D. Coursen, J. A. Dobrowolski, F. T. Goldstein, D. E. Gaustafson and R. A. Kemp, Appl. Opt., 1988, 27, 2832.

30. R. Ionov and D. Nesheva, Thin Solid Films, 1992, 213, 230.

31. J. Pouzet, J. C. Bernede, A. Khellil, H. Essaidi and S. Benhida, Thin Solid Films, 1992, 208 , 252.

32. P. O'Brien, Chemtronics, 1991, 5, 61.

33. M. Ohishi, H. Satio, M. Yoneta and Y. Fujisaki, J. Cryst. Growth, 1992,117, 125.

34. S. Bonilla and E. A. Dalchiele, Thin Solid Films, 1991, 204, 397.

35. J. M. Dona and J.Herrero., J. Electrochem. Soc., 1994, 141, 205.

36. Y. Endoh and T.T. Taguchi, Mater. Res. Soc. Symp. Proc., 1990, 161, 211.

37. Y. Endoh, T.T. Taguchi, J. T. Mnllins and Y. Nozue, in Proc. 20th Intern. Conf. on Physics of Semiconductors, Thessaloniki, 1990, Eds. E. M. Anastassakis and J. D. Joannopoulos (World Scientific, Singapore, 1990) p1158.

38. C. D. Lokhande, M. S. Jadhav, and S. H. Pawar, J. Electrochem. Soc., 1989, 136, 2756.

39. K. T. Ramakrishna Reddy and P. Jayarama Reddy, J. Mater. Sci. Lett. 1991, 10, 439

40 D. Zeng, M. J. Hampden, T. M. Alam and A. L. Rheingold, Polyhedron, 1994, 13, 2715.

41. J. L. Vossen, in G. Hass, M. H. Francombe and R. W. Hoffmann (eds.) Physics of Thin Films, Academic Press, New York, 1977, page 1.

42. A. L. Dawar and J. C. Joshi, J. Mater. Sci., 1984, 19, 1.

43. T. Minami, H. Nanto and S. Takata, Appl. Phys. Letters, 1982, 41, 958.

44. T. Minami, H. Nanto and S. Takata, Japan. J. Appl. Phys., 1985, 24, L605.

45. T. Minami, H. Nanto, H. Sato and S. Takata, J. Appl. Phys., 1985, 24, L781.

46. T. Minami, H. Nanto, H. Sato and S. Takata, J. Appl. Phys., 1986, 25, L776.

47. H. E. Brown, Zinc Oxide. Properties and Applications, Int. Lead Zinc Research Org., New York 1976, chapter 6.

48. A. L. Fahrenbruch and R. H. Bube, Fundamentals of Solar Cells, Academic Press, New York, 1983, page 473-477.

49. C. Eberspacher, A. L. Fahrenbruch and R. H. Bube, Thin Solid Films, 1986, 136, 1.

50. P. O'Brien, J. Auld, D. J. Houlton, A. C. Jones, S. A. Rushworth, M. A. Malik and G. W. Critchlow, J. Mater. Chem., 1994, 4, 1249.

51. M. Tammenmaa, T. Koskinen, and M. Leskela, Thin Solid Films, 1985, 124, 125.

52. M. D. Amersley and C. W. Pitt, Thin Solid Films, 1981, 80, 183.

53. J. Aronovich, A. Ortiz and R. H. Bube, J. Vac. Sci. Technol., 1979, 16, 994

54. P.O'Brien, T. Trindade and J. D. P. de Jesus, J. Mater. Chem., 1994, 4, 1611.

55. A. Chittofrati and E. Matijevic, Colloids Surf., 1990, 48, 65.

56. D. Ravindra and J. K. Sharma, J. Appl. Phys., 1985, 58, 838.

57. J. I. Pankove, "Offical Processes in Semiconductors", Dover Publications, Inc., New York, 1970.